

**A PARTICULAR MECHANISM OF ANTI-ASTHMATIC
ACTIVITY OF COMPOUNDS ISOLATED FROM
Zingiber cassumunar Roxb. THROUGH
COMPUTATIONAL CHEMISTRY
APPROACHES**

**BY
KULPAVEE JITAPUNKUL**

**A THESIS SUBMITTED IN PARTIAL FULFILLMENT OF THE
REQUIREMENTS FOR THE DEGREE OF MASTER OF SCIENCE
(ENGINEERING AND TECHNOLOGY)
SIRINDHORN INTERNATIONAL INSTITUTE OF TECHNOLOGY
THAMMASAT UNIVERSITY
ACADEMIC YEAR 2016**

**A PARTICULAR MECHANISM OF ANTI-ASTHMATIC
ACTIVITY OF COMPOUNDS ISOLATED FROM
Zingiber cassumunar Roxb. THROUGH
COMPUTATIONAL CHEMISTRY
APPROACHES**

**BY
KULPAVEE JITAPUNKUL**

**A THESIS SUBMITTED IN PARTIAL FULFILLMENT OF THE
REQUIREMENTS FOR THE DEGREE OF MASTER OF SCIENCE
(ENGINEERING AND TECHNOLOGY)
SIRINDHORN INTERNATIONAL INSTITUTE OF TECHNOLOGY
THAMMASAT UNIVERSITY
ACADEMIC YEAR 2016**



A PARTICULAR MECHANISM OF ANTI-ASTHMATIC ACTIVITY OF
COMPOUNDS ISOLATED FROM *Zingiber cassumunar* Roxb.
THROUGH COMPUTATIONAL CHEMISTRY
APPROACHES


A Thesis Presented

By
KULPAVEE JITAPUNKUL

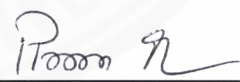
Submitted to
Sirindhorn International Institute of Technology
Thammasat University
In partial fulfillment of the requirements for the degree of
MASTER OF SCIENCE (ENGINEERING AND TECHNOLOGY)

Approved as to style and content by


Advisor and
Chairperson of Thesis Committee


(Assoc. Prof. Luckhana Lawtrakul, Dr.rer.nat.)


Committee Member and
Chairperson of Examination Committee


(Assoc. Prof. Pisanu Toochinda, Ph.D.)

Committee Member


(Prof. Orapan Poachanukoon, M.D.)

Committee Member


(Prof. Supa Hannongbua, Dr.rer.nat.)

APRIL 2017

Abstract

A PARTICULAR MECHANISM OF ANTI-ASTHMATIC ACTIVITY OF COMPOUNDS ISOLATED FROM *Zingiber cassumunar Roxb.* THROUGH COMPUTATIONAL CHEMISTRY APPROACHES

By

KULPAVEE JITAPUNKUL

Bachelor of Engineering (Chemical Engineering), Sirindhorn International Institute of
Technology, Thammasat University, 2015

Asthma has been a worldwide health problem including in Thailand and available medications are mostly imported and some have very severe side effects. Interestingly, Plai (*Zingiber cassumunar Roxb.*) is a herb which have anti-inflammation and anti-constriction properties. Compound D and DMPBD are considered as major compounds that have these properties. However, the inhibition mechanisms of them are not fully understand. Hence, molecular modeling are used to simulate complex systems between isolated compounds from Plai and two protein targets, 5-Lipoxygenase enzyme (5-LO) and Cysteinyl leukotriene receptors (CysLTRs), in comparison with natural substrates and commercial asthma drugs to investigate the possible antiasthmatic mechanism of these isolated compounds.

As the results, isolated compounds from Plai have possibility to bind with 5-LO enzyme and CysLTRs receptors. The possibility of their inhibition towards 5-LO is quite high because of following supported reasons. First, the calculate binding energy

of these compounds are similar to Zileuton which is commercial asthma drugs. Second, the binding characteristic of DMPBD is very similar to Zileuton. Third, solvent accessibility surface area calculation revealed the similarity of 5-LO binding pocket cavity between 5-LO complex with AA and Compound D. In other hand, binding with Zileuton and DMPBD can lead to reduction of 5-LO binding pocket cavity. Both properties give possibility to prevent the binding between 5-LO and AA. There are opportunities that these natural compounds will inhibit CysLTRs as well. But, with time-limit study, the movement of receptors which is important factor for activation or inhibition process cannot fully investigate. Hence, exact inhibition mechanism toward CysLTRs cannot be made. However, the binding affinity of isolated compounds from Plai on CysLTRs are similar to montelukast which is another commercial asthma drugs. This revealed opportunity that these compounds can inhibit CysLTRs. Moreover, Compound D shows interesting behavior which can lead to possible inhibition by limit receptor's structural movement. This behavior also found in CysLTR₁ structure after binding with montelukast. Consequently, with the current available information, isolated compounds from Plai have possibility to be antiasthmatic substances from natural source.

Keywords: Molecular Docking, Molecular Dynamics Simulations, Density Functional Theory, Asthma, *Zingiber cassumunar Roxb.*, Anti-Leukotriene Agents

Acknowledgements

Primarily, I would like to present my sincere appreciation to my esteemed advisor, Associate Professor Dr. Luckhana Lawtrakul, who have been dedicated many of her time and knowledge to support me. She have educated me in several ways for both academic materials and systematization in research performance. Moreover, she always expressed her attention with my health problem, endured with some troubles that had been occurred during my studied, and also provided me a lot of opportunities for my future study. Because of her encouragement, kindness and advices made my study much more valuable. I would like to express my truthful gratitude to all of my research committees; Professor Dr. Supa Hannongbua for her kindness and many helpful advices, Professor Dr. Orapan Poachanukoon for her useful advices and medical information that help me fulfilled my understand in this research, and Associate Professor Dr. Pisanu Toochinda for his kindness, valuable suggestion and many supports that he have given to me all along.

I would like to mention and express my thankfulness to those who have assisted and supported me during my study; Ms. Pimonluck Sittikornpaiboon, who have given me several suggestions, kind assistances that helped me solved many problems, and encouragement which supported me during this study. Mr. Krit Inthajak, who have always encouraged, assisted and supported me in many ways.

I would like to acknowledge the Excellent Thai Students (ETS) scholarship program of Sirindhorn International Institute of Technology (SIIT) which I had been financially supported. Moreover, this research was also supported by National Research Council of Thailand (NRCT) and I am gratefully acknowledge the Center of Nanotechnology, Kasetsart University for GAUSSIAN09 program package.

I am truly appreciate all of encouragement, support, and assistance from my parents Mr. Santichai Jitapunkul and Mrs. Vipavadee Jitapunkul. I would not have finished this research without their kind support and reassurance.

Ultimately, I would like to dedicate this research to all of those mentioned and I hope it would be useful for development of asthma medication in the near future.

Table of Contents

Chapter	Title	Page
	Signature Page	i
	Abstract	ii
	Acknowledgements	iv
	Table of Contents	v
	List of Figures	vii
	List of Tables	x
	List of Abbreviations	xi
1	Introduction	1
	1.1. Objectives	3
	1.2. Scope of Study	3
2	Literature Review	5
	2.1. Asthma and Drugs	5
	2.2. Leukotrienes and Its Roles in Asthma	7
	2.3. Characterization of Human 5-Lipoxygenase Enzyme	10
	2.4. Characterization of Human Cysteinyl Leukotriene Receptors	11
	2.5. Pharmacology of Anti-leukotriene Drug	15
	2.6. <i>Zingiber cassumunar Roxb.</i> Compositions and Properties	18
	2.7. Molecular Modeling with Computational Chemistry	21

3	Methodology	33
	3.1. Computational Devices and Software	33
	3.2. Operation Place	34
	3.3. Computational Procedure	34
	3.4. Flow Chart of Research Procedure	40
4	Computational Results	41
	4.1. 5-LO Systems	41
	4.2. CysLTRs Systems	59
5	Conclusions and Recommendations	99
	References	101
	Appendices	111
	Appendix A Amino Acids Sequences Information	112
	Appendix B Calculation Theory	122
	Appendix C Calculation Results	130

List of Figures

Figures	Page
1.1 Scope of study flow chart.	4
2.1 The illustration of airways comparing normal and inflamed airways.	5
2.2 Illustration of asthma symptoms stimulation pathways.	8
2.3 The biosynthesis pathway of LTs production.	9
2.4 Illustration of 5-Lipoxygenase enzyme (5-LO) structure.	10
2.5 Chemical structure of leukotriene D ₄ .	11
2.6 The conceptualized CysLTRs structure bounded with LTD ₄ .	12
2.7 Diagram shows the inhibition mechanism of anti-leukotriene drugs.	16
2.8 Chemical structure of Zileuton.	17
2.9 The chemical structures of commercial antagonists of CysLTRs.	17
2.10 Plai rootstock and types of extracted.	19
2.11 The chemical structures of isolated compounds from Plai.	19
2.12 Prediction of binding site and ligand structure with AutoSite.	25
2.13 Illustration of molecular docking concept.	25
2.14 Thermodynamics cycle of MM/PBSA and MM/GBSA calculation.	29
4.1 2-D structures and optimized structures of ligands in 5-LO systems.	41
4.2 Superimposition of two 5-LO x-ray structures.	42
4.3 Superimposition of 5-LO substrate complex from docking and x-ray.	45
4.4 5-LO binding site and conformation of each ligand from dockings.	45
4.5 Interacting amino acid residues for each 5-LO complexes from dockings.	46
4.6 2-D illustrations of 5-LO complexes interactions from docking.	46
4.7 5-LO complex systems energy.	47
4.8 5-LO systems total and average energy.	48
4.9 RMSD plot of 5-LO complex systems.	49
4.10 Total energy decomposition from selected interval of MD (15-20 ns).	52
4.11 Sidechain and backbone energy decomposition.	53

List of Figures (Continued)

Figures	Page
4.12 Superimposition of 5-LO substrate complex from MD snapshot and x-ray.	54
4.13 Superimposition of 5-LO structures from 19 ns snapshot.	55
4.14 Solvent accessible surface area (SASA).	56
4.15 Average solvent accessible surface area of 5-LO.	57
4.16 5-LO binding site and ligands conformations from 19 ns snapshot of MD.	58
4.17 2-D chemical interaction of selected frame from MD.	58
4.18 2-D structures and optimized structures of ligands in CysLTRs systems.	59
4.19 Generated 3-D structure of CysLTR ₁ and its component.	60
4.20 Generated 3-D structure of CysLTR ₂ and its component.	60
4.21 CysLTRs embed in phospholipid bilayer membrane.	61
4.22 Reference phospholipid bilayer membrane thickness.	62
4.23 Color map of constructed membrane thickness.	62
4.24 System energy of pure CysLTRs embed in membrane.	63
4.25 Alpha-carbon RMSD of pure CysLTRs embed in membrane.	64
4.26 CysLTR ₁ binding sites from AutoSite calculation.	67
4.27 CysLTR ₂ binding sites from AutoSite calculation.	67
4.28 Superimposition of CysLTR ₁ and CysLTR ₂ .	68
4.29 Intracellular binding site of CysLTR ₁ .	70
4.30 Extracellular binding site of CysLTR ₁ .	71
4.31 Extracellular binding pocket of CysLTR ₂ .	71
4.32 2-D chemical interaction of C1INT docking.	72
4.33 2-D chemical interaction of C1EXT docking.	73
4.34 2-D chemical interaction of C2EXT docking.	75
4.35 C1INT complex system energy.	77

List of Figures (Continued)

Figures	Page
4.36 C1EXT complex system energy.	78
4.37 C2EXT complex system energy.	78
4.38 RMSD plot of C1INT system.	79
4.39 RMSD plot of C1EXT system.	80
4.40 RMSD plot of C2EXT system.	80
4.41 Atomic fluctuation of CysLTRs systems.	82
4.42 Total energy decomposition from selected interval of C1INT systems.	85
4.43 Sidechain and backbone energy of C1INT systems.	86
4.44 Total energy decomposition from selected interval of C1EXT systems.	87
4.45 Sidechain and backbone energy of C1EXT systems.	88
4.46 Total energy decomposition from selected interval of C2EXT systems.	89
4.47 Sidechain and backbone energy of C2EXT systems.	90
4.48 Superimposition of C1INT complex systems.	91
4.49 Superimposition of C1EXT complex systems.	92
4.50 Superimposition of C2EXT complex systems.	93
4.51 Binding site and ligand conformation from selected snapshot of C1INT.	96
4.52 2-D chemical interaction of selected frames from C1INT systems.	96
4.53 Binding site and ligand conformation from selected snapshot of C1EXT.	97
4.54 2-D chemical interaction of selected frames from C1EXT systems.	97
4.55 Binding site and ligand conformation from selected snapshot of C2EXT.	98
4.56 2-D chemical interaction of selected frames from C2EXT systems.	98

List of Tables

Tables	Page
2.1 BLAST result between CysLTR ₁ receptor and difference species.	13
2.2 BLAST result between CysLTR ₂ receptor and difference species.	13
2.3 Amount of phenylbutanoids in Plai extract from different solvents.	20
4.1 RMSD of 5-LO x-ray structures (PDB ID: 3O8Y and 3V99).	42
4.2 Summary of molecular docking calculation of 5-LO systems.	43
4.3 Free binding energy calculated from MM/GBSA for 5-LO systems.	50
4.4 Alpha-carbon RMSD of selected frame at 19 ns of MD simulations.	55
4.5 CysLTR ₁ native contacts.	65
4.6 CysLTR ₂ native contacts.	66
4.7 Summary of molecular docking calculation for C1INT.	69
4.8 Summary of molecular docking calculation for C1EXT.	69
4.9 Summary of molecular docking result for C2EXT.	69
4.10 Comparison of experimental and calculated inhibitory constant of MON.	70
4.11 Free binding energy calculated from MM/GBSA for CysLTRs systems.	83
4.12 RMSD of selected frame from C1INT complexes and initial structure.	91
4.13 RMSD of selected frame from C1EXT complexes and initial structure.	92
4.14 RMSD of selected frame from C2EXT complexes and initial structure.	94

List of Abbreviations

Abbreviation	Description
5-LO	5-Lipoxygenase Enzyme
AA	Arachidonic acid
LTs	Leukotrienes
CysLTs	Cysteinyl leukotrienes
CysLTRs	Cysteinyl leukotriene receptors
CysLTR ₁	Cysteinyl leukotriene receptor 1
CysLTR ₂	Cysteinyl leukotriene receptor 2
Phyre	Protein Homology/Analogy Recognition Engine
GPCRs	G-Protein coupled receptors
PC	Phosphatidylcholine
PE	Phosphatidylethanolamine
LTD ₄	Leukotriene D ₄
DFT	Density Functional Theory
B3LYP	Becke, three-parameter, Lee-Yang-Parr
STOs	Slater-Type-Orbitals
GTOs	Guassian-Type-Orbitals
MD	Molecular dynamics simulation
NVT	Canonical ensemble
NPT	Isothermal-isobaric ensemble
MM/PBSA	Molecular Mechanics Poisson-Boltzman Surface Area

MM/GBSA	Molecular Mechanics Generalized Born Surface Area
CHARMM	Chemistry at Harvard Macromolecular Mechanics
EEL	Electrostatic energy
VDW	Van der Waals interaction
ZIL	Zileuton
MON	Montelukast
CD	Compound D
DMP	DMPBD
RMSD	Root Mean Square Deviation
C _α	Alpha-Carbon atoms
SASA	Solvent accessibility surface area
AS	AutoSite
C1INT	Intracellular Binding Pocket of CysLTR ₁
C1EXT	Extracellular Binding Pocket of CysLTR ₁
C2EXT	Extracellular Binding Pocket of CysLTR ₂
N-ter	N-terminal of protein
C-ter	C-terminal of protein
IL	Intracellular loop
EL	Extracellular loop

Chapter 1

Introduction

Asthma is a common chronic respiratory disease which symptoms can be stimulated by many factors such as genetic predisposition, environmental exposure, or exercise. Global Asthma Network (GAN) has reported in 2014 that approximately 334 million people have been suffered from asthma [1]. In present, major factors that can stimulate development of chronic airways disease especially asthma are rapid increase of pollutant or poisonous air in urban area and the crowded living circumstance, since, these could easily stimulate asthma symptoms.

Asthma symptoms occur from 3 basic components which are (1) narrowing of airways due to constriction of smooth muscle (2) inflammation of airways (3) production of mucus to obstruct the airways. These components will leads to cough, wheezing, and breathlessness; patients will have low quality of life because they have to constantly go to hospital and if the severity of symptoms is rapidly increase, it can be dangerous to death. In general, asthma drugs can be divided into 2 groups which are (i) anti-airways obstruction drug and (ii) anti-airways inflammation drug. Anti-airways obstruction drug can be used to relieve wheezing and breathlessness by reduce the constriction of airways. Anti-airways inflammation drug can be used to control the symptoms until it reach resting-state including both tablet (Montelukast and Zileuton) and inhaled corticosteroids. Since asthma is chronic disease that needs long-term therapy, thus, patients have to constantly use these medications in order to relieve symptoms. By using inhaled corticosteroids, the long-term side effects may occur such as osteoporosis, oral candidiasis, dysphonia, glaucoma, and adrenal insufficiency etc. [2] Moreover, there is a very high probability that patients will have the permanent resistant to corticosteroids [3]. In spite of corticosteroids severe side effects, the drug are still used in asthma treatment due to their low market price compared to others with the same range of effectiveness. Hence, the development for alternative asthma drugs with lower price and less side effects are necessary.

Leukotrienes (LTs) are potent lipid mediators that will be secreted out from cell when the immune system has been stimulated which similar to prostaglandin and histamine. These mediators will not spread throughout the body but its effects will be at specific location. Their responses are mediated through another G-protein couple receptor called cysteinyl leukotriene receptors (CysLTRs) [4] that will lead to airways inflammation, airways constriction and mucus production. In the past decade, there are many studies aimed to develop anti-leukotriene substances in order to use them as alternative asthma drugs. Some have been used in clinical practice which can be further divided into two sub-categories; (i) leukotriene biosynthesis inhibitors that inhibit activities of 5-Lipoxygenase enzyme (5-LO) and (ii) specific leukotriene receptor antagonists that inhibit response of CysLTRs [5]. However, those medications have lower efficacy than corticosteroids and contain some severe major drawbacks [6].

Interestingly, Plai or *Zingiber cassumunar Roxb.* has anti-inflammation and anti-histamine actions [7]. These medicinal properties of Plai extract were recorded in Thai herbal pharmacopoeia [8]. Researchers also found out that there are some important substances from Plai extraction by using hexane which responsible for anti-constriction and anti-inflammation activities on smooth muscle in small intestine and airways of guinea pig [9]. However, their inhibition mechanisms are not fully understand. Consequently, those isolated compounds have possibility to bind with both 5-LO and CysLTRs because they could reduce airways inflammation by inhibition of these protein-targets. Molecular modeling are used to simulate ligand-protein complex in order to study about inhibition mechanism of isolated compounds from Plai on 5-LO and CysLTRs in comparison with natural substrates and commercial asthma drugs by considering activities between each compound and amino acid residues around binding sites, binding energy and thermodynamics properties. Then, the suggestion regarding antiasthmatic mechanism of these isolated compounds from Plai based on binding modes and calculated binding energies are made to support future development of novel alternative asthma drug. This could reduce usage of chemicals and animal models in drug experiment. Moreover, this research result could be used to retrieve attention on traditional herbs like Plai and also stimulate the price of this herb.

1.1. Objectives

1. To study about molecular structure and binding interaction between isolated compounds from Plai in comparison with 2 commercial anti-leukotriene drugs (Montelukast and Zileuton) and natural substrates (Leukotriene D₄ and arachidonic acid) with cysteinyl leukotriene receptors (CysLTRs) and 5-Lipoxygenase enzyme (5-LO) in order to make suggestion concerning antiasthmatic mechanism of compounds for further development of novel asthma drug.
2. To study about binding site and 3-D crystal structure of 5-Lipoxygenase enzyme (5-LO), which is the target for isolated compounds from Plai.
3. To study about the amino acid sequences, binding sites and construct 3-D crystal structures of cysteinyl leukotriene receptors (CysLTRs), which are the targets for isolated compounds from Plai, since, there was no report regarding actual crystal structures of CysLTRs.

1.2. Scope of Study

This research aimed to study about antiasthmatic mechanism of isolated compounds from Plai or *Zingiber cassumunar Roxb.* Compound D (CD) or (E)-4-(3',4'-dimethoxyphenyl)-but-3-en-2-ol and DMPBD (DMP) or (E)-1-(3',4'-dimethoxyphenyl)-butadiene are considered as major anti-inflammation and anti-constriction substances. However, the inhibition mechanisms of these natural compounds are not fully understand. Therefore, several molecular modeling techniques are used to simulate and analyze complex system between those isolated compounds and two protein targets, 5-Lipoxygenase enzyme (5-LO) and Cysteinyl leukotriene receptors (CysLTRs), in comparison with natural substrates (AA and LTD₄) and commercial asthma drugs (Zileuton or ZIL and Montelukast or MON). Unfortunately, there is no reported about x-ray structures of CysLTRs and available x-ray structures of 5-LO were mostly incomplete. Thus, I have started with preparation of 5-LO structure from two x-ray structures. Following by construction of CysLTRs structures by homology modeling. Then, embedded them into phospholipid bilayer to mimic

environment of membrane protein. Construction and optimization of commercial asthma drugs, natural substrates, and isolated compounds from Plai under quantum mechanics modeling were performed. Afterwards, molecular docking with fixed-receptor and flexible-ligand have been used to observe possibility of binding between each ligand and amino acid residues around binding sites of CysLTRs or 5-LO by analysis on binding energy and modes of binding. The high possibility conformations are selected to perform MD simulation in order to study about inhibition mechanism of each anti-leukotriene agents by taking molecular motions of all atoms in the system into account and analysis of thermodynamics properties within each complex system. This can reveal the opportunities to used isolated compounds from Plai as antiasthmatic substances from natural source. The flow chart describing scope of study for this research is shown in Figure 1.1 below.

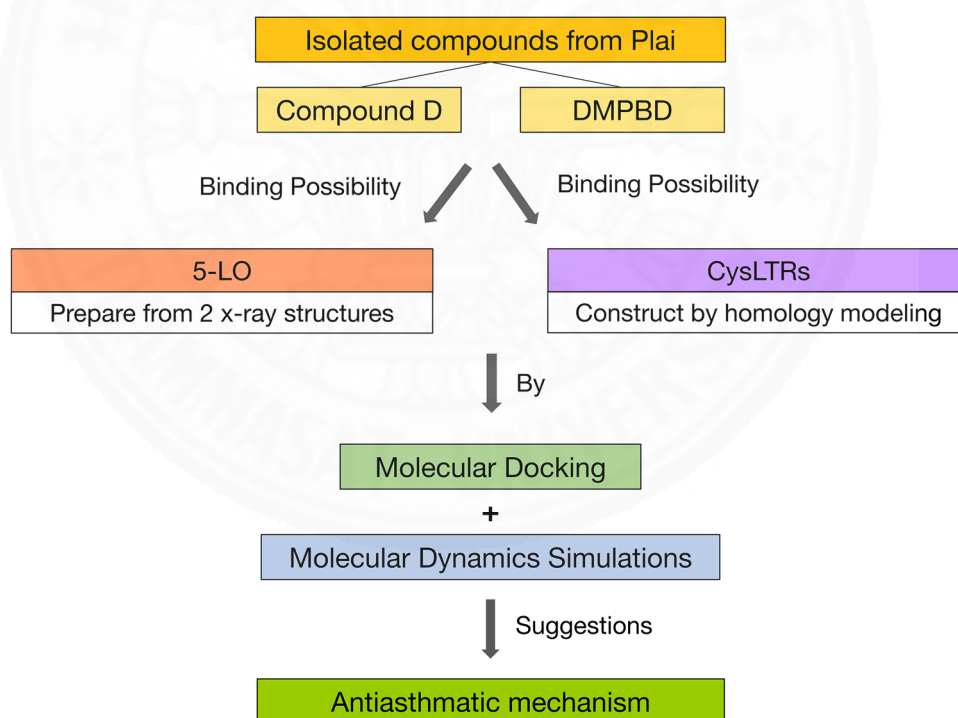


Figure 1.1: Scope of study flow chart.

Chapter 2

Literature Review

2.1. Asthma and Drugs

Asthma is a chronic respiratory disease that inflames and narrows the airways as shown in Figure 2.1, which will eventually lead to present of asthma symptoms such as wheezing, breathlessness, chest tightness, and coughing etc. The causes of asthma are not completely understood, but the main factors for developing asthma are a combination of genetic predisposition, environmental exposure, or stimulated by exercise. The severity ranges of symptoms varied from mild with occasional symptoms to severe with persistent symptoms that certainly impact patient's quality of life.

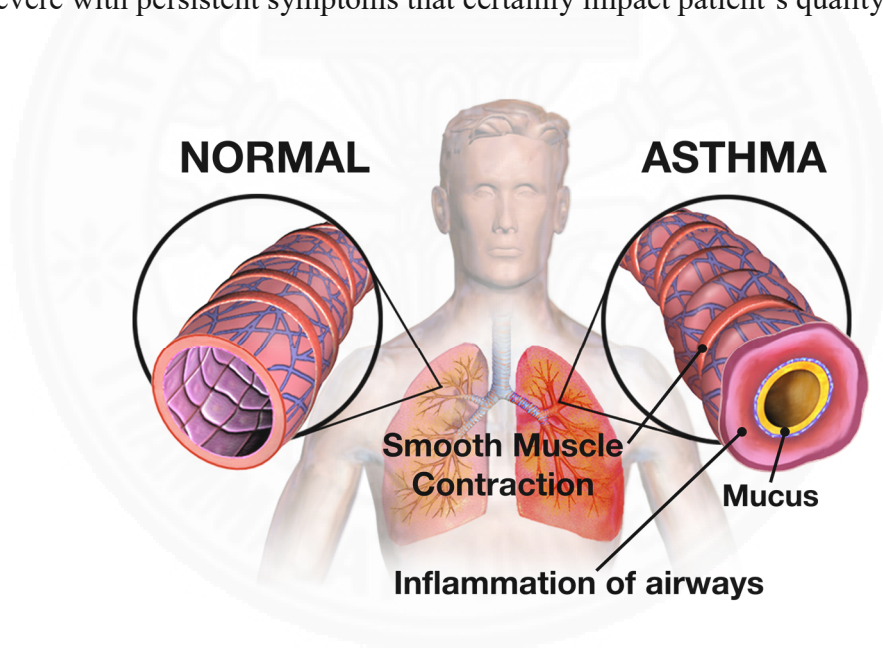


Figure 2.1: The illustration of airways comparing normal and inflamed airways.
(Source: [https://en.wikipedia.org/wiki/Asthma#/media/File:Asthma_\(Lungs\).png](https://en.wikipedia.org/wiki/Asthma#/media/File:Asthma_(Lungs).png))

Current available commercial asthma drug provide symptomatic relief to some, but not all patients. Medications used to treat asthma can be divided into two general classes: (i) quick-relief medications (Reliever) used to treat acute symptoms and (ii) long-term control medications (Controller) used to prevent further exacerbation.

2.1.1. Quick-Relief Medications: These medications provide fast relief of asthma attack symptoms such as cough, chest tightness, and wheezing, which include:

- Short-acting beta-agonists: A type of drug called bronchodilator, which opens your airways.
- Anticholinergics: These are bronchodilators that can be paired with or used instead of short-acting beta-agonists.
- Systemic corticosteroids (steroids): These are anti-inflammatory drugs that get asthma symptoms under control quickly, normally contained in inhaler.

2.1.2. Long-Term Control Medications: These drugs are taken daily over a long-time to get asthma under control and keep it stable. The most effective ones stop airways inflammation. The doctor may suggest the combine an anti-inflammatory drug with other drugs such as:

- Long-acting beta-agonists and inhaled corticosteroids (ICS).
- Mast cell stabilizers: Curb the release of chemicals that cause inflammation.
- Theophylline: A bronchodilator used to prevent nighttime symptoms.
- Leukotriene modifiers: Block chemicals that cause inflammation.

Controller medications are the most important because they prevent asthma attacks. However, since asthma is a chronic respiratory disease and the long-term symptoms relieve therapy is still necessary, some patients might have steroids drug resistance problem. In present, there are some alternative asthma drugs available such as the anti-leukotriene drugs that have been used in clinical practice of bronchial asthma. They can be divided into two categories: (i) specific leukotriene receptor antagonists (Montelukast, Zafirlukast, Pranlukast) and (ii) leukotriene biosynthesis inhibitors (Zileuton). Some organizations set guidelines on these drugs and classified the anti-leukotriene therapeutic agents as a group of drugs controlling the course of disease [5]. In addition, the anti-leukotrienes are the first new class of novel and effective therapy for asthma in more than 20 years. They have been shown to have a beneficial effect in treatment of both induced and spontaneously occurring asthma [10].

2.2. Leukotrienes and Its Roles in Asthma

Asthma symptoms stimulation involved with various biological pathways. In general, they was initiated by inhalation of antigen that will activates mast cells and Th2 cells in the airway which can induce production of mediators responsible for inflammation, such as histamine, leukotrienes, and cytokines including interleukin-4 and interleukin-5. Once mast cells were activated, it will secrete histamine and LTs out. Some Interleukin-5 that have been secreted out from activated Th2 cell were transported to bone marrow and causes terminal differentiation of eosinophils. Then, circulated eosinophils will enter inflammation area and migrate to lung by rolling through interactions with selectins, and eventually adhering to endothelium. After eosinophils enter matrix of airway through cytokine activation, their survival is prolonged by interleukin-5. Once activation occurred, eosinophil will releases inflammatory mediators such as leukotrienes and granule proteins. Leukotrienes production has started by conversion of arachidonic acid (AA) through many enzymes and eventually formed cysteinyl leukotrienes (CysLTs) that will give biological response through another G-protein couple receptors called cysteinyl leukotriene receptors (CysLTRs) and leads to airways injury including smooth muscle contraction as shown in Figure 2.2 [11; 12].

In this study, I was only interested in leukotriene pathway because most of the available alternative asthma drugs besides steroids hormones were anti-leukotriene substances shown as red text in Figure 2.2. Thus, additional detail about leukotrienes bio-synthesis and activities were studied. Leukotrienes (LTs) are potent biological lipid mediators that have been converted from arachidonic acid (AA) by catalytic activities of 5-Lipoxygenase enzyme (5-LO) and its activation protein (FLAP), AA have become available when cytosolic phospholipase A₂ (cPLA₂) cleaves it from cell-membrane phospholipids once the cell have been activated. LTs will not be found in resting cell and also be called as slow reacting substance of anaphylaxis (SRS-A).

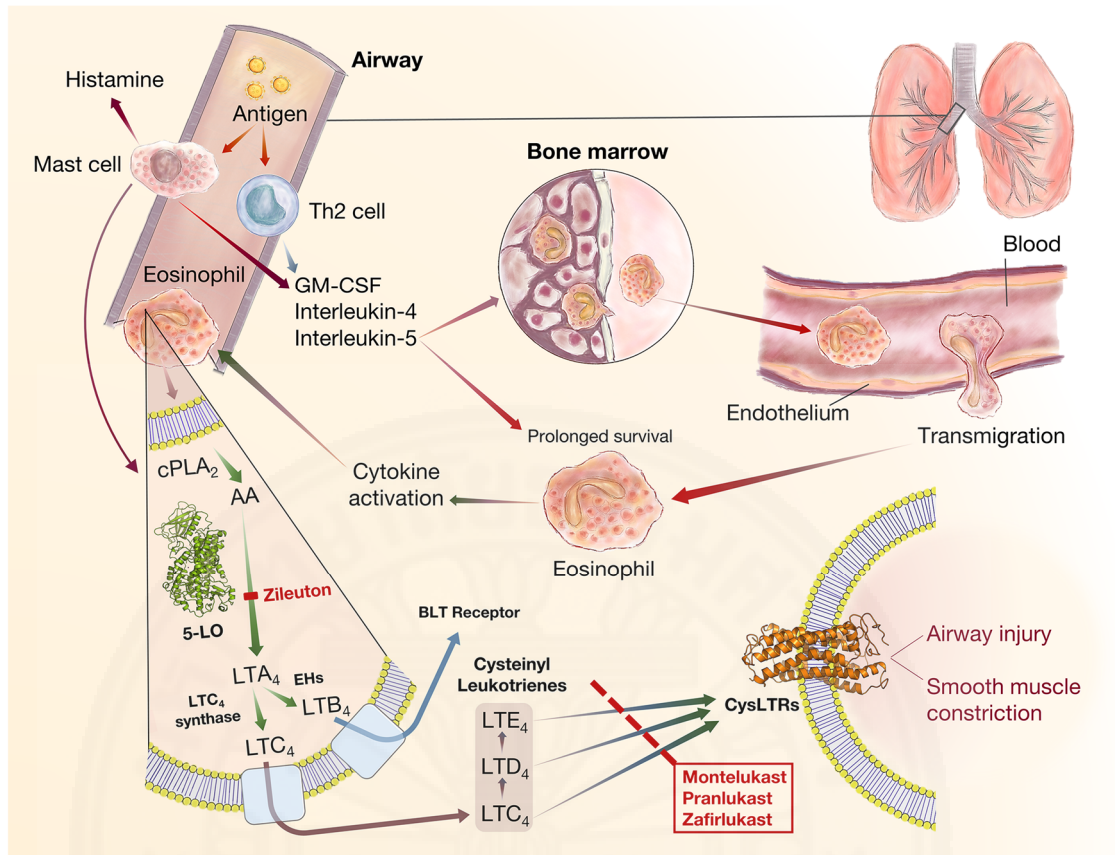


Figure 2.2: Illustration of asthma symptoms stimulation pathways.

After AA were released and catalyzed in sequential catalytic activities of 5-LO and FLAP, leukotriene A₄ (LTA₄) have been produced. Since, instability of LTA₄ it is immediately converted to leukotriene C₄ (LTC₄) or leukotriene B₄ (LTB₄). In two cell types associated with asthma symptoms activation pathway; mast cells and eosinophils, LTA₄ is converted to LTC₄ by the addition of glutathione at the C-6 position of LTA₄ by catalytic reaction of LTC₄ synthase. Then, LTC₄ is transported to extracellular through specific transmembrane transporter. Once LTC₄ presented in extracellular space, the glutamic acid moiety is cleaved from LTC₄ to form LTD₄ which alternately cleaved by extracellular dipeptidases to form LTE₄. Due to LTC₄, LTD₄, and LTE₄ contained essential amino acid cysteine, therefore, they have been called as cysteinyl leukotrienes as shown in Figure 2.2 and Figure 2.3 [12; 13].

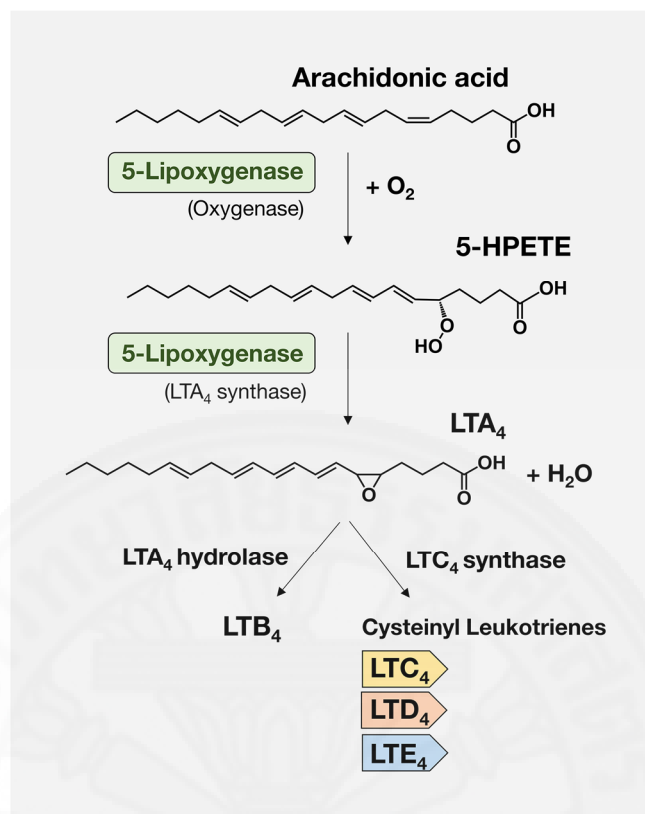


Figure 2.3: The biosynthesis pathway of LTs production.

There are several evidences suggested that CysLTs can be produced in the lung through interaction between different cells, structural, and infiltrating inflammatory. Some experiment data also support that CysLTs may be involved in airway smooth muscle proliferation and remodeling. Therefore, the concept that CysLTs mediate significant components of bronchoconstriction and inflammation evoked by common triggers of asthma e.g. allergen, exercise, and inhalation of dry cold air were proposed. By following the hypothesis, there are many studies about the mechanism of leukotriene in guinea pig, as the results; there are two G-protein couple receptors involved in activation process of asthma symptoms which are 2 types of cysteinyl leukotriene receptors (CysLTRs), CysLTR₁ and CysLTR₂, that will bind with CysLTs to give the biological responses in asthma. LTC₄ and LTD₄ are reported as potent inducers of bronchoconstriction in airways of guinea pig and caused contraction of isolated human bronchi. Meanwhile, LTE₄ has been studied less because this leukotriene was found to be incomplete and less potent agonist than LTC₄ and LTD₄. However, LTE₄ has been documented to possess a bronchoconstrictor activity, which is similar to LTC₄ and

LTD₄. Moreover, the prolonged exposure to LTE₄ may produce enhancement of the responsiveness of smooth muscle to histamine which is an organic nitrogenous compound involved in the inflammatory response. Therefore, CysLTs are the most potent endogenous bronchoconstrictors so far known [14; 15].

2.3. Characterization of Human 5-Lipoxygenase Enzyme

Human 5-LO is monomeric enzyme with 673 amino acids, which consist of two major domains; N-terminal domain β -sandwich (residues 1-114) and C-terminal catalytic domain (residues 121-673) as shown in Figure 2.4 [16]. It catalyzes the first two steps in biosynthesis of LTs which are potent lipid mediators derived from AA and leukotriene responses are mediated through another G-protein couple receptor, which are CysLTRs that will eventually leads to appearance of asthma symptoms. In resting cell, 5-LO will locate either in cytosol or inside nucleus but once it has been activated by binding with Ca^{2+} ion at N-terminal β -sandwich domain, it will migrate close to nuclear envelope due to Fe^{2+} ion inside catalytic domain was oxidized to be Fe^{3+} ion. Then, it is ready to catalyze the oxygenation reaction of AA to form 5(S)-hydroxy-6-trans-8,11,14-cis-eicosatetrenoic (5-HETE) in first step and covert 5-HETE to be LTA₄ in second step by dehydration as shown in Figure 2.3 [17; 18].

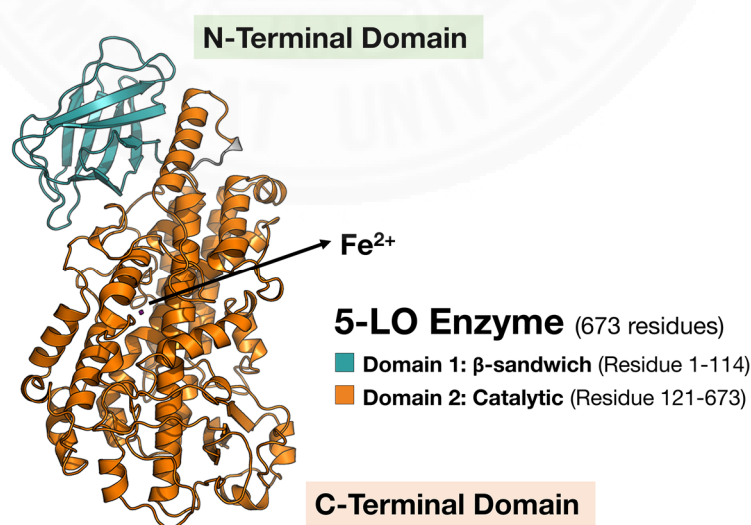


Figure 2.4: Illustration of 5-Lipoxygenase enzyme (5-LO) structure.

Consequently, this research will focus on interaction between each compound and amino acid residues around binding site in catalytic domain of 5-LO only, since there was a scientific study reported regarding binding site of AA which located within catalytic domain of 5-LO [19], therefore, the binding area for simulation have been set followed this reference in order to observe competitive inhibition activity of each compound.

2.4. Charaterization of Human Cysteiny Leukotriene Receptors

Pharmacological and clinical studies have shown that cysteinyl leukotriene receptors (CysLTRs) are 7 hydrophobic transmembrane-spanning domains linked by 6 hydrophilic loops receptors [20] which coupled to G-proteins and activated intracellular signaling pathways in response to their endogenous ligands, CysLTs [21]. Currently, there are two types of these membrane receptors that have been identified to specifically bind with CysLTs; CysLTR₁ which selective for LTD₄ and LTE₄, and CysLTR₂ which selective for LTC₄ and LTD₄. Consequently, there is an assumption that CysLTRs antagonist/inhibitor may bind to the same site as natural substrates (CysLTs) based on the observation that minor change of LTD₄ can results in competitive antagonist, and the reason that LTD₄ was used as representative for other CysLTs is because both CysLT₁ and CysLT₂ receptors selective for LTD₄ [22; 23]. The 2-D chemical structure of LTD₄ is shown in Figure 2.5.

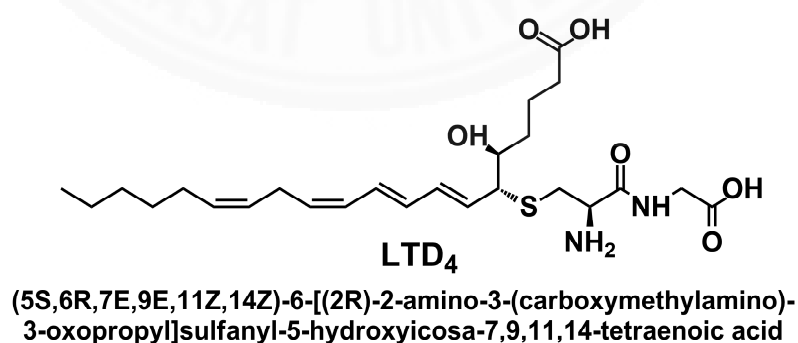


Figure 2.5: Chemical structure of leukotriene D₄.

In order to analyze the interaction between competitive inhibitor of CysLTRs, understanding about interactions between natural substrate and CysLTRs is necessary.

Therefore, the essential structure requirements for CysLTRs ligands are listed below [24; 25];

- i. A lipophilic anchor which fits into the lipophilic pocket of CysLTRs.
- ii. A central lipophilic and flat unit to mimic triene system of LTD₄.
- iii. One or two acidic groups as potential mimics of peptide unit and/or carboxylic acid of LTD₄.
- iv. Spacers to connect and pre-organize the elements.

The illustration of CysLTRs structure complex with LTD₄ is shown in Figure 2.6.

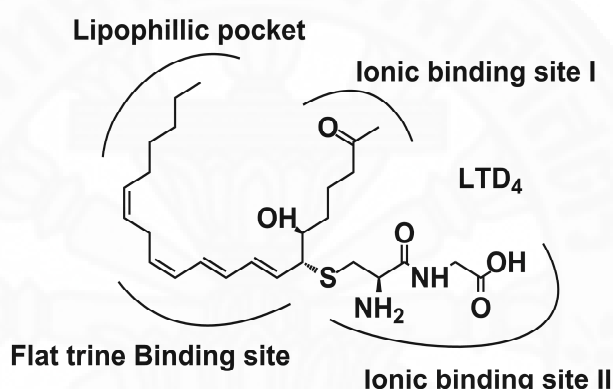


Figure 2.6: The conceptualized CysLTRs structure bounded with LTD₄.

CysLTR₁ receptor consist of 337 amino acid residues and CysLTR₂ receptor consist of 346 amino acid residues as reported in Appendix A (A-1 and A-2) and the similarity between these two receptors were reported in Appendix A (A-3) with definition of single letter abbreviation of essential amino acid in Appendix A (A-5). Since the x-ray structures of CysLTRs are not available in any database, therefore, in order to predict and construct crystal structure of proteins, the amino acid sequences should be consider in detail. By using BLAST (Basic Local Alignment Search Tool) [26] among difference amino acid sequences from many species in order to make comparison between human CysLTRs and others. BLASTP (Standard protein-protein BLAST) is available online on UniProt website (BLASTP version 2.2.29+) which linked to database called UniProtKB that was generated to support BLAST via UniProt (last updated on March 14, 2016). The results are shown in Table 2.1 and Table 2.2.

Table 2.1: BLAST result between CysLTR₁ receptor and difference species.

Entry (ID)	Protein Name	Identity
Q9Y271	CysLTR ₁ (<i>Homo sapiens</i> :: Human)	100.00%
Q2NNR5	CysLTR ₁ (<i>Cavia porcellus</i> :: Guinea pig)	87.00%
Q99JA4	CysLTR ₁ (<i>Mus musculus</i> :: House mouse)	87.50%
Q99JA4-2	Isoform 2 of CysLTR ₁ (<i>Mus musculus</i> :: House mouse)	87.50%
Q95N02	CysLTR ₁ (<i>Sus scrofa</i> :: Wild boar)	87.90%
Q924T8	CysLTR ₁ (<i>Rattus norvegicus</i> :: Brown rat)	87.40%

Table 2.2: BLAST result between CysLTR₂ receptor and difference species.

Entry (ID)	Protein Name	Identity
Q9NS75	CysLTR ₂ (<i>Homo sapiens</i> :: Human)	100.00%
Q95N03	CysLTR ₂ (<i>Sus scrofa</i> :: Wild boar)	79.30%
Q920A1	CysLTR ₂ (<i>Mus musculus</i> :: House mouse)	73.10%
Q924T9	CysLTR ₂ (<i>Rattus norvegicus</i> :: Brown rat)	73.10%

From Table 2.1 and Table 2.2, by considering identity percentage of each entry; for CysLTR₁ receptor, amino acid sequences of guinea pig, house mouse, wild boar, and brown rat are similar to human with approximately 87-88% identity. For CysLTR₂ receptor, amino acid sequences of wild boar is the most resemble with human (79.30% identity), house mouse, and brown rat are less resemble with 73.10% identity. Consequently, drugs testing that have done with animal models such as guinea pig and mouse could be reliable due to high similarity of receptors compared to human. However, since we intend to reduce experimental cost and animals testing, molecular modeling based on computational chemistry theory would support that intention. To perform simulation, the x-ray structures of CysLTRs will be needed, in this case amino acid sequences of human CysLTRs have been selected and homology modeling of CysLTRs is necessary. Therefore, I have studied some fundamental of homology modeling as described below.

2.4.1. Homology Modeling

Homology modeling refer to protein's comparative modeling, which involve the construction of protein structure in atomic-resolution level from amino acid sequence incorporate with experimental three-dimensional structures of related protein or template. This technique depends on identification of one or more known protein structures probably to imitate structure of the query sequence from the alignment of amino acid residues in query sequence to residues in template sequence. According to the past result, it revealed that protein structures are more conserved than protein sequences among homologues. However, sequences falling below 20% sequence identity can have very different structure [27].

The quality of generated structure depend on quality of sequence alignment with template structure. The complication could arise from alignment gaps in target that specify the presence of structure in target but not in template, and structure gaps in template that occur from poor x-ray crystallography resolution in the experimental procedure. The quality also degenerates with reduction of sequence identity. Normally, model has approximately 1–2 Å root mean square deviation (RMSD) between matched C_{α} atoms at 70% sequence identity, but, 2–4 Å C_{α} -RMSD at 25% sequence identity. Nonetheless, errors are much higher in loop regions which amino acid sequences of target and template proteins can be entirely distinct. Loop regions were constructed without a template by loop modeling. They normally have low accuracy when compare to the other regions of model. Errors in side chain position and packing also rise with reduction of sequence identity. Because deviations in packing configurations have been proposed as a dominant reason for poor quality model at low sequence identity [28].

Phyre and Phyre² (Protein Homology/Analogy Recognition Engine) are web-based services for protein structure prediction that are free of charge for non-commercial use [29; 30]. It is popular methods for protein structure prediction and has been cited for more than 1500 times (from Google scholar citation statistic). Similar to other remote homology modeling techniques, it can be used to repeatedly generate decisive protein structures when other vastly used methods cannot. Usage and application of the predicted structural models by homology modeling include protein–protein interaction prediction, protein–protein docking, protein–ligand docking, and

functional annotation of genes identified in an organism's genome [31]. Even the low-accuracy homology models can still be useful for these purposes, because the inaccuracy normally located in loops regions on protein surface, which are generally more deviate even between intimately related proteins. The functional regions of the protein, especially its active site, tend to be more highly conserved and thus more precisely modeled [32].

However, since CysLTRs are the transmembrane spanning G-protein coupled receptor (GPCRs) that have been categorized as rhodopsin sub-family GPCRs [33]. In order to imitate the reality of that environment, the constructed 3-D structure of CysLTRs by homology modeling have to be embedded in the phospholipid bilayer with assistance of membrane-builder program, thus, the type and amount of phospholipids used to build the membrane have to be specified, since, rhodopsin protein had been simulated in membrane-bounded environment before by Grossfield group [34]. Consequently, in this study, I have been specified similar properties of phospholipid-bilayer membrane with their study as described below.

A bilayer containing a 2:2:1 mixture of SDPC:SDPE:cholesterol (total of 124 lipid molecules). SDPC is a type of phospholipid in phosphatidylcholine (PC) category and SDPE is a type of phospholipid in phosphatidylethanolamine (PE) category which both of them are considered as crucial component of phospholipid-membrane. For the hydration number, which is variable that control the number of water molecules in the system, value 59.67 have been used, thus, there are present of 59.67 water molecules per 1 molecules of lipid and this have given 7,400 water molecules in total.

2.5. Pharmacology of Anti-leukotriene Drug

Asthma symptoms are caused by LTs biosynthesis process followed with CysLTRs activation through CysLTs in order to release biological response which present as asthma symptoms. Therefore, the inhibition of LTs biological pathway may be directed towards their formation (LTs biosynthesis) or actions (CysLTRs activation process) as shown in Figure 2.7 [13].

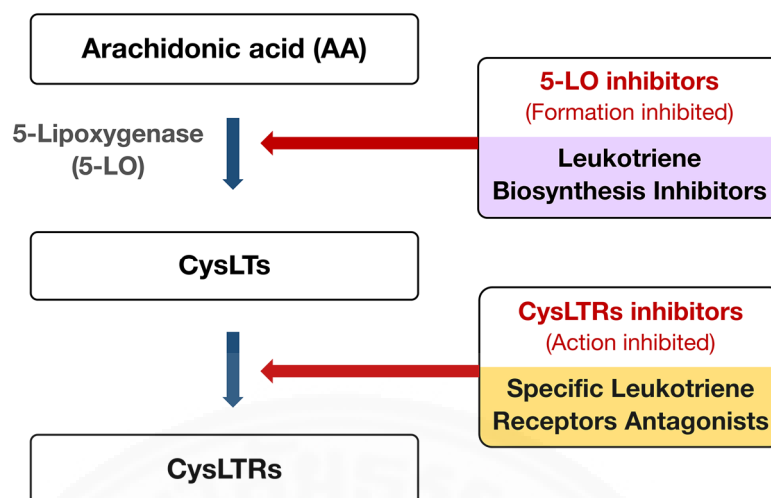


Figure 2.7: Diagram shows the inhibition mechanism of anti-leukotriene drugs.

Over the past two decades, there are many developments for selective and potent pharmacological agents that can inhibit biological pathway of LTs. In this regards, there are 2 schemes have been pursued which are inhibition of biosynthesis of LTs and inhibition of LTs action. Therefore, to achieve inhibition of LTs formation, preferred target is 5-LO due to the direct inhibition of 5-LO activity is assumed to be the most effective approach to reduce leukotriene biosynthesis. Because the formation of 5-HETE will be blocked and as the result, the formation of LTA₄ will also be blocked. The direct 5-LO inhibitors can be classified based on the molecular mode of action as redox-active 5-LO inhibitors, iron-ligand inhibitors, and non-redox 5-LO inhibitors. Redox-active 5-LO inhibitors will reduce the active site iron and uncoupling the catalytic cycle of enzyme, therefore, it is an efficient inhibitor to prevent formation of 5-LO enzyme in vitro and in vivo. Iron ligand inhibitors normally are hydroxamic acids; generally they are amides wherein the N-H center has been replaced by a hydroxyl (OH) that will chelate the active site iron. However, they have low reducing properties such as N-hydroxyurea derivatives A-64077 or Zileuton (ZIL) as shown in Figure 2.8. Unfortunately, ZIL is the only commercial alternative asthma drug which target 5-LO and it has many major drawbacks such as liver toxicity, low potency, and short half-life [35]. Non-redox 5-LO inhibitor could be the competitive inhibitor of AA, it will compete with AA to bind with 5-LO, and normally contain structurally diverse molecules which are potent and highly selective inhibitors of 5-LO. Even though they

have tremendous potency which have been observed in intact cells, but their efficacy depends on the stimulus such as Ca^{2+} ions and also the redox tone [6].

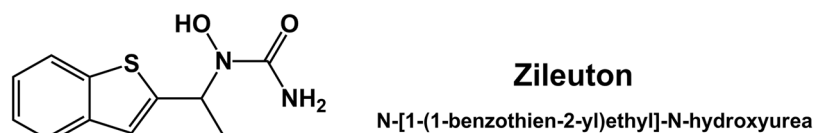


Figure 2.8: Chemical structure of Zileuton.

Nevertheless, the therapeutic efficacies of 5-LO inhibitors did not reach the expectation that those inhibitors should be at least effective as the inhibitor for blocking only CysLT_1 receptor, which is the inhibition of LTs action by inhibiting subtype receptor that induce asthma symptoms [6].

For inhibition of LTs action, some drugs in this category have been use in clinical practices for bronchial asthma as mentioned earlier. From Figure 2.9, Motelukast (MON) contains acid residue (carboxylic acid) and both Zafirlukast and Pranlukast contain quinolone nitrogen that can form hydrogen bounds with amino acid residues, especially arginine, or the ionic binding sites of CysLTRs [23].

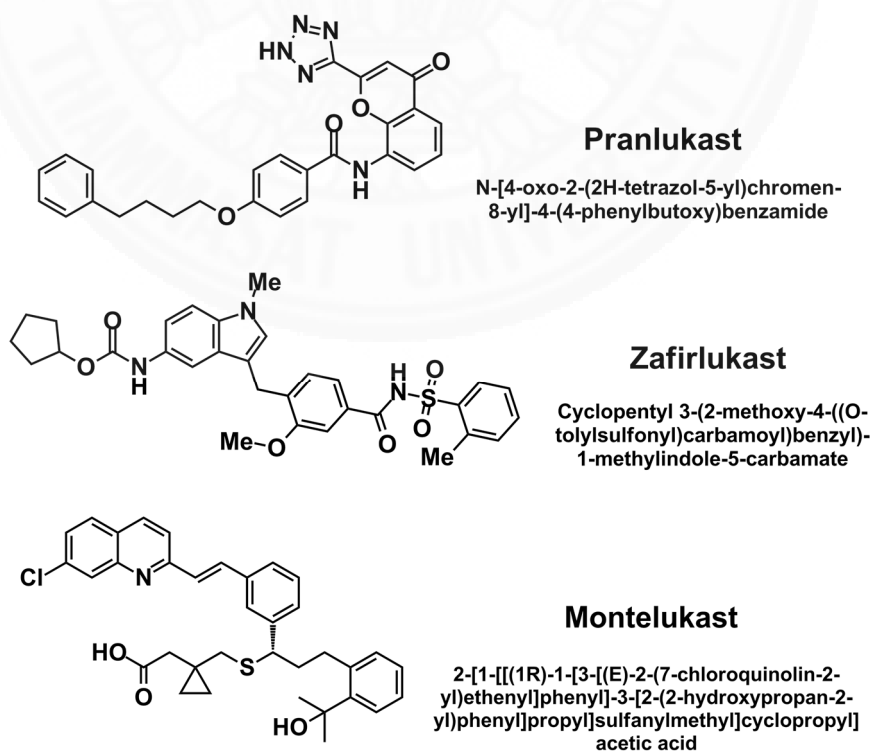


Figure 2.9: The chemical structures of commercial antagonists of CysLTRs .

2.6. *Zingiber cassumunar Roxb.* Compositions and Properties

Thai herbal pharmacopoeia indicated that approximate 50% of drug recipe contained Plai or *Zingiber cassumunar Roxb.* [8] Interestingly, it has antiasthmatic activity in children with no acute toxicology effect. Phytochemical study of Plai have shown that, there are varieties of compounds that can be extracted out of Plai rhizome by using hexane as solvent. Study about pharmacological properties of each isolated compound revealed that Compound D (CD) or (E)-4-(3',4'-dimethoxyphenyl)but-3-en-2-ol has anti-constriction of airways property in guinea pig [36] and DMPBD (DMP) or (E)-1-(3',4'-dimethoxyphenyl)-butadiene has anti-inflammatory and anti-swelling activity in laboratory rats [9; 37; 38]. However, there is only a few report about the antiasthmatic mechanism of isolated compounds from Plai (CD and DMP) [39]. By considering laboratory result and chemical structure of these isolated compounds, there was a possibility that they will inhibit synthesis or action of LTs' biological pathway. Consequently, I have studied further about composition and pharmacological properties of Plai extracted as described below.

Plai can also be called as Bengal root and cassumunar ginger. It is an herbs in ginger family which has originated in South East Asia region, including Thailand. An article published in *Journal of Thai Traditional and Alternative Medicine Vol. 11 No. 2 (2013)* has reported about chemical properties, pharmacological properties, and toxicology of Plai that it can be used as anti-inflammatory drug, analgesic, and asthma drug [7]. The substances that have been considered to have anti-inflammatory and antiasthmatic property were extracted from rhizome or rootstock of Plai (Figure 2.10) by using organic solvents such as hexane, palm oil, soybean oil, or mineral oil. The Plai crude extract consist of many compounds which can be divided into 5 categories; phenylbutanoids, curcuminoids, naphthoquinone derivatives, monoterpenoids, and sesquiterpenoids. The phenylbutanoid monomers is a group of compounds that have been reported as effective anti-inflammatory substances and analgesic, therefore, I have focused on substances in phenylbutanoids group [7].



Figure 2.10: Plai rootstock and types of extracted.

(Source: <http://www.munyatra.com/wp-content/uploads/2015/02/Mangoesteem.jpg>, http://thumbs3.picclick.com/d/w1600/pict/191601998498/_Bottle-of-Plai-Massage-Oil-100ml-Genuine.jpg, and <http://frynn.com/wp-content/uploads/2013/09/เหง้าไพล.jpg>)

2.6.1. Phenylbutanoid monomers

There are 2 compounds in this group of extracted substances which were reported to have anti-inflammatory and anti-allergy properties called Compound D (CD) and DMPBD (DMP). The structures of these isolated compounds are shown in Figure 2.11.

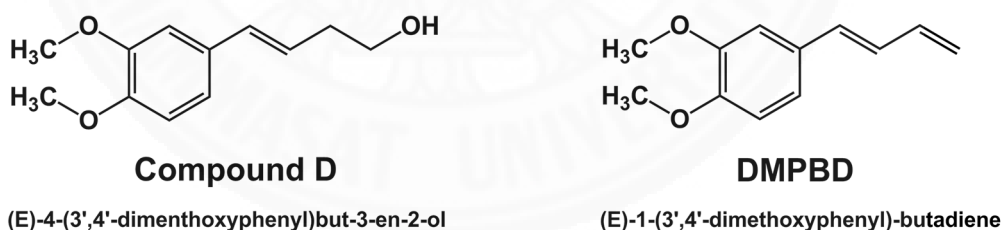


Figure 2.11: The chemical structures of isolated compounds from Plai.

- i. Anti-inflammatory, Analgesics, and Antipyretic Activities of Phenylbutanoids
 - CD has been reported that it has anti-inflammatory activity similar to some of the commercial drugs such as Aspirin, Indomethacin, and Prednisolone when tested with animal models [7].

- DMP has been reported that it has better anti-inflammatory activity than the commercial drug, Diclofenac, when tested in animal models which were induced the inflammation with AA [7].

ii. Smooth Muscle Relaxation Activities

CD has been reported that it has non-specific smooth muscle relaxation activity and increasing the capacity of airways by resistance of histamine activity when tested in guinea pig. Consequently, it has been reported to use as asthma drug but there is a disadvantage; it can resist the shrinking of diaphragm [7].

iii. Anti-allergic Activity

The anti-histaminic activity of Plai extract (11-25 mg/kg) in young asthma patients age 8-16 years result in reduction of blisters size caused by histamine injection [7].

iv. Green Extraction

Originally, the extraction of phenylbutanoids out of Plai rhizome will use hexane as solvent. However, since hexane has to be evaporated out from the Plai extract before those extract can be used, therefore, this process could leads to high operating cost. Thus, several researchers have studied on alternative solvents such as palm oil, soybean oil, and mineral oil which are environmental friendly solvents and this could be called as green extraction technology [7].

Table 2.3: Amount of phenylbutanoids in Plai extract from different solvents.

Solvent	Phenylbutanoids (%w/w)			
	CD	CD acetate	DMP	Total
Hexane	0.23	0.38	1.04	1.66
Palm oil	0.17	0.23	0.63	1.02
Soybean oil	0.16	0.22	0.63	1.01
Mineral oil	0.10	0.22	0.71	1.02

From Table 2.3, hexane is the most effective solvents to extract phenylbutanoids out of Plai rhizome. Palm oil, soybean oil, and mineral oil can extract phenylbutanoids out of Plai rhizome slightly less than hexane. Therefore, those alternative solvents can be considered as good solvents to extract phenylbutanoids out of Plai rhizome because they are safer and do not need evaporation process; which can reduce operation cost for extraction. Nevertheless, hexane is the best option due to the high amount of phenylbutanoids production. For alternative, the acute toxicological testing of 50/50 alcohol and hexane mixing ratio as solvent in Plai extraction process reported that there was no poisonous effect to laboratory mouse.

2.7. Molecular Modeling with Computational Chemistry

Study about computational chemistry will be important option in research and drug development. Computational chemistry is a study about properties of compound at molecular level. The concept of designing compounds for further drug development is finding out compounds that have stronger binding interaction between them and amino acid residues in target protein than natural substrate, consequently, computational chemistry will take the role in calculation of binding energy between protein and each compound in order to let researcher choose only compound with similar or higher binding energy than natural substrate to further pharmacological study. Advantages of computation chemistry are reduction of experimental/test cost, chemical free, reduction of clinical practice on animal models, and environmental friendly. The result from different computational chemistry approaches such as quantum chemistry calculations, molecular docking, and molecular dynamics simulation will be processed and analyzed in order to get chemical and thermodynamic properties, and then use it to support or explain experimental result and provide basic information regarding possibility before performed experiment. Even though computational chemistry was widely accepted and also played crucial role in research for drug development, but it cannot completely replace laboratory experiment due to every discovery needs proof, therefore, it must be finished with laboratory testing, so, in order to get accurate and correct results for further actual usage, the simulation results should match with actual laboratory results. Nonetheless, this study aimed to investigate

the possibility of inhibition activities by computational chemistry only. Therefore, basic information about each technique that have been used and results from previous researches are described below.

Firstly, in order to do structural optimization of small-molecules or ligands prior further complex system simulation in this study, the Density functional theory (DFT) in quantum chemistry program package will be used, hence, the fundamental and theory behind the calculation have been studied and briefly explained as followed.

2.7.1. Density Functional Theory (DFT)

DFT can be considered as a versatile and renowned computational quantum modeling technique that have been used in many fields such as physics, material science, and computational chemistry etc. It normally used to investigate the electronic structure in particular atom or molecule of macroscopic system that contain many interacting atoms, which applicable to this study; since, the structural optimization by minimization of energy was performed with molecule solvated in water system. By applying DFT, the property of several electrons system can be determined with electron density functionals. There are many models and theorem were developed by several scientists since 1927, the first model was proposed by Llewellyn Thomas and Enrico Fermi, which called Thomas-Fermi model (TF model) [40; 41], it was developed shortly after introduction of Schrödinger equation to investigate the electronic structure of system with interacting atoms by concern only electronic density. Thus, TF model is correct only in the limit of infinite nuclear charge aspect. However, applying the calculation for investigation of realistic systems produce poor quantitative predictions. Hence, Hohenberg and Kohn have come up with developed theorem called Hohenberg-Kohn Theorems (H-K Theorem) which consisted of two sub-theorems [42], The first H-K theorem have shown that the ground state properties of many-electron system can be determined with 3-coordinates electron density functional. From the first theorem, reduction of many-body or many interacting atoms problem which consist of N electrons with $3N$ coordinates to only 3 spatial coordinates by usage of electron density functionals have been proposed. In addition, this theorem can be applied to the time-dependent domain for development of time-dependent density functional theory

(TDDFT) in order to describe excited states of electrons. The second H–K theorem defines an energy functional for the system and proves that the minimization of energy could be achieved from correct ground state electron density. Nonetheless, in 1965 Walter Kohn and Lu Jeu Sham have discover new theorem called Kohn-Sham equation [43], it can change the difficult many-body problem to easier problem by considering particles in the system as non-interacting electrons that generate the same density as system of interacting particles, calculation details are described in Appendix B (B-1).

2.7.2. Hybrid Functional

It is an approximation for exchange-correlation energy in DFT that incorporate a part from Hartree–Fock theory with other sources. The correlation exchange energy is determined as Kohn–Sham orbitals rather than electron density. The approximation that generally used and have been selected to use with this study is called B3LYP, which referred to Becke, three-parameter, Lee-Yang-Parr [44; 45]. The involved function as description are shown in Appendix B (B-2).

2.7.3. Pople Basis Set

Basis set is a set of function used in computational chemistry by combining the linear combination to produce molecular orbitals, which is the atomic orbitals at atom center. Originally, these atomic orbitals can be described by Slater-Type-Orbitals (STOs); STOs will be decayed exponentially with respect to distance from atom nuclei and reach maximum distance with zero STOs, thus, this could be accurately determine the overlap range between atoms incorporate with charge and spin around nuclei. However, STOs is difficult technique to compute which have been realized and further developed by Frank Boy who came up with Gaussian-Type-Orbitals (GTOs) [46]. Presently, there are many basis set consisted of GTOs; the smallest set is called minimal basis set which included the minimum number of basis function to express all electrons of each atom in system by applying single function to each orbital in Hatree-Fock approximation of free atom. Nonetheless, there are additional function that need to add in minimal basis set which is the polarization function, denoted as asterisk (* or **), in order to describe the polarization of atoms in the system including light atom such as hydrogen. In addition, for precision notation of what function are added to the basis set,

the asterisk sign can be change to type of orbital that have been added such as (d,p) is equals to double asterisk (**) notation etc. Split-valence basis sets is developed basis set to describe molecular bonding, in term of valence electron with several basis function corresponding to each valence atomic orbital. Due to different orbitals have different range, the combination provided adjustment of electron density to the particular molecular environment. Minimum basis sets are fixed and are unable to adjust to any different molecular environments. The most commonly used one is called Pople basis set [47] , which have been proposed by group of John Pople. Thus, in this study one of basis set from this split-valence type have been selected , which is the 6-31G basis set that have been added the d polarization to non-hydrogen atoms plus with addition of p polarization function to hydrogen atoms called as 6-31G(d,p) or 6-31G**.

Afterwards, the simulation of ligand-protein complex have to be performed in order to investigate the chemical interaction. Two modeling techniques have been selected, which are molecular docking and molecular dynamics simulation (MD), thus, basic theory incorporated with computation detail had been studied as briefly explained below.

2.7.4. Molecular Docking

Unlike 5-LO, CysLTRs have no available x-ray structure, consequently, there is no proposed binding site/pocket within CysLTRs structure. With assistance of additional package from docking program (AutodockFR) called AutoSite [48], the possible binding site could be predicted, since, AutoSite (AS) used the computational algorithm for identification and characterization of small molecules binding sites with known receptor 3-D structure by observation on energetic aspects in order to select high affinity points in space around the receptor incorporate with clustering technique for segregating these points into clusters (fills point) which corresponding to potential binding pockets. In addition, this algorithm also capable to predict the structure of ligand in each predicted binding site as illustrated in Figure 2.12.

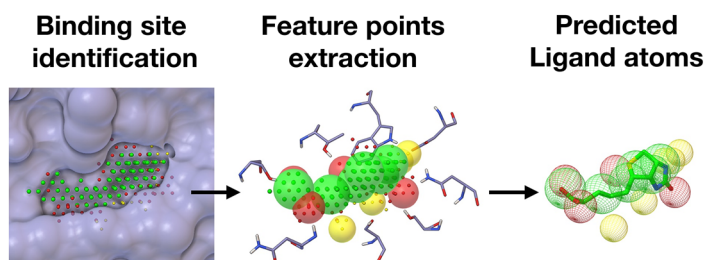


Figure 2.12: Prediction of binding site and ligand structure with AutoSite.
(Source: <http://adfr.scripps.edu/AutoDockFR/autosite.html>)

The result from AutoSite will be categorized in ranking system based on default AutoSite score of each predicted site (fills point ≥ 50) as shown in eq. (2.7.4-1)

$$\frac{\text{No. of fills points} \times \text{buriedness}^2}{\text{Radius of gyration}} \quad (2.7.4-1)$$

After the possible binding site have been specified to help reduce calculation time, the molecular docking can be initiated. However, in order to correctly perform simulation, fundamental of this technique should be understand as described below.

Molecular docking with fixed-receptor and flexible-ligand is computational chemistry technique that can be used to predict the possibility of binding between ligand and protein-target by considering the orientation/conformation of ligand within binding site which form a stable complex as shown in Figure 2.13.

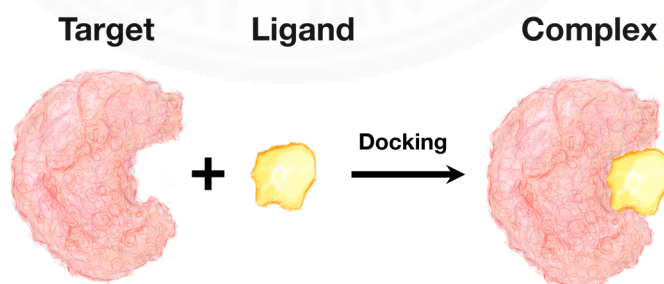


Figure 2.13: Illustration of molecular docking concept.

There are 2 molecular docking approaches that have been widely used, the first approach is to describe the complimentary surface of ligand and protein by matching technique [49-51]. The second approach is to simulate the molecular docking and

calculate ligand-protein interaction energy [52]. In this study, the second approach has been selected and the simulation outline are explained as followed.

In this second approach of molecular docking technique, ligand will move toward protein's active site and finds its position in conformational space. The motion of ligand incorporate with rigid body transformations such as translations, rotations, internal changes of structure, and torsion angle rotations. At the end of every move, the total energy of system will be calculated because the motion of ligand induce the system energy. Hence, the advantage of this approach is the incorporation of ligand flexibility was easy to obtain and produce more accurate result, unlike the first approach that used the shape complimentary method to incorporate ligand flexibility. Nonetheless, the second approach which is the simulation technique will be definitely expensive to produce more realistic result due to increase of computer speed and specification result in more expensive price of the computer.

In order to be able to perform the molecular docking screening, general docking algorithm have to be understand also, thus, the steps of calculation are described as followed. The first requirement as input for molecular docking simulation are 3-D structures of ligand and target protein which can be obtained from several biophysical techniques such as x-ray crystallography and NMR spectrometry etc. Nonetheless, the structure can be produced from homology modeling technique, which also applied to this study. Then, in order to successfully perform simulation, there are 2 important components that need to be carefully investigated before include them in the docking algorithm; which are (i) search algorithm and (ii) scoring function. For this study, the genetic algorithm will be used as search algorithm to do iteration for finding the low energy conformations. The scoring function will be used to estimate energy of each ligand conformation in the binding site as shown in eq. (2.7.4-2).

$$G_{\text{bind}} = G_{\text{solvent}} + G_{\text{conf}} + G_{\text{int}} + G_{\text{rot}} + G_{\text{t/t}} + G_{\text{vib}} \quad (2.7.4-2)$$

Where, G_{solvent} denotes energy from solvent effect

G_{conf} denotes energy from conformation change

G_{int}	denotes free energy from complex interaction
G_{rot}	denotes energy from internal rotation
G_{vib}	denotes energy from change in vibrational modes

The low binding energy (G_{bind}) indicates a stable system with stable binding interaction [53]. However, the binding energy cannot be considered alone to make the conclusion regarding binding possibility, but, the number of ligand orientations in each cluster incorporate with inhibitory constant (K_i) have to be investigated along with binding energy. Thus, the inhibitory constant can be determined from the calculated binding energy with the following relationship as shown in eq. (2.7.4-3) and (2.7.4-4).

$$G_{\text{bind}} = RT \ln K_i \quad (2.7.4-3)$$

$$K_i = \exp\left(\frac{G_{\text{bind}}}{RT}\right) \quad (2.7.4-4)$$

Where, R denotes gas constant ($1.9858775 \text{ cal K}^{-1}\text{mol}^{-1}$)
 T denotes temperature of simulation (298.15 K)

2.7.5. Molecular Dynamics Simulation (MD)

MD is the computational tool used to calculate the time dependent molecular behavior, in this case the complex biological molecules, by investigate the thermodynamics properties of the system. MD will generate the information about atomic position and velocity in the defined system, which can be considered as microscopic level properties. Thus, in order to investigate the thermodynamics properties of the whole system such as pressure and energy, which considered as macroscopic level properties, the statistical mechanics will be used to observe macroscopic system properties from properties of each molecule in the system. Hence, there are two states of system properties that have to be interchangeably investigated, which are (i) thermodynamics state and (ii) microscopic/mechanical state; the definition of each state are described below.

Thermodynamic state usually expressed by temperature (T), pressure (P), volume (V) and number of particles (N). Nonetheless, other thermodynamic parameters can be calculated from equations of state and other fundamental equations.

Microscopic/mechanical state expressed by particle position and momentum which can be defined as coordinate in multi-dimension space called phase space. Ensemble is a set of points in phase space that match the conditions of thermodynamic state. MD will generate a series of time dependent points in phase space and those points will be included to the same ensemble that corresponding to the different conformations and momentum of the system. In other word, ensemble is a set of possible system that have different microscopic properties but can satisfy same macroscopic properties. Currently, there are several available ensembles. However, only three of them will be used and also briefly explained in this study as followed.

Canonical ensemble (NVT) will control the number of particles (N), volume (V), and temperature (T) to remain constant. This ensemble can also be called as constant temperature molecular dynamics (CTMD). In NVT, endothermic energy and exothermic energy will be exchanged with thermostat, in this study the Langevin thermostat have been selected.

Isothermal-isobaric ensemble (NPT) will control the number of particles (N), pressure (P), and temperature (T) to remain constant. Thus, in addition of thermostat, the barostat is also require to perform pressure control that considered as isotropic system. This ensemble correspond to the reality of laboratory experiment with open system at ambient pressure and temperature. Nevertheless, for system with bilayer-membrane the ensemble that considered as the most appropriate have to slightly change from NPT to NPAT because the isotropic pressure control will not suitable for the system, but, the pressure control will occur under constant membrane area instead which can be called as anisotropic pressure control.

Consequently, in order to obtain the microscopic properties of each particle in the system, MD will use fundamental of Newton's second law which is an equation of motion to produce trajectory and specify location, velocity, and acceleration of each particle in the system with respect to time as explained in Appendix B (B-3).

However, the potential and kinetic energy of the system are considered as important thermodynamics parameters that have to be calculated and analyze. But, due to difficulty in solving the potential energy equation which depend on position of all particles in the system, there are many numerical methods that have been developed and for this study, the selected MD program has used the integration algorithm called Leap-frog algorithm which briefly described in Appendix B (B-4). Then, after obtaining the potential energy and kinetic energy, the total energy of system can be determined by relationship described in Appendix B (B-5)

Even though, determination of whole system energy can explain the system behavior, but, in order to investigate regarding binding interaction between protein target and ligand; the system energies are not considered as decent representative because interactions between solvent particles in the system can result in fluctuation of total energy. Therefore, MM/PBSA (Molecular Mechanics Poisson-Boltzman Surface Area) and MM/GBSA (Molecular Mechanics Generalize Born Surface Area) method can be used to calculate binding free energy between protein target and ligand in the system by followed a particular thermodynamics cycle as shown in Figure 2.14.

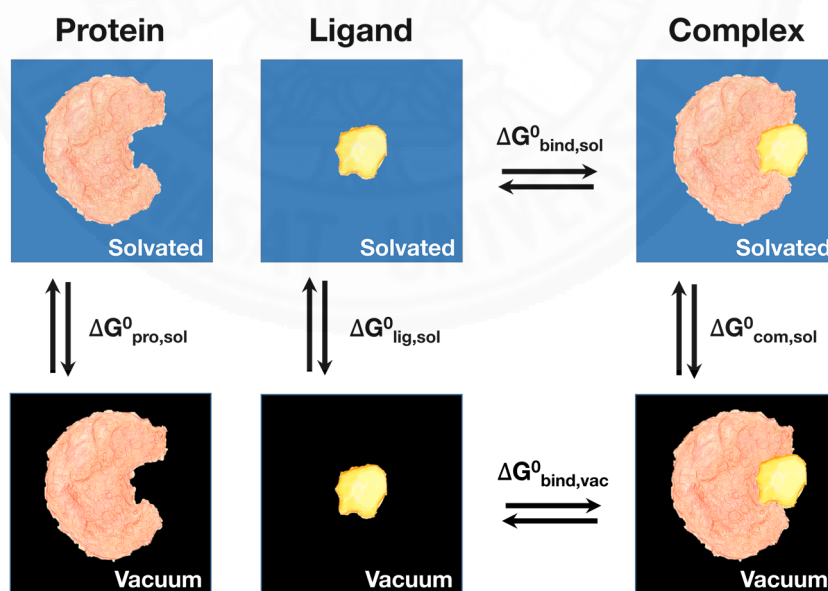


Figure 2.14: Thermodynamics cycle of MM/PBSA and MM/GBSA calculation.

Thus, the binding free energy of protein target and ligand in solvated system can be calculated as indicated in eq. (2.7.5-1).

$$G_{\text{bind,sol}}^0 = G_{\text{bind,vac}}^0 + G_{\text{com,sol}}^0 \left(G_{\text{pro,sol}}^0 + G_{\text{lig,sol}}^0 \right) \quad (2.7.5-1)$$

In MM/PBSA and MM/GBSA approaches, the solvation free energy of each state ($G_{\text{pro,sol}}^0$, $G_{\text{lig,sol}}^0$, and $G_{\text{com,sol}}^0$) can be calculated from solving the linearized Poisson-Boltzman (MM/PBSA) or Generalized Born (MM/GBSA) equation. Thus, the solvation free energy with electrostatic contribution can be obtained incorporate with addition of empirical term for hydrophobic contributions as shown in eq. (2.7.5-2).

$$G_{\text{s,sol}}^0 = G_{\text{elec, } \epsilon=80}^0 - G_{\text{elec, } \epsilon=1}^0 + G_{\text{hydrophobic}}^0 \quad (2.7.5-2)$$

Where,

$G_{\text{s,sol}}^0$	denotes solvation free energy of each state
$G_{\text{elec, } \epsilon=80}^0$	denotes electrostatic contribution with permittivity of free space (ϵ) = 80
$G_{\text{elec, } \epsilon=1}^0$	denotes electrostatic contribution with permittivity of free space (ϵ) = 1
$G_{\text{hydrophobic}}^0$	denotes hydrophobic contribution

For binding free energy in vacuum environment ($G_{\text{bind,vac}}^0$), it can be obtained by calculation of average interaction energy between protein target and ligand. In addition, if necessary or desired the calculation can also include the entropy change upon binding as shown in eq. (2.7.5-3).

$$G_{\text{bind,vac}}^0 = E_{\text{molecular mechanics}}^0 - T S_{\text{normal mode analysis}} \quad (2.7.5-3)$$

Where,

$E_{\text{molecular mechanics}}^0$	denotes interaction energy
$S_{\text{normal mode analysis}}$	denotes entropy change
T	denotes temperature (298.15 K)

The entropy change can be calculated by using normal mode analysis on the 3 states (protein, ligand, and complex), however, the entropy change in system can be neglected if consider the comparison of similar entropy state such as two ligands binding to the same protein target. Since, normal mode analysis calculations are computationally expensive and might produce large margin of error that introduces significant uncertainty in the result.

The average interaction energies of protein and ligand are normally calculated on ensemble of uncorrelated snapshots derived from equilibrated MD trajectory.

2.7.6. Previous Research Results

Molecular dynamics simulations of CysLTs (LTC₄, LTD₄, and LTE₄) were first study by Herron's group [54]. They investigate the LTs structures in water systems and they found T-shaped conformation of LTD₄ and the cup-shaped conformation of LTC₄ while LTE₄ shown the overlap T-shaped and cup-shaped conformations. Liu and team studied the affinity of anti-leukotriene agents (Zafirlukast and Montelukast) and leukotriene to carbon nanotubes by using molecular dynamics simulations approach [55]. Both of Herron and Liu used AMBER program for their investigations. Parravicini's group applied docking and molecular dynamics simulations to analyze the binding and the forced unbinding of a hybrid G-protein coupled receptor ligand (Pranlukast) using AutoDock and Gromacs programs. They found out that aromatics interactions are play a predominant role in the recognition of Pranlukast binding subsites [56]. Thangapandian and team used Gromacs program to study the molecular dynamics simulations of hybrid pharmacophore model development in Human Leukotriene A₄ hydrolase which use to convert LTA₄ to LTB₄. Binding mode analysis shown that the additional thiophene moiety of most active inhibitor helps the pyrrolidine moiety to interact the most important amino acid residues [57].

Eren and team were performed molecular docking between 5-LO and 50 non-redox inhibitors with GOLD program in order to observe inhibitory activity, they revealed the key hydrophobic interactions an their results also demonstrated probable binding conformations and key interactions of ligands in different structural classes at the active site of 5-LO [58]. De Lucia and team were used docking protocol to predict

the possible interaction between 5-LO and 18 compounds, which were reported as potential 5-LO inhibitor, in comparison with Zileuton and caffeic acid as references structures; they used Autodock Vina program to perform molecular docking. They reported that compounds with triazole linker demonstrated excellent and higher potency than clinical drugs like Zileuton, moreover, the linker length was proved to be importance factor in determining potency against 5-LO [59]. Loza-Mejía and team were suggested that some triterpiens and sterols can be good candidates for produce active compounds that interfere with inflammatory process; consequently, they have selected some of triterpiens to perform molecular docking with 5-LO by using Molegro Virtual Docker program. They revealed that the present of carboxylic groups in ligand could improve 5-LO binding, evidently, carboxylic groups are crucial for enzyme binding because they interact with histidine residues around binding site [60].

Chapter 3

Methodology

3.1. Computational Devices and Software

3.1.1. Computers

- 2 computers with Intel® core™ i7-3770 CPU @ 3.40GHz (4 cores), RAM 8 GB, Windows 8, Intel® display graphics 4000.
- 2 computers with Intel® core™ i7-4790 CPU @ 3.60GHz (8 cores), RAM 8 GB, Ubuntu 14.04 LTS, NVIDIA GeForce GT 720/PCIe/SSE2.
- 2 computers with Intel® Core™ i7-6700 CPU @ 3.40GHz (8 cores), RAM 16 GB, Ubuntu 14.04 LTS, NVIDIA GeForce GTX 960/PCIe/SSE2.
- 1 workstation (Exxact: Quantum TXR4340064R) with 2 Intel® Xeon® processor E52640 CPU @ 2.6 GHz (8 cores), RAM 64 GB, GPU up to 1 TB, CentOS 7, NVIDIA GeForce GTX 1080, Pascal, 8GB GDDR5X 4.

3.1.2. Software

- GaussView 5.0 [61] and GAUSSIAN09 [62] program package for structural construction and optimization of small molecules.
- Phyre² [29] online program for performing the homology modeling.
- AutoSite package from AutodockFR [48] for specification of unknown binding site in protein structure.
- Autodock 4.2 [63] for molecular docking calculation.
- CHARM-GUI online membrane builder [64-71] for embedded the protein into phospholipid bilayer system.
- Discovery Studio Visualizer 4.0 [72] for perform structural superimposition and visualize the protein-ligand interactions.
- PyMOL 1.3 [73] for rendering protein-ligand complexes figures.
- Bio3d program package [74-76] for formatting result file from CHARM-GUI membrane builder to match with MD program files format.

- GRIDMAT-MD [77] for measure the thickness of constructed phospholipid bilayer membrane.
- AMBER12 [78] and AMBER16 [79] program package for performing MD with AMBER force fields [80-82]
- MM/PBSA and MM/GBSA calculation method [83] in AMBER program package to determine the free binding energy of protein target and ligand incorporated with energy decompositions between each amino acid residue and ligand.

3.2. Operation Place

Computer lab located on 5th floor of laboratory building at Sirindhorn International Institute of Technology (SIIT) – Rangsit campus, Thammasat University, which own by School of Bio-Chemical Engineering.

3.3. Computational Procedure

Computer-aided molecular modeling can be used to find out about binding interaction and thermodynamics properties of interested complex system, therefore, the operation steps are described below.

3.3.1. Ligand Preparation and Structural Optimization

- Ligands: AA, LTD₄, ZIL, MON, CD, and DMP.
- Construction: create 3-D structure in GaussView 5.0 program package or extracted structure from x-ray structure (only AA).
- Optimization: using DFT at B3LYP/6-31G(d,p) level in water solvated system by GAUSSIAN09 program package.

3.3.2. Host Preparation and Structural Minimization

- Host: 5-LO, CysLTR₁, and CysLTR₂.
- Preparation: for 5-LO, use protein structure from RCSB Protein Data Bank (PDB ID: 3O8Y with x-ray diffraction resolution

equals to 2.39 Å [84]) and extracted coordinated of AA from another x-ray structure (PDB ID: 3V99 with x-ray diffraction resolution equals to 2.25 Å [85]).

- Construction: for CysLTR₁ and CysLTR₂, create 3-D protein structure by homology modelling in Phyre² server.
- Minimization: perform protein structures minimization in AMBER force field by AMBER12 program with constant volume.

3.3.3. Embedded Protein in Phospholipid Bilayer Membrane

- Protein: CysLTR₁ and CysLTR₂.
- Input: minimized structure of CysLTRs from 3.3.2.
- Setting: for CHARMM-GUI online membrane builder
 1. Set format for uploaded pdb file as CHARMM.
 2. Set orientation of protein to align along z-axis, due to this orientation is the appropriate setting for small helical bundle protein.
 3. Calculation of lipid number, followed reference [34], from 2:2:1 mixture of SDPC:SDPE:cholesterol, thus, the amount of each lipid can be described below;

SDPC	= 50 molecules (ref. 49 molecules).
SDPE	= 50 molecules (ref. 50 molecules).
Cholesterol	= 24 molecules (ref. 24 molecules).
Total	= 124 molecules.

Therefore, specification of number of lipid will be divided into 2 part as followed;

Upper leaflet = 25 POPC : 25 POPE : 12 cholesterol.

Lower leaflet = 25 POPC : 25 POPE : 12 cholesterol.

Since, lipid11 and lipid14 force field in AMBER program package did not included SDPC and SDPE, consequently, POPC and POPE have been used instead. Then, set the length in x and y direction to followed the specified lipid component.

4. Calculation of hydration number, followed reference [34], thus, from reference the total number of water molecules is 7,400 molecules. Since, the hydration number specify the number of water molecules per one lipid, the calculation can be done by division of total water molecules with total number of lipid. As the result, hydration number is 59.67 and specify number should slightly exceed the calculated value which approximately 60. Then, set the length in z-direction followed the specified hydration number to form rectangular box system.
5. Set system building option to replacement method, which is a method that protein is first packed by lipid like spheres whose positions are subsequently used to randomly place the specified lipid molecules from library.
6. Neutralizing system by adding ions with Monte-Carlo ion placing method.

3.3.4. Formatting Protein Chain in Membrane system

- Input: generated files from 3.3.3.
- Program: Bio3D program package.
- File format: format protein chain in the files to AMBER format.

3.3.5. Formatting Lipid Molecules in Membrane system

- Input: formatted files from 3.3.4.
- Program: charmm lipid2amber function in AmberTools13 package.
- File format: format lipids molecules from CHARMM format to AMBER format.

3.3.6. Measure Thickness of Constructed Phospholipids Bilayer Membrane

- Input: completely formatted files from 3.3.5.

- Program: GRIDMAT-MD program package.
- Comparison: compare measured thickness with reference [86].

3.3.7. MD of Pure CysLTRs Embedded in Bilayer Membrane system

- Input: completely formatted files from 3.3.5.
- Program: AMBER12 program package with lipid11, gaff, ff12SB, and TIP3P water box force fields.
- Simulation:
 1. Minimization: constant volume, no pressure scaling.
 2. Heating (step 1): from 0-100 K for 5 ps with constant volume and Langevin thermostat.
 3. Heating (step 2): from 100-300 K for 100 ps with anisotropic pressure control and Langevin thermostat.
 4. Production MD: equilibrate system for 15 ns with NPAT ensemble.
- Analysis: investigate C α -carbon RMSD and take snapshot from stable interval for performing molecular docking.

3.3.8. Molecular Docking

- Host: minimized 5-LO, equilibrated CysLTR₁, and CysLTR₂.
- Ligands: optimized AA, LTD₄, ZIL, MON, CD, and DMP.
- Binding site: specify binding site of CysLTRs in AutoSite package.
- Docking: perform molecular docking in Autodock 4.2 program.
 1. Fixed-host and flexible-ligands.
 2. Assign Gasteiger charges to all molecules.
 3. Use Lamarkian genetic algorithm with 100 dockings at maximum number of 25,000,000 energy evaluation.
- Analysis: select ligands conformation based on binding energy (G), inhibitory constant (K_i), and number of ligand conformation in cluster (frequency) for performing MD of each complex system.

3.3.9. Molecular Dynamics Simulation (MD)

(i) 5-LO system

- Input: complex system between 5-LO and each ligand (AA, ZIL, CD, DMP) from 3.3.8.
- Program: AMBER12 program package with gaff, ff12SB, and TIP3P water box force fields.
- Simulation:
 1. Minimization
 2. Heating: from 0-300 K for 20 ps with constant volume and Langevin thermostat.
 3. Production MD: equilibrate system for 20ns with NPT ensemble.
- Analysis:
 1. Investigate energy and other thermodynamic property of complex system.
 2. Investigate C $_{\alpha}$ -carbon RMSD and take stable interval for calculating free binding energy between 5-LO and ligand incorporated with energy decomposition with MM/GBSA method

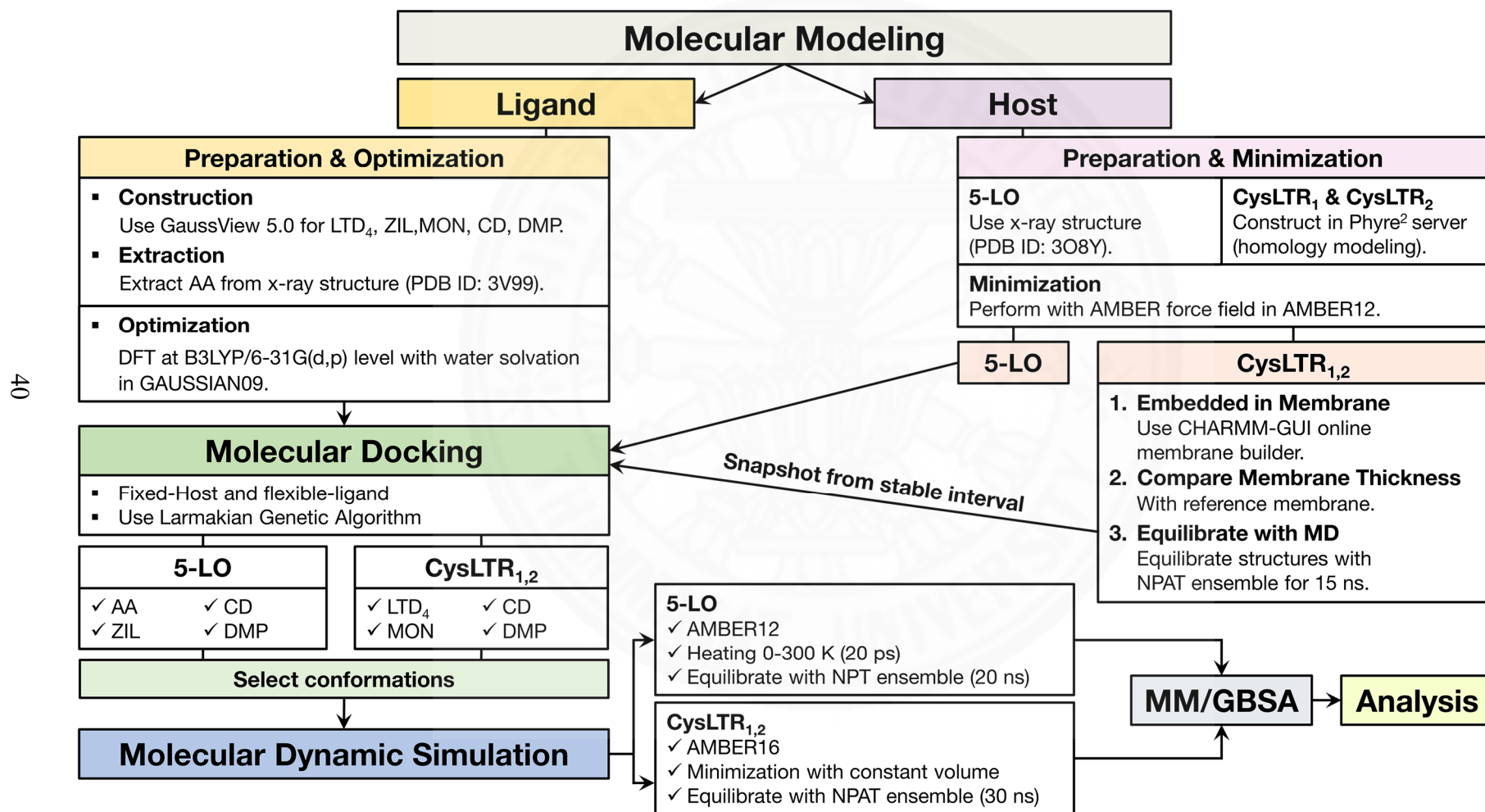
(ii) CysLTRs system

- Input: complex system between CysLTRs and each ligand (LTD₄, MON, CD) from 3.3.8.
- Program: AMBER16 program package with lipid14, gaff, ff14SB, and TIP3P water box force fields.
- Simulation:
 1. Minimization: constant volume, no pressure scaling.
 2. Production MD: equilibrate system for 30 ns with NPAT ensemble.
- Analysis:
 1. Investigate energy and other thermodynamics property of complex system.
 2. Investigate C $_{\alpha}$ -carbon RMSD and take stable interval for calculating free binding energy between CysLTRs and ligand incorporated with energy decomposition with MM/GBSA method

3.3.10. Calculate Binding Free Energy and Energy Decomposition with MM/GBSA

- Input: selected frames from stable RMSD interval from 3.3.9.
- Program: MM/GBSA.py within AMBER12 (for 5-LO) and AMBER16 (for CysLTRs)
- Setting:
 1. Calculate binding free energy incorporated with entropy approximation.
 2. Select amino acid residues around each ligand in range within 6 Å to calculate pairwise energy decomposition with addition of 1-4 non-bonded interaction energies (1-4 EEL and 1-4 VDW).
- Analysis:
 1. Investigate calculates binding free energy.
 2. Investigate energy decomposition between selected amino acid residues of protein and each ligand.

3.4. Flow Chart of Research Procedure



Chapter 4

Computational Results

4.1. 5-LO Systems

Ligands in this system compose of AA, ZIL, CD, and DMP, which have been constructed following the reported 2-D chemical structures and extracted from x-ray structure (PDB ID: 3V99 for AA only) then performed structural optimization in GAUSSIAN09 program package, as shown in Figure 4.1.

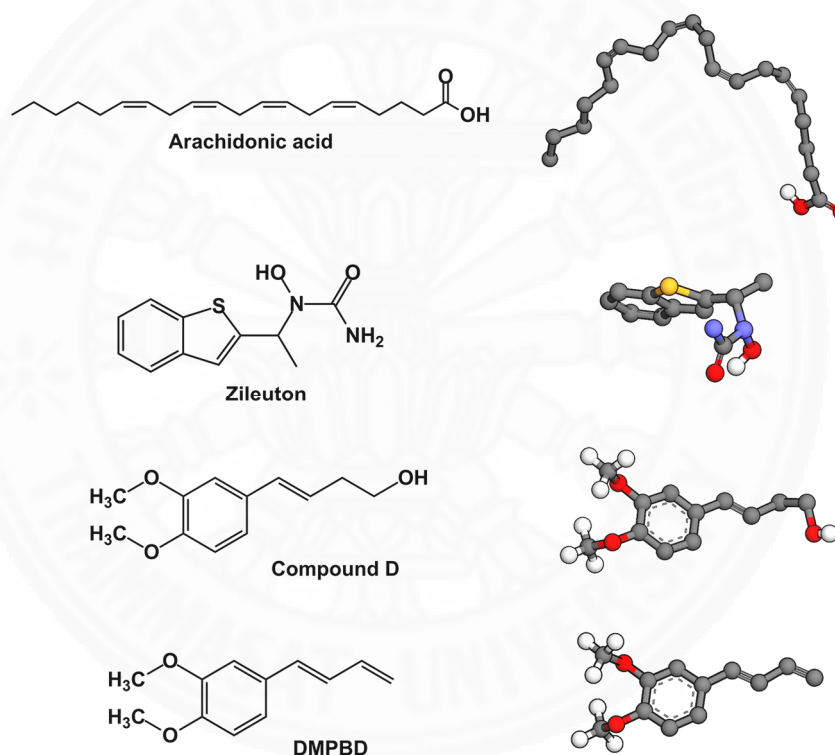


Figure 4.1: 2-D structures and optimized structures of ligands in 5-LO systems.

Afterwards, 5-LO which is protein target of this system has been prepared from 2 available x-ray structures in RCSB protein data bank (PDB ID: 3O8Y and 3V99). Consequently, the difference between these two x-ray structures have been observed by structural superimposition in Discovery Studio Visualizer as shown in Figure 4.2 incorporated with amino acid sequences comparison as described in Appendix A (A-4) with definition of single letter abbreviation of essential amino acid specified in Appendix A (A-5).

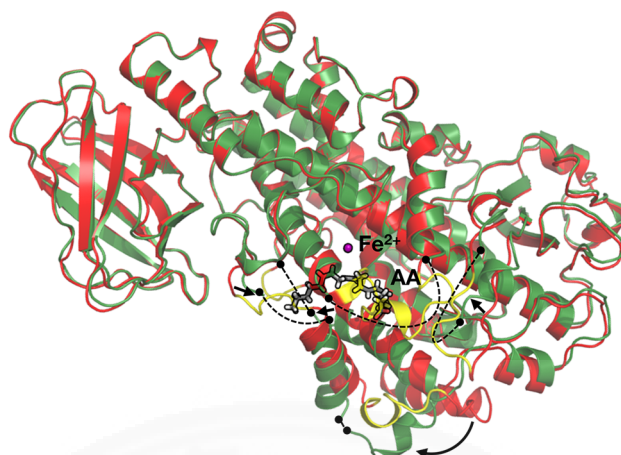


Figure 4.2: Superimposition of two 5-LO x-ray structures. Substrate-bound structure (PDB ID: 3V99) presented as green ribbon with AA as stick model. Substrate-free structure (PDB ID: 3O8Y) presented as red ribbon. Fe^{2+} ions in both structure presented as purple sphere. The missing amino acid residues are highlighted in yellow.

The protein chain of 5-LO around AA of these two x-ray structures are distinctly deviate from each other at catalytic domain as shown in Figure 4.2. Moreover, some section of protein chain from substrate-bound 5-LO structure (PDB ID: 3V99) are missing. Hence, from this observation, when AA binding with 5-LO the cavity of binding pocket has change and this assumption will be used with other ligands in this research also. However, in order to show the deviation between this 2 x-ray structures, alpha-carbon root mean square deviation (C_{α} -RMSD) of 5-LO have been calculated as explained in Table 4.1.

Table 4.1: RMSD of 5-LO x-ray structures (PDB ID: 3O8Y and 3V99).

Component	Residues	RMSD (Å)
Overall structure	1-673	2.22
β -sandwich domain	1-114	0.66
Catalytic domain	121-673	2.43
Fe^{2+} ion		0.10

From Table 4.1, C_{α} -RMSD of all amino acids residues is 2.22 Å, nevertheless, when investigate on two separated domains (catalytic and β -sandwich) the deviation of

catalytic domain was higher than β -sandwich domain. Consequently, the most deviation of two 5-LO x-ray structures could come from deviation of catalytic domain which reported to be AA binding pocket. Thus, this can be used to support assumption on differentiation of binding pocket when 5-LO bound with ligands. Moreover, the position of Fe^{2+} ion within catalytic of these two x-ray structures are similar. Therefore, the position of Fe^{2+} might not affect the binding characteristic between 5-LO and AA or other ligands. Thus, substrate-free 5-LO structure (PDB ID: 3O8Y) is used as host in all 5-LO complex simulations due to completeness of protein chain. Then, prepared 5-LO structure has been performed structural minimization with AMBER12 program package before starting the molecular docking calculation of each complex systems.

4.1.1. Molecular Docking Calculation Results

Molecular docking have been used to calculate the binding energy and possibility of binding between each protein-ligand complex by fixed protein structure and let ligand flexible in specified grid box ($80 \times 80 \times 80 \text{ \AA}$) which center has been set following center of geometry of AA in substrate-bound 5-LO structure (PDB ID: 3V99). The criteria for selection of ligand conformations in each complex system depended on 2 variables which are binding energy (B.E.) and number of conformations in cluster (frequency). Thus, if frequency is equal or greater than 50 that cluster will be selected, but, if there is no frequency in any cluster equal or greater than 50, the cluster with lower binding energy will be selected. The selected cluster have been listed in Table 4.2 and complete calculation results have been combined in Appendix C (C-1).

Table 4.2: Summary of molecular docking calculation of 5-LO systems.

Ligand	Cluster	Lowest B.E. (kcal/mol)	Mean B.E. (kcal/mol)	Frequency	K_i (μM)	$K_{i,avg}$ (μM)
AA	1	-7.49	-6.68 ± 0.40	26	3.21	12.63 ± 11.18
ZIL	2	-7.28	-7.22 ± 0.05	51	4.57	5.09 ± 0.43
CD	1	-5.93	-5.73 ± 0.12	32	44.71	62.54 ± 12.82
DMP	2	-5.74	-5.70 ± 0.06	50	61.62	65.97 ± 8.26

The model validation have been considered based on the position of AA by superimposition with x-ray structure (PDB ID: 3V99). As the result, hydroxyl group of AA structure from x-ray and docking are close to each other. However, the movement of long chain hydrocarbon can be observed within the same binding site close to Fe^{2+} ion as presented in Figure 4.3. Thus, all ligands are possible to bind on 5-LO in the specified region, not far from Fe^{2+} ion, as shown in Figure 4.4. The detail interaction of each ligand with amino acid residues in their binding pockets are presented in Figure 4.5 and Figure 4.6. AA and ZIL are located in the same binding site leading by two strong hydrogen bonds which occur between the hydroxyl group of AA and ZIL with the carbonyl group of Leu420 and the amino group of Ala424 (Figure 4.6). Moreover, the aliphatic and aromatic hydrocarbon atoms of AA and ZIL occur the interaction with the hydrophobic amino acid residues on 5-LO which help to stabilize these protein-ligand complexes indicated by low B.E. (Table 2). Even though, CD and DMP have the similar chemical structure, but their binding mode on 5-LO are quite difference. The oxygen ether atom of DMP forms a hydrogen bond with the amino group of Ala424 and its hydrocarbon atoms occur the Van der Waals interaction with hydrophobic amino acid residues which very similar to the binding mode of AA and ZIL on 5-LO. Unlike CD that have no similar interaction with other ligands. Nevertheless, it still bound within the same binding site. But it made interaction with difference amino acid residues. The hydroxyl of CD occurs the hydrogen bond network with the carbonyl oxygen atom of Asn554 and the hydrogen atom of amino group of Gln557 (Figure 4.6). This network is also found in other four clusters of CD docking calculations as well. However, due to the rigidity of protein target and vacuum environment in docking calculations which are not mimic reality of enzyme behavior. Thus, we have to further investigated the system by using MD simulation to study the dynamics motion of 5-LO with different four ligands and possible interacting amino acid residues which could be change after perform MD simulations because of flexibility of all atoms in complex systems that have been solvated in water environment.

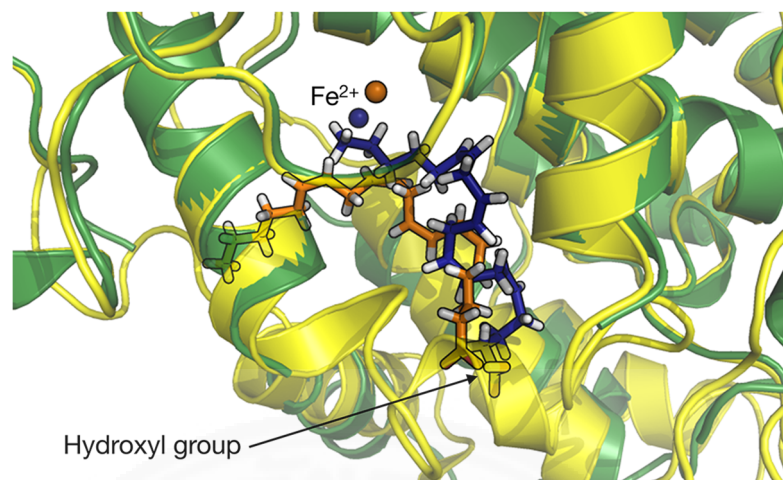


Figure 4.3: Superimposition of 5-LO substrate complex from docking and x-ray. 5-LO structure from x-ray and docking shown as green and yellow ribbon, respectively. AA from x-ray and docking shown as orange and blue stick model, respectively. Fe^{2+} ion shown as non-bonded sphere with the same color as AA in each complex structure.

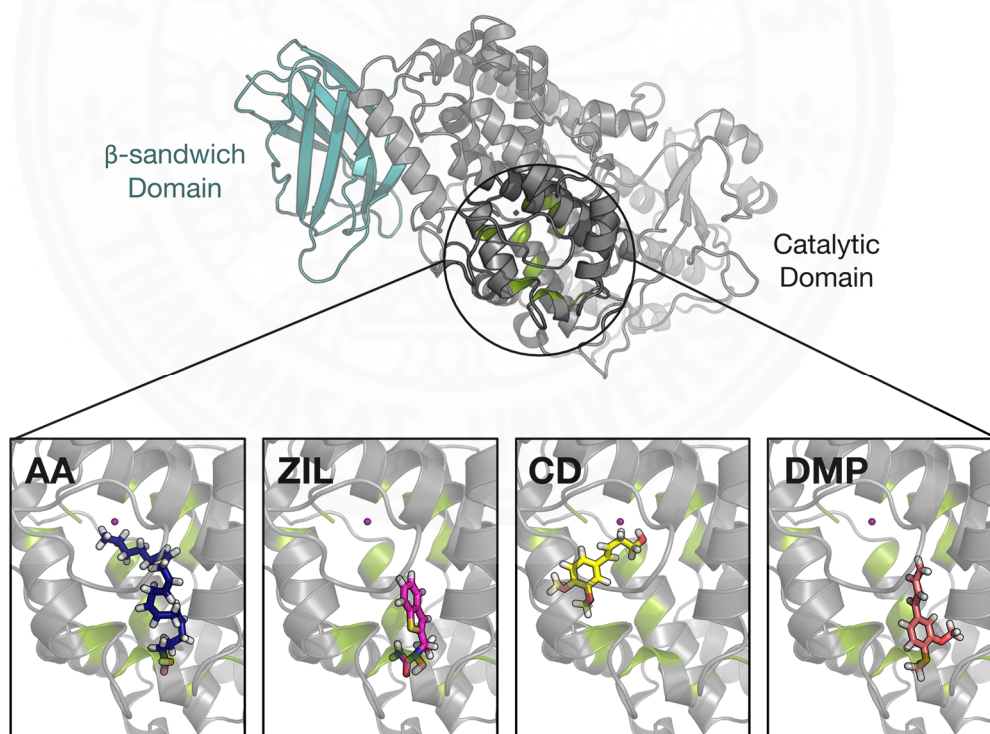


Figure 4.4: 5-LO binding site and conformation of each ligand from dockings. 5-LO represented by grey ribbon structure. All ligands represented by stick model and Fe^{2+} ion presented as non-bonded sphere. The green highlighted amino acid residues represented the interacting residues (binding pocket).

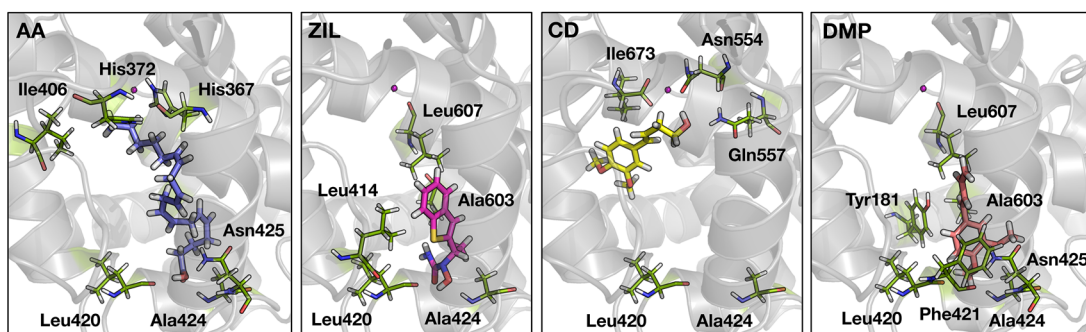


Figure 4.5: Interacting amino acid residues for each 5-LO complexes from dockings. 5-LO structure presented as grey ribbon model. The interacting amino acid residues shown as green stick model. AA, ZIL, CD and DMP shown as blue, magenta, yellow, and pink stick model, respectively. Fe^{2+} ion shown as purple non-bonded sphere.

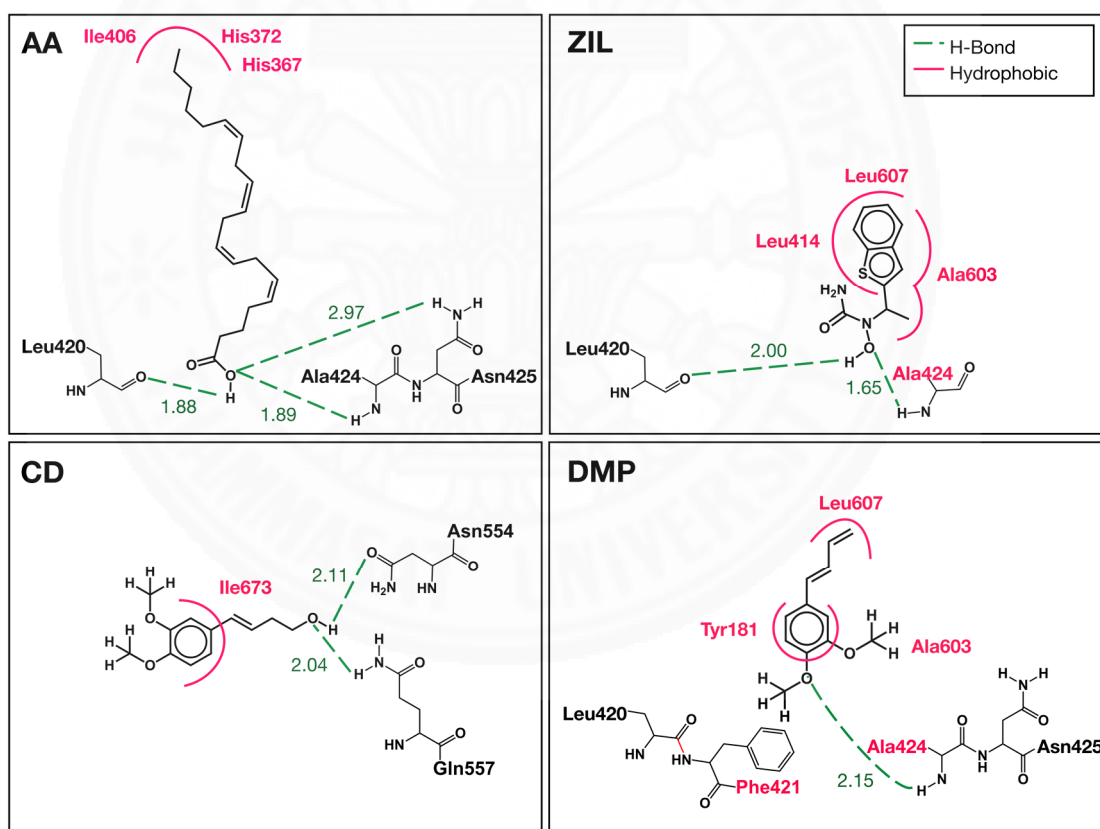


Figure 4.6: 2-D illustrations of 5-LO complexes interactions from docking. The presented chemical interactions were within 5 Å distance around ligands. Hydrogen bonds shown as green dash lines. Hydrophobic interactions (Van der Waals) shown as pink curve lines and pink amino acid labels represented the amino acid residues that formed hydrophobic interactions with ligands. All distance labels presented in Å unit.

4.1.2. Molecular Dynamic Simulation Results

The selected conformations of ligands from molecular docking have been prepared with 5-LO structure that have been cut β -sandwich domain out in order to reduce calculation time. Then, solvated 5-LO complex into truncated octahedral water box which will be heated and equilibrated with isothermal-isobaric ensemble (NPT) for 20 ns. First, energies of complex systems have been calculate in order to observe behavior of systems (Figure 4.7). Energies of each complex system are steady throughout whole simulation (approximately -2 kcal/mol in total energy). Therefore, in order to emphasize systems equilibrium, total energies have been average every 5 ps interval and plot along with original total system energy (Figure 4.8). As the result, average total energy present stability in every complex systems after approximately 2 ns of MD simulation. The rapid increase of energy at the beginning of simulation was occurred due to the heating step (20 ps) and the decline after that was an adjustment to reach equilibrium. Hence, the interval between 2 ns to 20 ns can be used to clearly represent complex systems equilibrium.

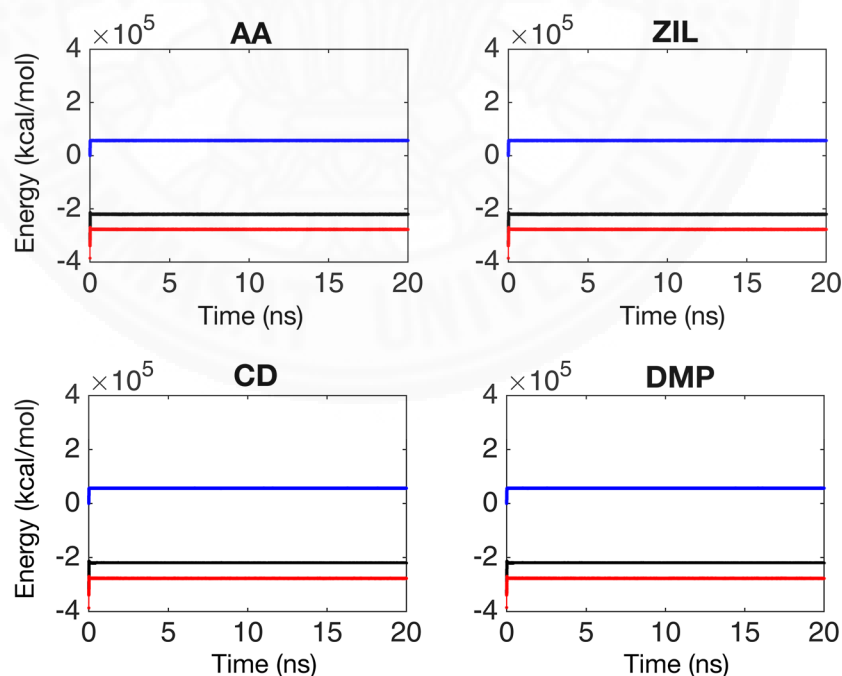


Figure 4.7: 5-LO complex systems energy. Kinetic energy of each complex system shown as blue line. Potential energy of each complex system shown as red line. Total energy of each complex system shown as black line.

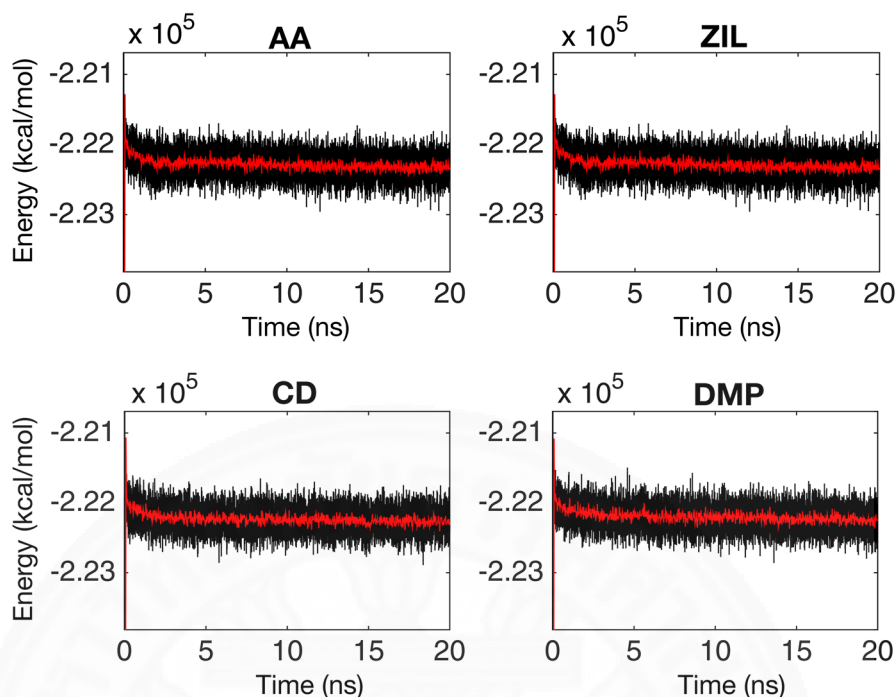


Figure 4.8: 5-LO systems total and average energy. The total system energy throughout MD of each 5-LO complex system represented by black line. The average total energy (every 5 ps interval) represented by red line. All sub-plots have been magnified in vertical axis for 50 percent in order to emphasize the change in total energy.

In order to observe the stability of 5-LO structure in each complex system, the C_{α} -RMSD of 5-LO was observed with reference frame (last frame of heating step) as shown in Figure 4.9. Last frame of heating step has been selected as reference frame in order to avoid the bias for RMSD comparison due to temperature difference. As the result, the C_{α} -RMSD of 5-LO complexes with AA was stable after 2 ns with small fluctuation between 1.2 to 1.4 Å. For 5-LO complexes with ZIL, 5-LO structure has high fluctuation (sharp peak) at simulation time around 5 ns. Afterwards, the fluctuation reduced and started to form stable pattern (fluctuate between 1.1 to 1.3 Å). For 5-LO complexes with CD, the fluctuation of protein structure was higher than other systems. However, the fluctuation from 12 ns until 20 ns approximately varied from 1.5 to 2.2 Å in the repeated behavior and no sharp peak during this interval. For 5-LO complexes with DMP, high fluctuation has occurred for two different simulation time which are 4 ns and 11 ns. Then, enzyme structure's fluctuation reduced and presented stable behavior (fluctuate between 1.2 to 1.4 Å).

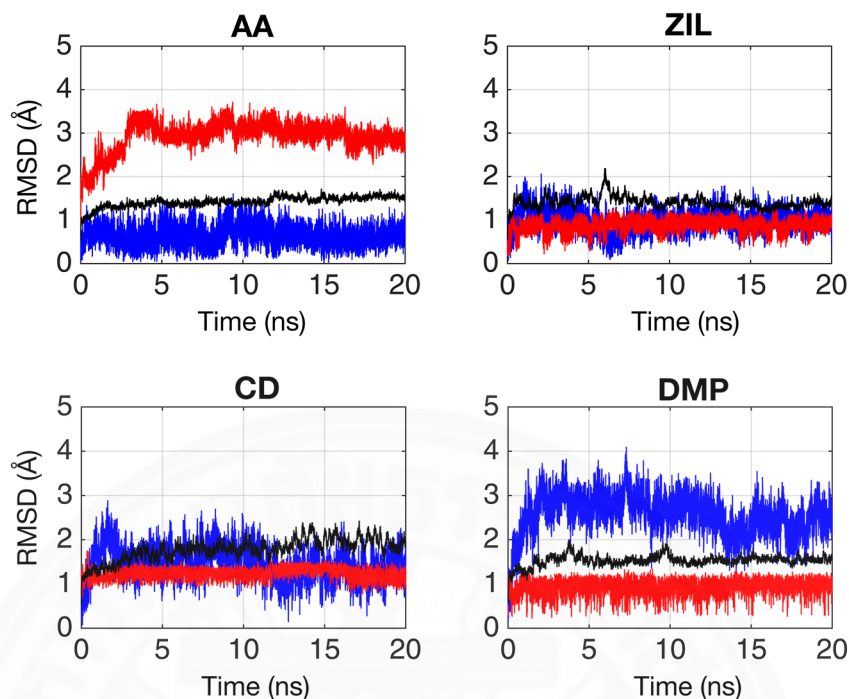


Figure 4.9: RMSD plot of 5-LO complex systems. Alpha-carbon RMSD of 5-LO shown as black line. All atoms RMSD of ligands shown as red line. Single atom distance of Fe^{2+} ion shown as blue line.

Nonetheless, the stability of enzyme structure in each system has been investigated as discussed above. But, each complex system included other components which are ligand and metal ion (Fe^{2+}). Consequently, the all atoms RMSD of both components have been observed in order to understand behavior of whole systems. As the result, RMSD of AA was highly fluctuate due to long chain of hydrocarbon in its structure. However, the fluctuation decreased after 3 ns and repeated around 2.5 to 3.5 Å. For ZIL, the fluctuation of RMSD was repeated in pattern around 0.2 to 1 Å. For CD, the fluctuation was repeated from 0 to 20 ns approximately 0.8 to 1.2 Å. For DMP, the RMSD fluctuate in pattern between 0.2 to 1 Å. For Fe^{2+} ion, single atom RMSD is the comparison of ion's distance between reference frame and each frame during whole simulation by superimposition of the enzyme structures together. As the result, high fluctuation of ion's RMSD in each system have occurred. However, there are noticeable drop down peak at difference time as specified in Figure 4.9 and then it started to present repeated behavior. Therefore, the high fluctuation of Fe^{2+} ion might not effect in the stability of ligand-protein complex system. Thus, all complex systems have been

considered as stable enough to perform further analysis. For this reason, the last 5 ns interval of each system will be selected to perform free binding energy calculation with MM/GBSA method.

4.1.2.1. Free Binding Energy Calculation (MM/GBSA)

For 5-LO systems, 5000 frames (1 frame equals to 1 ps) in specified interval (15-20 ns) have been averaged and calculated binding energy between enzyme and each ligand as shown in Table 4.3.

Table 4.3: Free binding energy calculated from MM/GBSA for 5-LO systems.

Ligand	MM/GBSA Results (kcal/mol)		
	G_{Total}^a	Entropy (T S)	$G_{Binding}^b$
AA	-48.21 \pm 2.78	-61.17	12.96
ZIL	-29.40 \pm 2.78	-31.28	1.88
CD	-26.83 \pm 2.58	-27.57	0.74
DMP	-29.15 \pm 1.87	-36.07	6.92

^a $G_{Total} = G_{complex} - G_{protein} - G_{ligand}$

^b $G_{Binding} = G_{Total} - T S$

If considered only total energy difference between bound and unbound state of 5-LO (G_{Total}) which neglect the entropy approximation (T S), 5-LO complexes with AA has highest binding affinity (low energy) which reasonable because it is 5-LO natural substrate followed by ZIL, DMP, and CD, respectively. The detail of energy approximation are explained in Appendix C (C-2). However, binding energy should include the entropy contribution for more accuracy. According to second law of thermodynamics, the entropy of system tends to be maximum which leads to disorder of system. On the contrary, for 5-LO systems, the entropy difference are negative which mean that all systems tend to be ordered when enzyme and ligand are bound. Nevertheless, normally this law will be used to describe whole isolated system (such as cell) not individual part of system like this 5-LO complexes. For this reason, due to 5-LO is enzymatic protein, the very stable protein-ligand complex should occur at first

and then after carried out particular chemical interaction converted ligand tends to be released out in order to generate further biological response which could lead to disorder of whole cell. Thus, negative entropy difference of 5-LO complex systems were quite reasonable because the performed MD simulations represent behavior of protein-ligand complex only, not the enzymatic reaction of 5-LO. Interestingly, binding energies (G_{Binding}) of all 5-LO complex systems turned out to be positive value which is not expected. This occurred due to magnitude of entropy difference is larger than total energy difference in all complex systems. However, the entropy approximation by normal mode analysis that included in MM/GBSA calculation can produce very large error. Moreover, it is a time consuming step which cannot be used to accurately produce entropy difference within short interval as I have selected. In addition, sometimes when comparing the binding affinity of different ligands with same protein target, entropy difference can be neglected because they tends to be similar in those protein-ligand complex system. Therefore, the comparison of binding affinity between 5-LO and each ligand have been considered from average energy difference (G_{Total}) instead.

The pairwise energy decomposition between each ligand and amino acid residues 5 Å around them are calculated in order to investigate major amino acid residues that interact with each ligand. The interacting amino acid residues are considered following criteria that amino acid residue residues with energy lower than -0.2 kcal/mol for one system out of four systems will be selected as shown in Figure 4.10. Moreover, the total energy decomposition has been further analyze in context of backbone and sidechain effect as shown in Figure 4.11. Energy decomposition of 5-LO complex with AA, ZIL and DMP show quite similar pattern in arched helix (Ile406, Leu414, Leu420, and Phe421) and specific amino acid residues in another alpha helix (Trp599, His600, Ala603, Val604, Ala606 and Leu607) which indicate edges of active site. However, 5-LO complex with CD show different pattern of energy decomposition, which mainly came from the interaction with C-terminus (Ile673) and helix α_2 (Phe177, Asn180, and Tyr181) which define another edge of active site [84]. According to average energy difference (G_{Total}), AA gave much lower binding energy than other ligand because it occur van der Waals interaction with many amino acid residues.

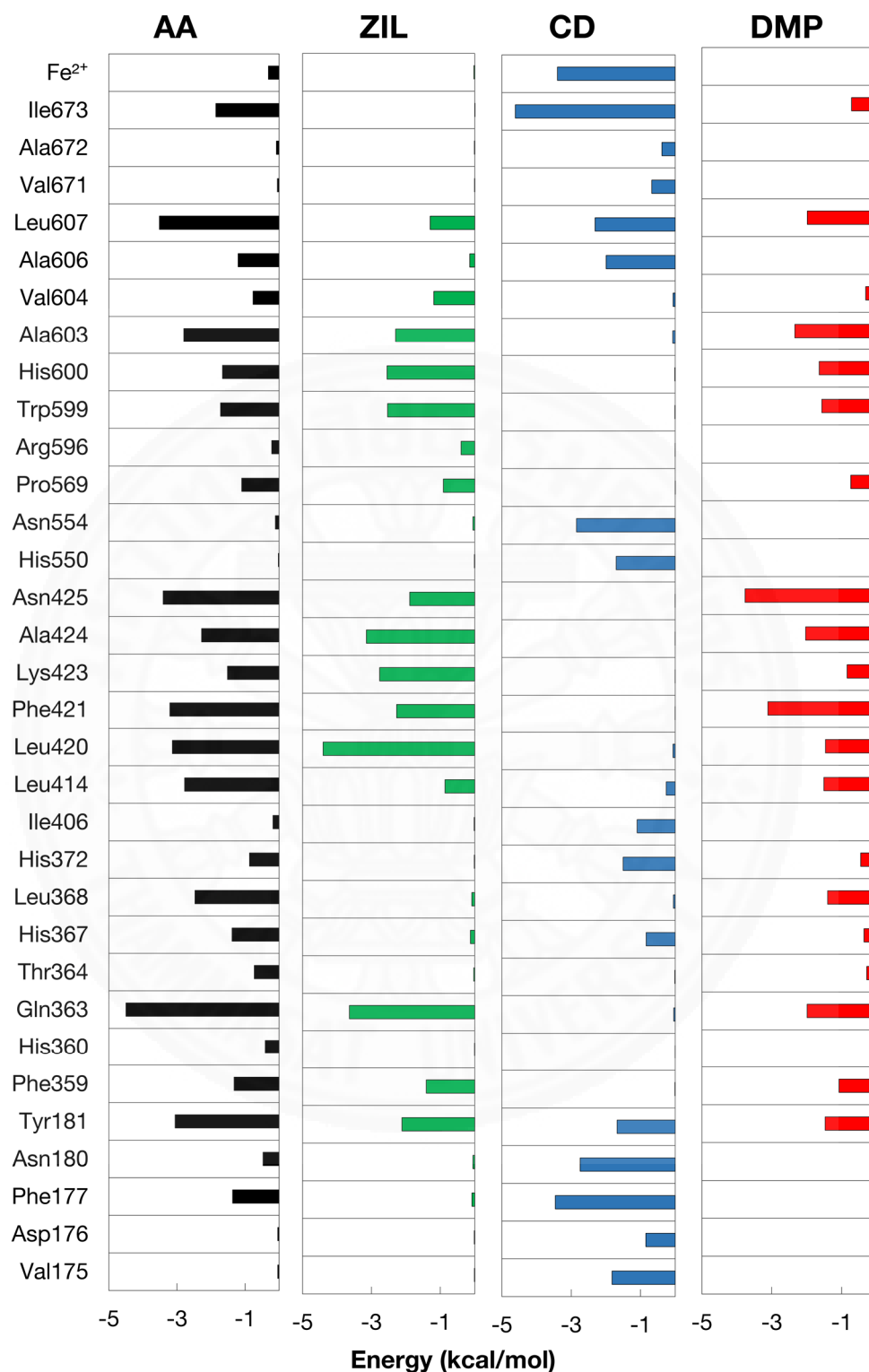


Figure 4.10: Total energy decomposition from selected interval of MD (15-20 ns).



Figure 4.11: Sidechain and backbone energy decomposition. The backbone and sidechain energy decomposition shown as orange and purple bar plot, respectively. The combination of backbone and sidechain energy equals to total energy decomposition.

Model validation have been performed again by considering AA position from the selected snapshot, at 19 ns of MD simulations, compared to the x-ray structure (PDB ID: 3V99) as shown in Figure 4.12. The C_{α} -RMSD between them is 2.98 Å. The hydroxyl group of AA from both structures are closed to each other but further movement of long chain hydrocarbon can be noticed. Moreover, the positions of Fe^{2+} ion in the MD simulations and in the x-ray structure are not far from each other. These results indicated that MD simulations are able to mimic the behavior of 5-LO enzyme when binding with AA substrate molecule and should able to provide the reliable prediction models of 5-LO in complexed with another ligands.

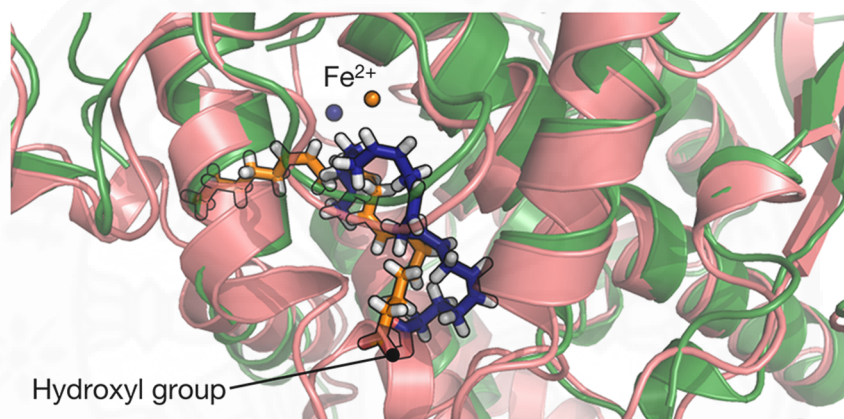


Figure 4.12: Superimposition of 5-LO substrate complex from MD snapshot and x-ray. 5-LO structure from x-ray and MD snapshot shown as green and pink ribbon. AA from x-ray and MD snapshot shown as orange and blue stick model. Fe^{2+} ion shown as non-bonded sphere with the same color as AA in each complex structure.

The specific frame of each ligand-protein complex systems at 19 ns of MD simulations were selected to investigate molecular interaction and dynamics properties. Superimpositions between systems have been performed in order to observe the difference between each of 5-LO complex systems as shown in Figure 4.13. Then, measure C_{α} -RMSD between extracted frames and x-ray structures as listed in Table 4.4.

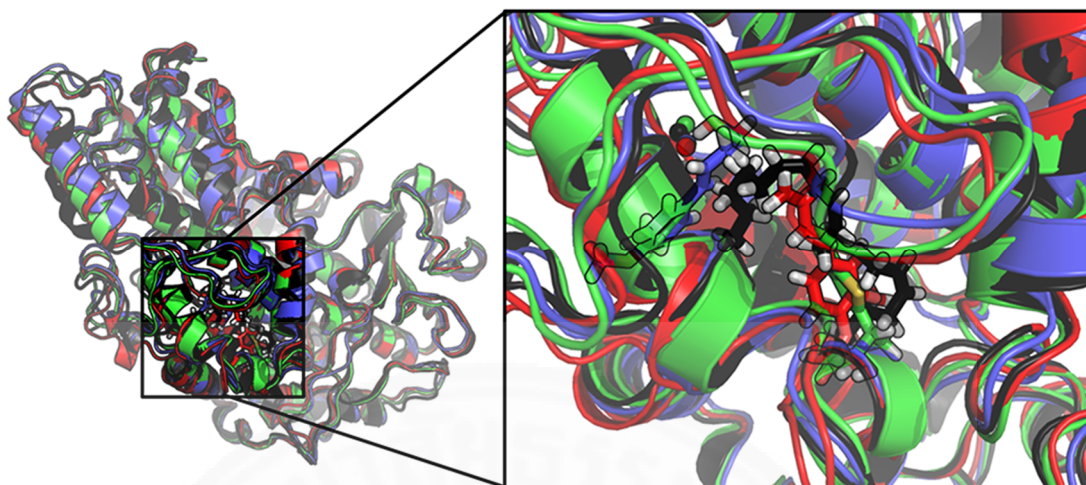


Figure 4.13: Superimposition of 5-LO structures from 19 ns snapshot. For 5-LO complexes with AA, ZIL, CD and DMP, enzyme structure shown as black, green, blue and red ribbon structure, respectively. All ligands are presented as stick model and Fe^{2+} ion shown as non-bonded sphere with color following enzyme structure.

Table 4.4: Alpha-carbon RMSD of selected frame at 19 ns of MD simulations.

C_α - RMSD (Å)	AA	ZIL	CD	DMP
AA	0.00	1.74	1.79	1.79
ZIL	1.74	0.00	1.35	1.52
CD	1.79	1.35	0.00	1.66
DMP	1.79	1.52	1.66	0.00

All 5-LO C_α -RMSD have been measured after cut out the catalytic domain (residue 1-114). Therefore, the deviation specified the change in catalytic domain only. The overall structures of 5-LO in complexed with each of ligands from our MD simulations are very similar, with RMSD 1.66 Å -1.79 Å, which indicated that the 5-LO enzyme has the same dynamics motion even though it was binding with different four ligands. This also support our assumption that CD and DMP are the competitive substrate inhibitors, same as the ZIL commercial drug.

Solvent accessibility surface area (SASA) has been used to investigate the change of internal surface area of specified binding pocket that have been selected based on energy decomposition as illustrated in Figure 4.14.

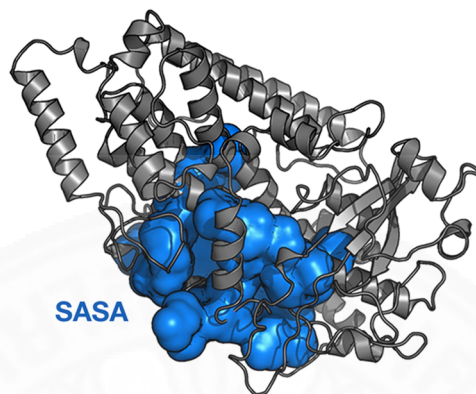


Figure 4.14: Solvent accessible surface area (SASA). SASA of interacting amino acid residues shown as blue surface embedded in ribbon structure of 5-LO.

SASA were calculated by movement of circular molecule (probe) inside specified amino acid residues that formed binding pocket which present as internal surface area. Probe that I have used was water molecule with radius equals to 1.4 Å. Average SASA were calculated from 5 frames (each frame equals to 1 ns) in specified interval (15-20 ns) in order to emphasize the difference of specified 5-LO binding pocket in each system as shown in Figure 4.15. As the result, binding pocket of simulated 5-LO complex systems were larger than x-ray structure (PDB ID: 3O8Y) due to the presence of ligands inside those pockets. However, binding pocket of 5-LO complexes with AA and CD were larger than ZIL and DMP. Thus, CD presented the similarity of binding characteristic with AA even though it has small molecular size, but, it can expand binding pocket like AA. Conversely, smaller cavity of 5-LO binding pocket when complexes with ZIL and DMP could prevent binding of 5-LO and AA.

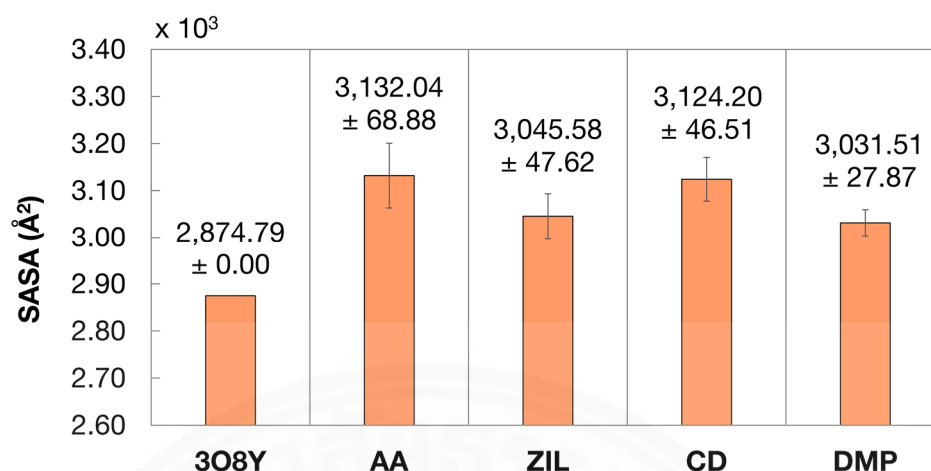


Figure 4.15: Average solvent accessible surface area of 5-LO. The grey error bar represented 1 interval standard deviation.

The ligand-protein complexed conformations at 19 ns of each MD simulations systems are used to present the ligand's alignment and the molecular interactions with amino acid residues inside the binding pocket on 5-LO, as shown in Figure 4.16. The detail interaction of each ligand with amino acid residues in their binding pockets are presented in Figure 4.17. AA and ZIL are located in the same binding site leading by two hydrogen bonds between hydroxyl group of AA and ZIL with carbonyl group of Leu420 and amino group of Ala424. Moreover, the aliphatic and aromatic hydrocarbon atoms of AA and ZIL occur the interaction with the hydrophobic amino acid residues on 5-LO which help to stabilize these protein-ligand complexes indicated by their low average energy difference (G_{Total}) in Table 4.3. Even though, CD and DMP have the similar chemical structure, but their binding mode on 5-LO are difference. The oxygen ether atom of DMP forms a hydrogen bond with the amino group of Asn425 and its hydrocarbon atoms occur the van der Waals interaction with hydrophobic amino acid residues which very similar to the binding mode of AA and ZIL on 5-LO. Unlike CD that have no similar interaction with other ligands. Nevertheless, it still bound within the same binding site but it made interaction with difference amino acid residues. The hydroxyl group of CD occurs three hydrogen bonds with imidazole ring of His550, amino group of Asn554 and carbonyl group of Ile673. Moreover, it forms Pi-Pi interaction between its aromatic ring and the phenyl ring of Phe177.

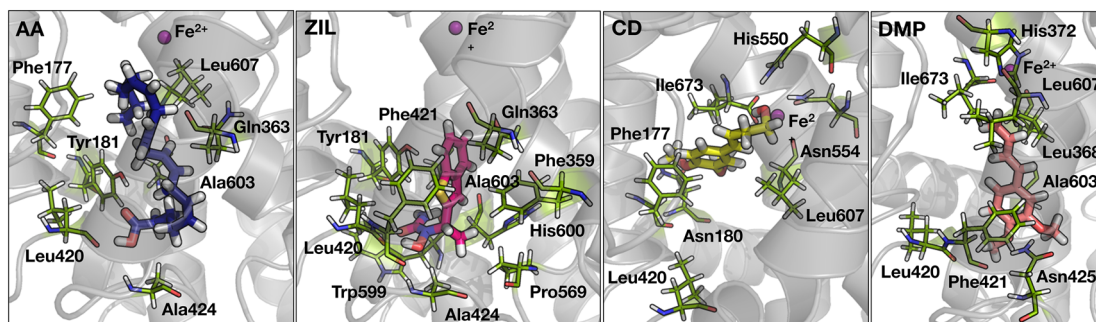


Figure 4.16: 5-LO binding site and ligands conformations from 19 ns snapshot of MD. 5-LO structure shown as grey ribbon. The binding pocket amino acid residues shown as green stick model. AA, ZIL, CD and DMP shown as blue, magenta, yellow, and pink stick model, respectively. Fe^{2+} ion shown as purple non-bonded sphere.

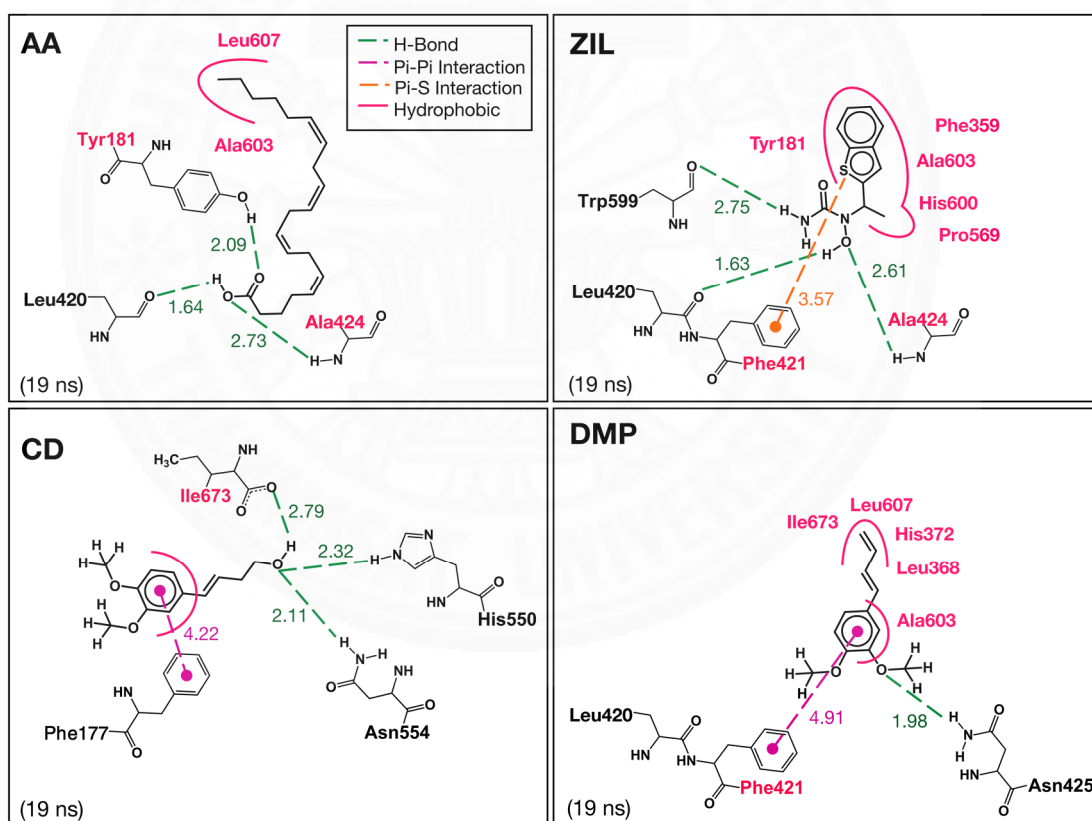


Figure 4.17: 2-D chemical interaction of selected frame from MD. Hydrogen bonds shown as green dash lines. Hydrophobic interactions (Van der Waals) shown as pink curve lines and pink amino acid labels represented the amino acid residues that formed hydrophobic interactions with ligands. Pi-Pi and Pi-Sulfur interaction shown as purple and orange dash line, respectively. All distance labels presented in Å unit.

4.2. CysLTRs Systems

Ligands in this system compose of LTD₄, ZIL, CD and DMP which have been constructed following the reported 2-D chemical structures. Then, performed structural optimization in GAUSSIAN09 program package, as shown in Figure 4.18

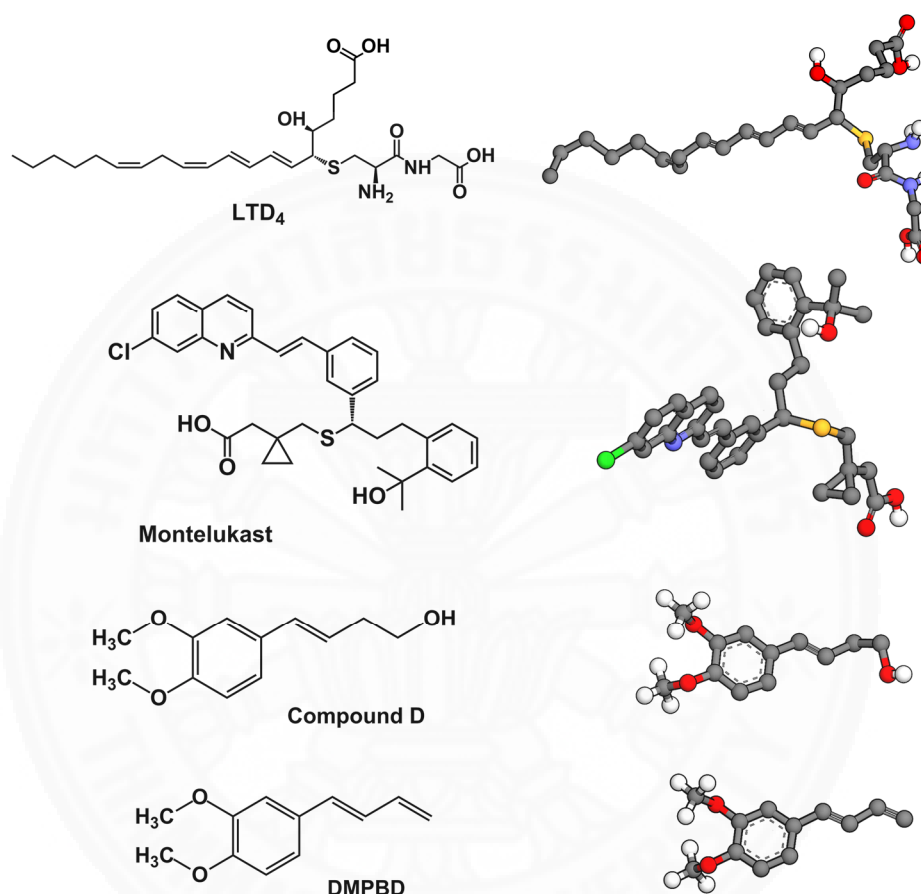


Figure 4.18: 2-D structures and optimized structures of ligands in CysLTRs systems.

Due to CysLTRs have no reported x-ray structures, thus, 3-D structures of these receptors have to be generated by homology modeling with Phyre² server which available online. The amino acid sequence data of CysLTRs are compiled in Appendix A (A-1 and A-2). Phyre² modelled both receptors from template of G-protein couple receptors in rhodopsin-like family. In addition, I have set the alias for each alpha-helix transmembrane of both receptors in order to simplify the receptors component for better understanding as illustrated in Figure 4.19 and Figure 4.20. However, reliability of generated CysLTRs structures have to be checked by construction of 5-LO structure in

Phyre² server. As the result, 5-LO structure was modelled from x-ray template (PDB ID: 3O8Y). Therefore, the generated CysLTRs structures are reliable enough for this time period with the current available templates.

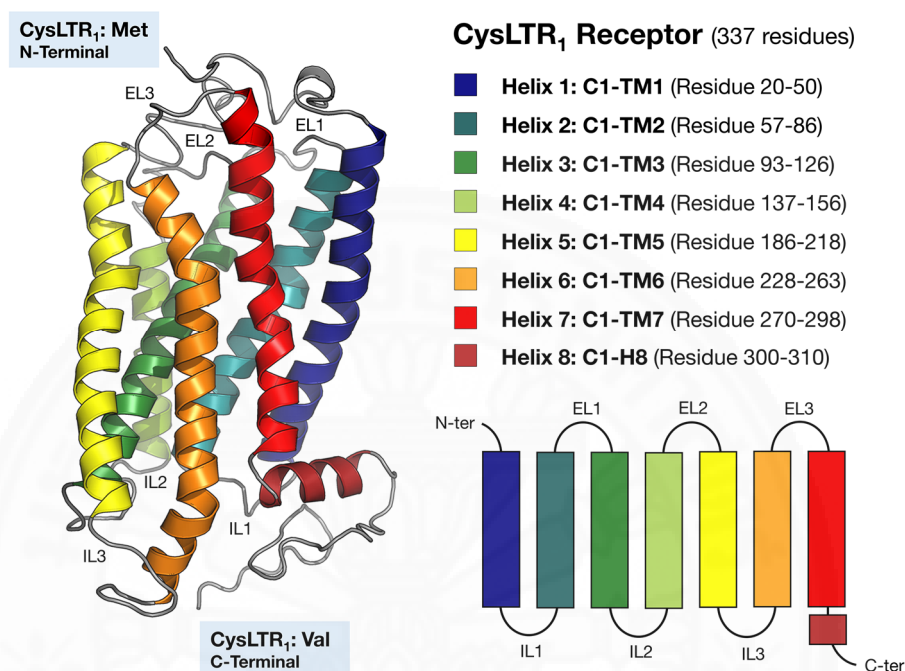


Figure 4.19: Generated 3-D structure of CysLTR₁ and its component.

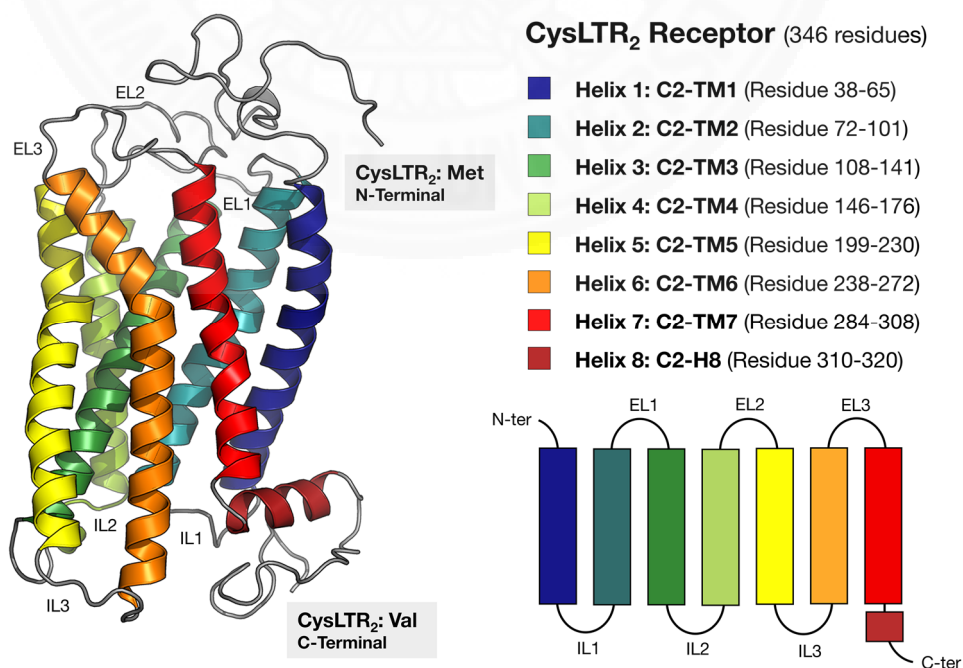


Figure 4.20: Generated 3-D structure of CysLTR₂ and its component.

4.2.1. Study of Pure CysLTRs

Both 3-D structures of CysLTRs have been performed structural minimization in AMBER force field. Afterwards, they are embedded into phospholipid bilayer membrane via CHARM-GUI online membrane builder. The membrane component and properties that I have used are followed the reported data for rhodopsin receptor. Because CysLTRs have been reported to be sub-type of G-protein couple receptor in rhodopsin family. The illustration of embedded CysLTRs are shown in Figure 4.21.

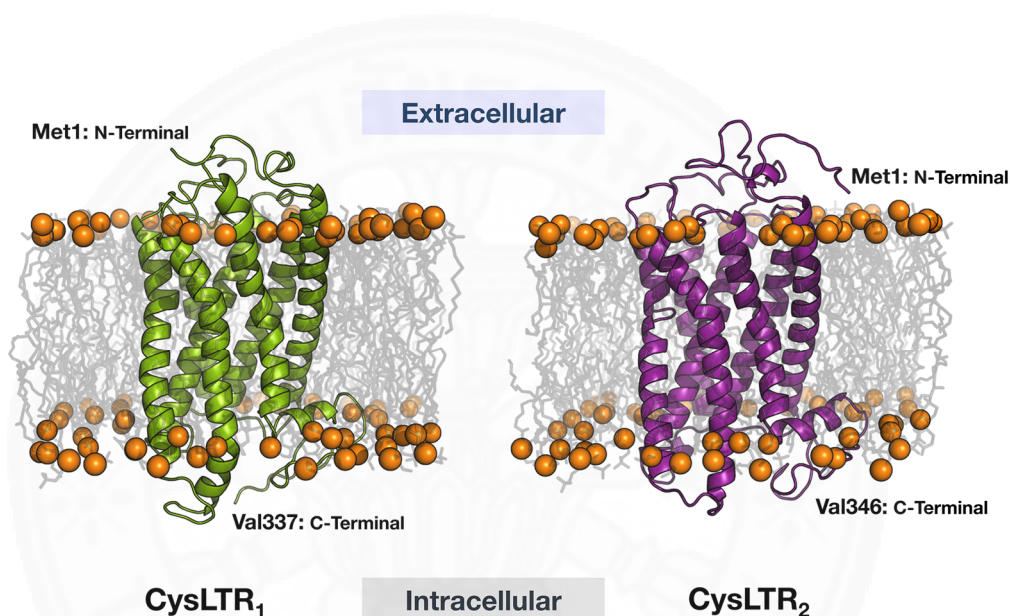


Figure 4.21: CysLTRs embed in phospholipid bilayer membrane. CysLTR₁ and CysLTR₂ shown as green and purple ribbon, respectively. The phosphate head and tail of phospholipids shown as orange sphere and grey stick model, respectively.

The approximate thickness of phospholipid bilayer membrane have been reported in reference [86] as specified in Figure 4.22. Consequently, I have measured the constructed membranes thickness by division of membrane cross-sectional area into 20 x 20 grid boxes first and then measure the thickness of each box as shown in Figure 4.23. In addition, the average membrane thickness of both CysLTRs systems have been calculated for better comparison (Figure 4.23). As the result, comparison showed that thickness of constructed membranes are quite similar to the reference with small deviation around 0.8 nm.

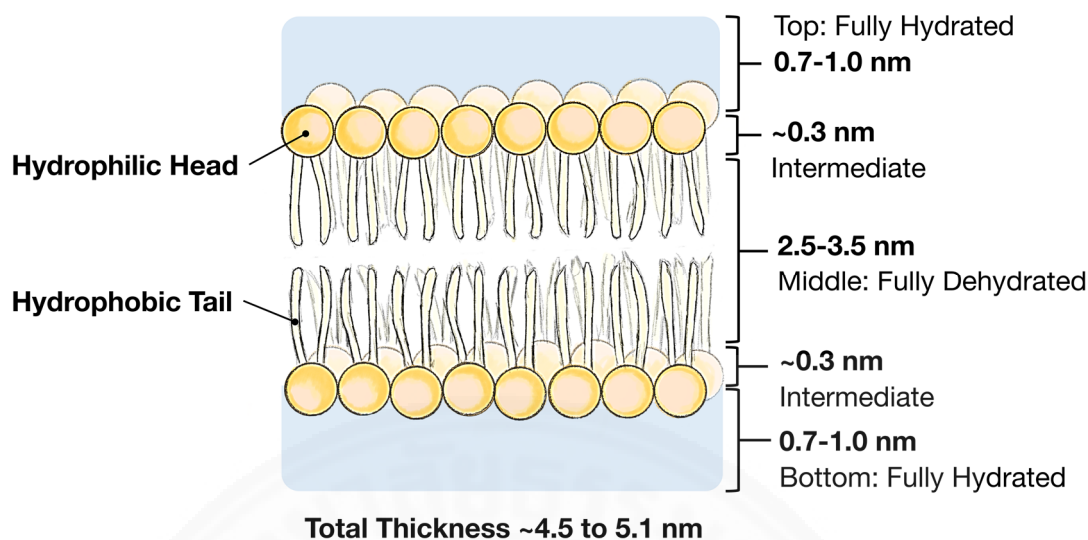


Figure 4.22: Reference phospholipid bilayer membrane thickness.

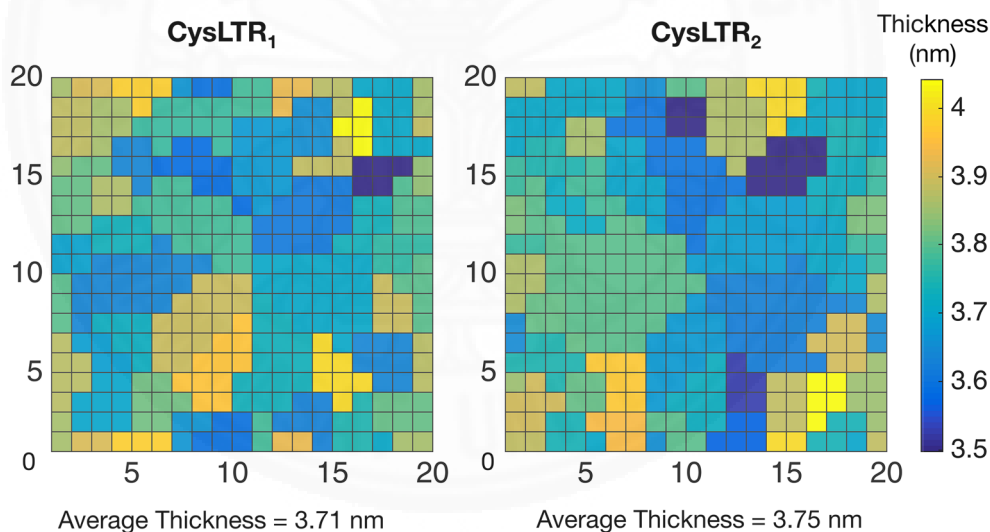


Figure 4.23: Color map of constructed membrane thickness.

Additionally, MD simulations of pure CysLTRs solvated in water and CysLTRs embed in membrane with water environment have been performed in order to observe the difference. Because simulation time depend on size of system (number of atoms in system). Thus, if the difference between these two systems are not significant, I can further perform simulations without membrane in order to reduce calculation time. However, distinctive difference in stability of receptor's structure can be observed by

comparison of C_{α} -RMSD in both system. Hence, I should not perform further MD simulation without presence of membrane because the different motion of protein will definitely lead to incorrect calculation. The comparison detail of MD simulation results can be found in Appendix C (C-3).

For this reason, CysLTRs in membrane systems have been equilibrate further for another 10 ns (15 ns in total). In order to observe behavior of pure CysLTRs prior performing further calculation which involve receptor-ligand complex. First, system energy have been calculated to investigate systems equilibrium as shown in Figure 4.24.

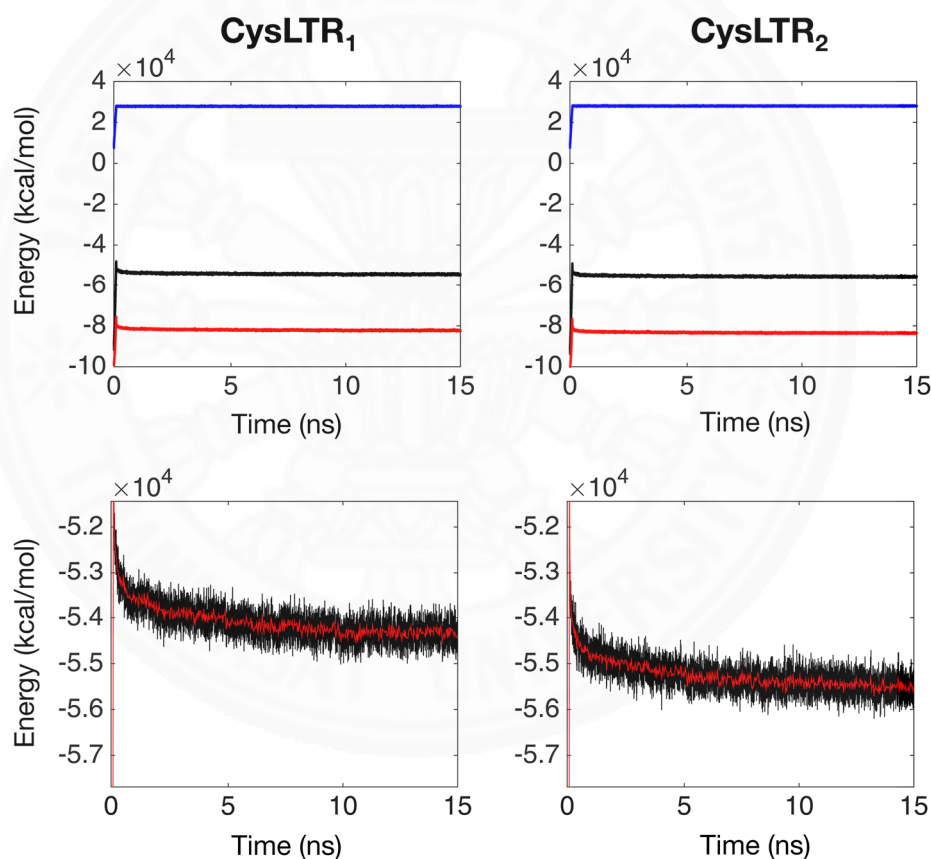


Figure 4.24: System energy of pure CysLTRs embed in membrane. For upper two sub-plot; kinetic energy shown as blue line, potential energy shown as red line, and total energy shown as black line. For lower two sub-plot; total energy shown as black line and average total energy (every 5 ps interval) shown as red line. These two sub-plots have been magnified in vertical axis for 50 percent in order to emphasize the change in total energy.

Both CysLTRs systems have stable behavior in energy throughout whole simulations. Average total energy (every 5 ps interval) have been used to emphasize system equilibrium. As the result, both systems approached equilibrium after approximately 2 ns. The drastic increase at beginning of both simulations were occurred due to heating step (105 ps) and the decline after that was adjustment to equilibrium. However, the stability of receptor have to be investigated as well by considering C α -RMSD (reference frame was last frame of minimization step) as shown in Figure 4.25. Both receptors have high structural fluctuation during heating step which consider as normal because protein tends to change folding pattern after heating. CysLTR₁ structure presented stable behavior after 1 ns, but, there was slight fluctuation between 6 to 11 ns and then its structure start to form stable pattern again. CysLTR₂ structure presented stable behavior after 1 ns and keep maintaining the RMSD in that pattern. Thus, last frame from both CysLTRs simulations have been extracted out in order to use them as host for further receptor-ligand docking calculations (molecular docking).

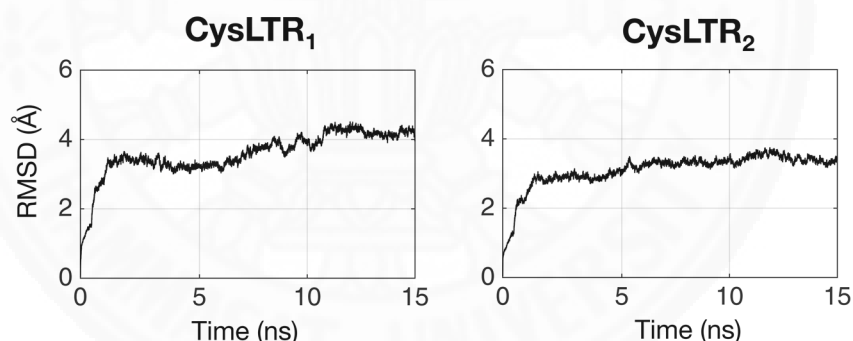


Figure 4.25: Alpha-carbon RMSD of pure CysLTRs embed in membrane.

Nevertheless, before start performing molecular docking, native contact of both receptors have been investigated throughout 15 ns of MD simulation. Native contact is intermolecular contact, normally hydrogen bond, between sidechains of two amino acid residues in protein structure that not adjacent to each other (more than 4 residues apart). Therefore, native contacts have major role in protein folding and can be used to observe contacts between transmembrane helixes (TM) of pure CysLTRs before binding with ligand or inhibitors. Because movement of TM (native contacts break) after binding with those small molecules could lead to activation or inhibition process of receptors.

AMBER12 program package is included tool for measurement of native contact in each frame during MD simulation. The cut-off distance that I have set is 3.4 Å (maximum efficient distance of hydrogen bond). The tool will record pair of residues that have their sidechain atoms come in close contact within cut-off distance in reference frame (last frame of heating step) and then compare contacts in other frames with these native contacts. Results came out in form of fraction, presence of native contact in each frame will be recorded as 1 and added up until last frame after that this summation will be divided by total number of used frames (15000 frames). Thus, the pair of residues that have native contact in every frames will result in fraction equals or greater than 1. Nonetheless, in this study I interested in native contacts between different TM only. Hence, the generated results have been screened for only interested contacts as listed in Table 4.5 and Table 4.6.

Table 4.5: CysLTR₁ native contacts.

Res 1	Res 2	Fraction	Contact	Hydrogen bond (Donor-Acceptor)	Distance (Å)
Ser27	His85	5.53	TM1-TM2	Ser27:H-His85:N	2.04
Tyr30	Val278	1.47	TM1-TM7	Tyr30:H-Val278:O	1.78
Tyr61	Ala140	1.74	TM2-TM4	Tyr61:H-Ala140:O	1.98
Asp69	Ser110	4.60	TM2-TM3	Ser110:H-Asp69:O	1.82
Leu103	His258	1.53	TM3-TM6	His258:H-Leu103:O	2.03
Gln164	Asn262	1.55	EL2-TM6	Asn262:H-Gln164:O	2.43
Asn169	Met273	1.05	EL2-TM7	Asn169:H-Met273:O	1.98
Lys183	His261	1.76	EL2-TM6	Lys183:H-His261:O	1.87
Ser220	Met234	1.86	IL3-TM6	Ser220:H-Met234:O	1.83
His250	Asp291	4.04	TM6-TM7	His250:H-Asp291:O	1.77
Thr254	Asn287	1.99	TM6-TM7	Thr254:H-Asn287:O	2.10

Table 4.6: CysLTR₂ native contacts.

Res 1	Res 2	Fraction	Contact	Hydrogen bond (Donor-Acceptor)	Distance (Å)
Arg38	Leu99	1.98	TM1-TM2	Arg38:H-Leu99:O	1.92
Gln65	Glu343	2.72	TM1-C-ter	Gln65:H-Glu343:O	1.77
Asn79	Trp163	3.94	TM2-TM4	Trp163:H-Asn79:O	1.87
Asp84	Ser125	2.02	TM2-TM3	Ser125:H-Asp84:O	1.73
Asp84	Asn301	1.16	TM2-TM7	Asn301:H-Asp84:O	1.87
Thr90	Ser117	2.34	TM2-TM3	Thr90:H-Ser117:O	1.67
Arg94	Ser117	1.62	TM2-TM3	Arg94:H-Ser117:O	1.92
Tyr98	His284	2.69	TM2-TM7	His284:H-Tyr98:O	2.31
Tyr221	Ile249	2.04	TM5-TM6	Tyr221:H-Ile249:O	1.75
Glu232	Arg243	1.90	IL3-TM6*	Arg243:H-Glu232:O	1.97
Thr252	Asn301	4.45	TM6-TM7	Thr252:H-Asn301:O	1.95
Glu310	Lys331	1.49	H8-C-ter*	Lys331:H-Glu310:O	1.85

*Salt bridge (hydrogen bond between hydrogen atom of protonated amine and oxygen)

4.2.2. Molecular Docking Calculation Results

Last frame snapshot from MD simulation of both CysLTRs have been prepared by removing water, neutralize ions, and phospholipids molecules. Due to molecular docking will be used to calculate binding energy and possibility of binding between each receptor-ligand complex only by neglect effect from phospholipids molecules. However, because information about binding pocket of CysLTRs are not available, AutoSite tool has been used to predict binding sites based on receptor structure as shown in Figure 4.26 and Figure 4.27. The AutoSite calculation results in detail are compiled in Appendix C (C-4).

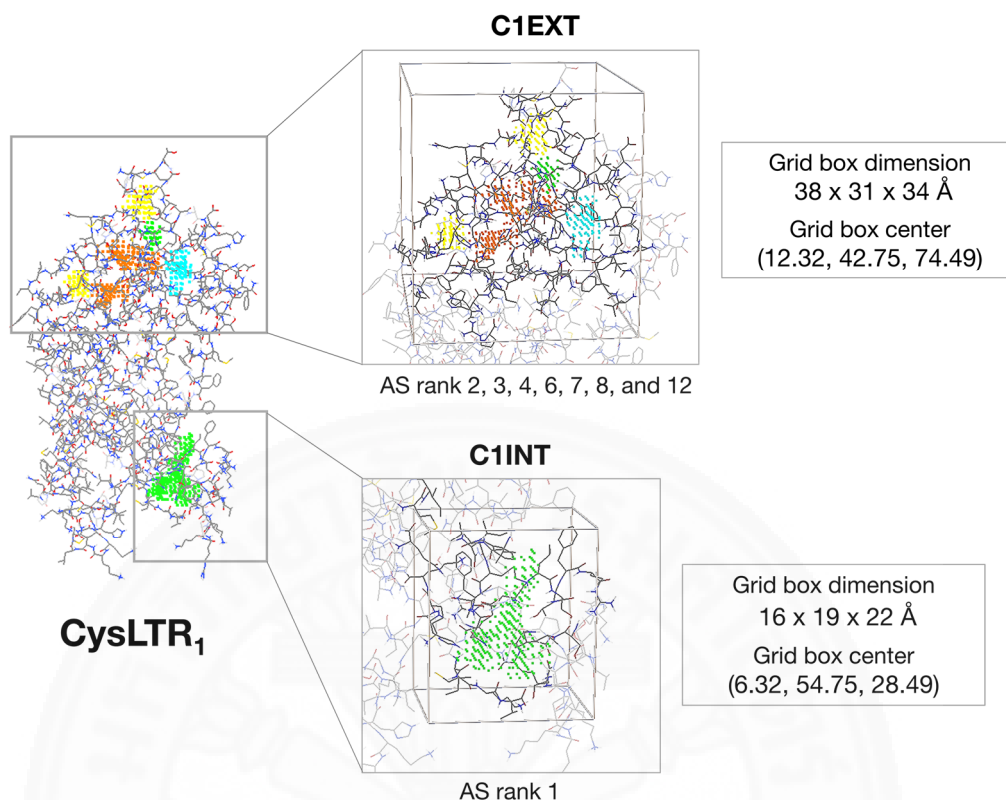


Figure 4.26: CysLTR₁ binding sites from AutoSite calculation. CysLTR₁ structure shown as line model. AutoSite fills points shown as colored-dot inside receptor. C1EXT refers to extracellular binding pocket. C1INT refers to intracellular binding pocket.

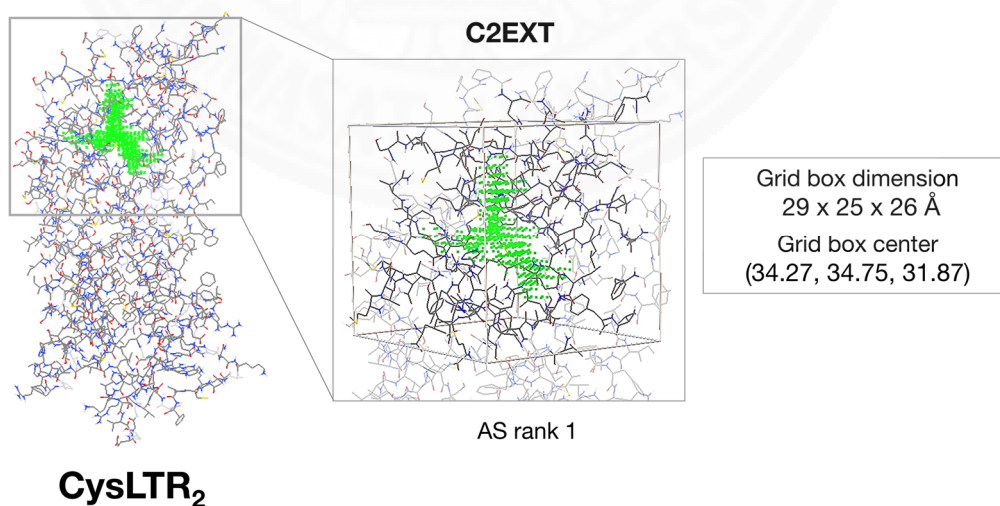


Figure 4.27: CysLTR₂ binding sites from AutoSite calculation. CysLTR₂ structure shown as line model. AutoSite fills points shown as colored-dot inside receptor. C2EXT refers to extracellular binding pocket.

According to predicted binding pockets of both receptors, CysLTR₁ has two possible binding pockets and CysLTR₂ has one possible binding pocket (Figure 4.26 and Figure 4.27). CysLTR₁ has two possible binding pockets because the binding site which has a high AS score is located in the intracellular region and it is quite difficult for an extracellular ligand to bind in that location. Therefore, the binding sites with lower AS scores but located in the extracellular region have been selected to form an extracellular binding pocket. Since, after equilibration by MD simulation, the extracellular region of CysLTR₁ is quite narrow when compared to CysLTR₂. The narrowness mainly came from the deviation of TM5, TM6, and TM7 toward the remaining 4 transmembrane helices as shown in Figure 4.28 and that could lead to the distribution of possible binding sites into a smaller cavity.

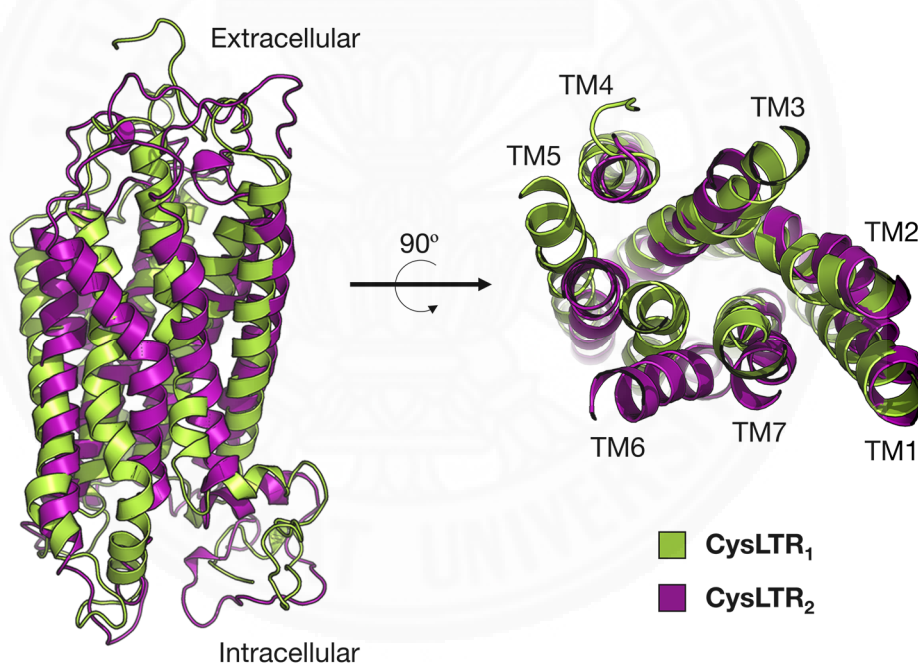


Figure 4.28: Superimposition of CysLTR₁ and CysLTR₂. Front view of superimposition is presented on the left and top view of superimposition is presented on the right. CysLTR₁ and CysLTR₂ structures shown as green and purple ribbon, respectively

In this study, molecular docking has been performed by fixed receptor structure and let ligand flexible in specified grid box (Figure 4.26 and Figure 4.27). The criteria for selection of ligand conformations in each CysLTRs complex will be followed the one I have used for 5-LO systems. The selected clusters have been listed in

Table 4.7, Table 4.8, and Table 4.9. In addition, the complete calculation results have been combined in Appendix C (C-5).

Table 4.7: Summary of molecular docking calculation for C1INT.

Ligand	Cluster	Lowest B.E. (kcal/mol)	Mean B.E. (kcal/mol)	Frequency	K _i (μ M)	K _{i,avg} (μ M)
LTD ₄	1	-7.68	-7.68 \pm 0.00	1	2.33	2.33 \pm 0.00
MON	1	-11.37	-10.56 \pm 0.59	8	0.005	0.02 \pm 0.03
CD	2	-5.76	-5.44 \pm 0.19	54	59.58	101.48 \pm 35.41
DMP	1	-6.17	-5.98 \pm 0.13	36	29.81	40.82 \pm 9.10

Table 4.8: Summary of molecular docking calculation for C1EXT.

Ligand	Cluster	Lowest B.E. (kcal/mol)	Mean B.E. (kcal/mol)	Frequency	K _i (μ M)	K _{i,avg} (μ M)
LTD ₄	1	-6.35	-5.35 \pm 1.02	3	21.99	118.40 \pm 362.88
MON	1	-8.36	-8.36 \pm 0.00	1	0.74	0.74 \pm 0.00
CD	1	-6.98	-6.68 \pm 0.21	96	7.59	12.65 \pm 5.29
DMP	1	-6.56	-6.50 \pm 0.06	99	15.43	16.96 \pm 2.26

Table 4.9: Summary of molecular docking result for C2EXT.

Ligand	Cluster	Lowest B.E. (kcal/mol)	Mean B.E. (kcal/mol)	Frequency	K _i (μ M)	K _{i,avg} (μ M)
LTD ₄	1	-7.18	-6.36 \pm 0.89	3	5.41	21.63 \pm 54.76
MON	1	-12.44	-11.39 \pm 0.95	3	0.001	0.004 \pm 0.01
CD	1	-6.25	-5.63 \pm 0.34	23	26.04	74.31 \pm 43.72
DMP	1	-5.61	-5.50 \pm 0.07	68	76.75	91.80 \pm 10.25

The validation of calculated results have been performed by comparison between experimental inhibitory constant (K_i) of MON on CysLTR₁ in guinea pig lung (absence of human serum albumin) and the calculated values as shown in Table 4.10.

Table 4.10: Comparison of experimental and calculated inhibitory constant of MON.

Type	Name	K_i (nM)	Reference
Experimental K_i	$K_{i,exp1}$	0.18 ± 0.03	[87]
	$K_{i,exp2}$	8.30 ± 2.00	[88]
Calculated K_i	$K_{i,C1INT}$	17.88 ± 32.10	-
	$K_{i,C1EXT}$	737.88 ± 0.00	-

The calculated K_i of MON at intracellular binding pocket of CysLTR₁ ($K_{i,C1INT}$) is closer to the experimental K_i ($K_{i,exp1}$ and $K_{i,exp2}$) than the calculated K_i from extracellular binding pocket ($K_{i,C1EXT}$). This indicated that MON prefer to bind on CysLTR₁ at intracellular binding pocket. However, according to calculated binding energy of all ligands at two binding pockets of CysLTR₁ (extracellular and intracellular) and one binding pocket of CysLTR₂ (extracellular), they are possible to bind on both CysLTRs in specified regions as shown in Figure 4.29, Figure 4.30, and Figure 4.31.

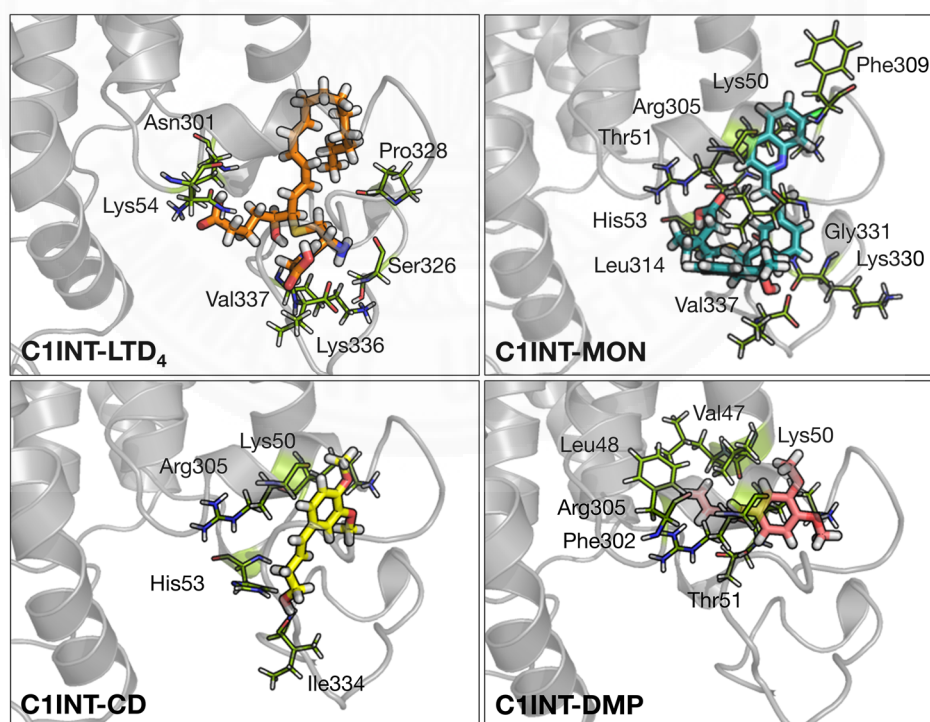


Figure 4.29: Intracellular binding site of CysLTR₁. Receptor structure shown as grey ribbon. The interacting amino acid residue shown as green stick model. LTD₄, MON, CD, and DMP shown as orange, teal, yellow, and pink stick model, respectively.

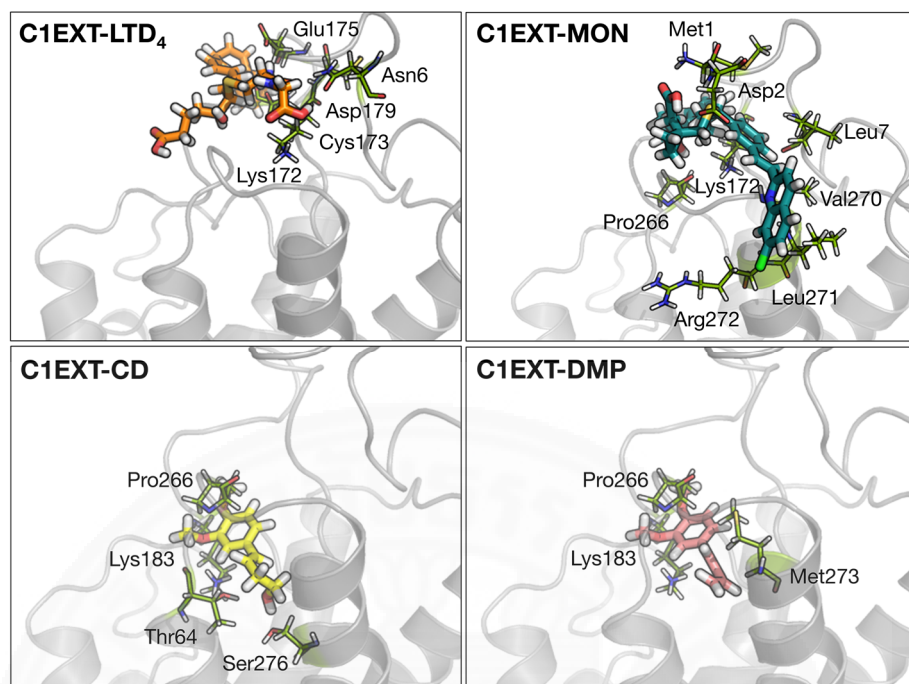


Figure 4.30: Extracellular binding site of CysLTR₁. Receptor structure shown as grey ribbon. The interacting amino acid residue shown as green stick model. LTD₄, MON, CD, and DMP shown as orange, teal, yellow, and pink stick model, respectively.

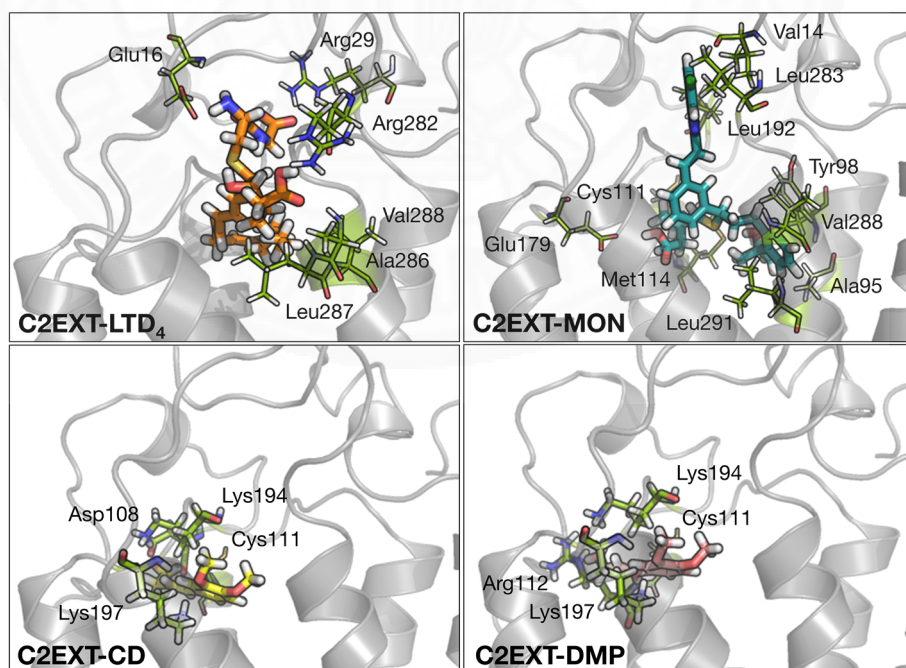


Figure 4.31: Extracellular binding pocket of CysLTR₂. Receptor structure shown as grey ribbon. The interacting amino acid residue shown as green stick model. LTD₄, MON, CD, and DMP shown as orange, teal, yellow, and pink stick model, respectively.

LTD₄ and MON are preferred to bind on CysLTR₁ in intracellular binding pocket. But, CD and DMP are preferred to bind on CysLTR₁ in extracellular binding pocket. Moreover, the binding possibility of MON on CysLTR₂ is slightly higher which is not expected because there is no evidence regarding inhibition effect of MON on CysLTR₂. Nevertheless, the comparison of binding affinity based on binding energy alone are not complete. Thus, the interaction between each ligand and amino acid residues in each binding pocket are investigated as illustrated in Figure 4.32, Figure 4.33, and Figure 4.34.

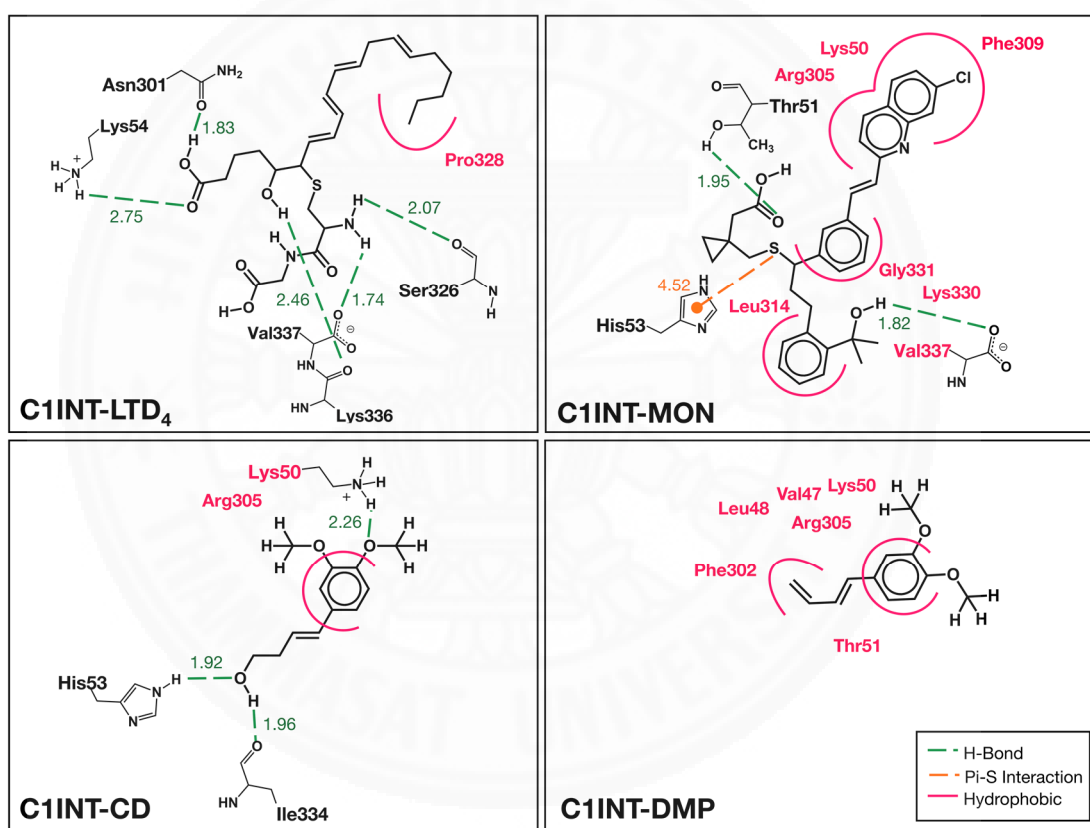


Figure 4.32: 2-D chemical interaction of C1INT docking. The presented chemical interactions were within 5 Å distance around ligands. Hydrogen bonds shown as green dash lines. Hydrophobic interactions (Van der Waals) shown as pink curve lines and pink amino acid labels represented the amino acid residues that formed hydrophobic interactions with ligands. Pi-Sulfur interaction shown as orange dash line. All distance labels presented in Å unit.

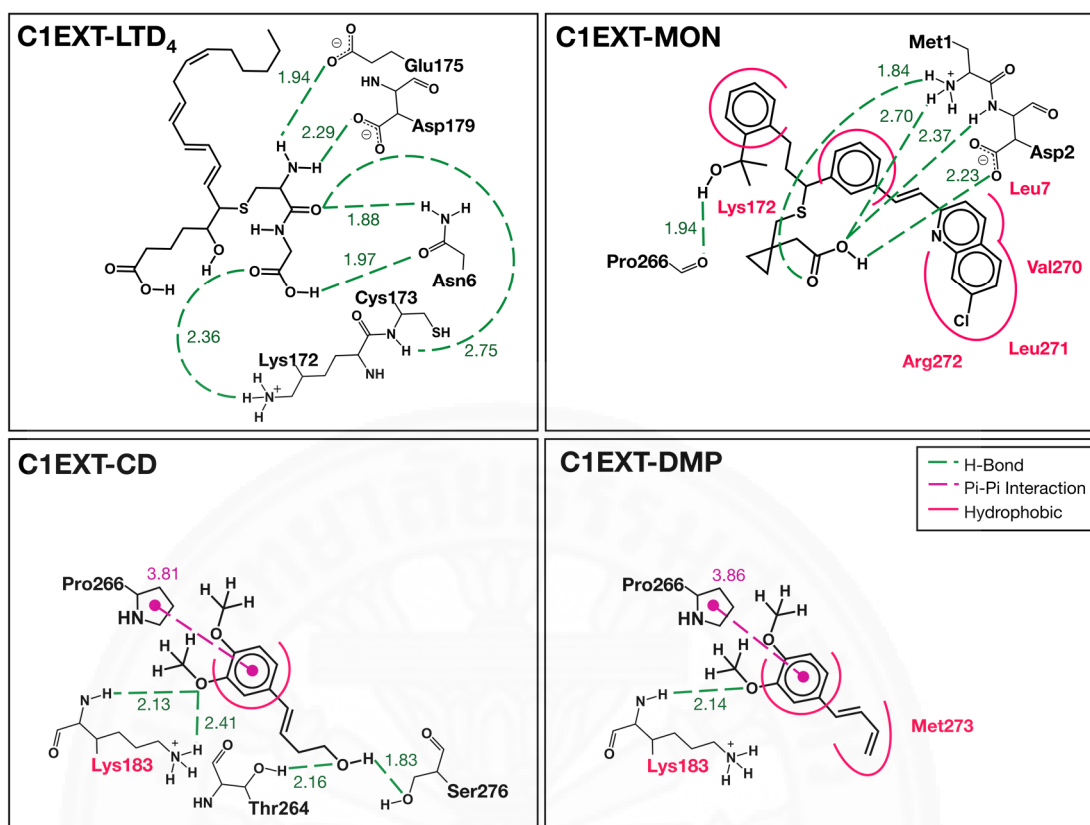


Figure 4.33: 2-D chemical interaction of C1EXT docking. The presented chemical interactions were within 5 Å distance around ligands. Hydrogen bonds shown as green dash lines. Hydrophobic interactions (Van der Waals) shown as pink curve lines and pink amino acid labels represented the amino acid residues that formed hydrophobic interactions with ligands. Pi-Pi interaction shown as purple dash line. All distance labels presented in Å unit.

Intracellular binding pocket of CysLTR₁ (C1INT) is located near Helix8. All ligands are bound within the same area, but, they interact with different amino acid residues. LTD₄ forms two hydrogen bonds between its carboxyl group with protonated amine group of Lys54 and carbonyl group of Asn301. It also forms another three hydrogen bonds between its hydroxyl and amino group with carbonyl group of Ser326, Lys336, and carboxylate group of Val337. In addition, the aliphatic hydrocarbon atoms of LTD₄ occur van der Waals interaction with nearby residue to stabilize the receptor-ligand complex which result in low B.E. MON forms two strong hydrogen bonds between its carboxyl and hydroxyl group with hydroxyl group of Thr51 and carboxylate

group of Val337, respectively. Similar to LTD₄, aromatic hydrocarbon atoms of MON occur the interaction with nearby residues leading by Pi-sulfur interaction with imidazole ring of His53 which make it have the most stable receptor-ligand complex. CD forms two hydrogen bonds between its hydroxyl group with imidazole ring of His53 and carbonyl group Ile334. Its oxygen ether atom also forms hydrogen bond with protonated amine group of Lys50. As expected, aromatic hydrocarbon atoms of CD also occur interaction with nearby residue as well. Unlike others, DMP did not form any hydrogen bond with pocket residues. But, its aliphatic and aromatic hydrocarbon atoms occur van der Waals interaction with nearby residues which quite similar to MON and CD.

Extracellular binding pocket of CysLTR₁ (C1EXT) is located in extracellular region of receptor. Because the difference in molecular structure among ligands, LTD₄ and MON which have large structure cannot penetrated through the network of amino acid interaction and they bound on receptor close to N-terminal area. But, CD and DMP which have smaller structure can go slightly deeper and bound on extracellular loop near TM7 instead. LTD₄ forms four hydrogen bonds between its carboxyl and carbonyl group with amino and carbonyl group of Asn6, protonated amine group of Lys172, and amino group of Cys173. It also forms another two hydrogen bonds between its amino group with carboxylate group of Glu175 and Asp179. Nevertheless, there is no interaction between LTD₄ and nearby residue to help stabilize the complex which result in higher B.E when compare to binding in intracellular site. MON forms four hydrogen bonds between its carboxyl group with amino and carboxylate group of Asp2 and protonated amine group of Met1. Its hydroxyl group also form hydrogen bond with carbonyl group of Pro266. Moreover, aromatic hydrocarbon atoms of MON occur the interaction with nearby residues but the strength of those interactions are weaker when compare to binding in intracellular site. CD forms two hydrogen bonds between its hydroxyl group with hydroxyl group of Thr264 and Ser276. Its oxygen ether atom also forms another two hydrogen bonds with protonated amine and amino group of Lys183. As expected, aromatic hydrocarbon atoms of CD also occur interaction with nearby residue leading by Pi-Pi interaction with pyrrolidine ring of Pro266 which result in lower B.E. when compare to binding in intracellular site. Due to resemble in chemical

structure and binding position, DMP and CD have quite similar interaction. The oxygen ether atom of DMP forms hydrogen bond with amino group of Lys183. In addition, its aliphatic and aromatic hydrocarbon atoms also occur interaction with nearby residues which very similar to CD.

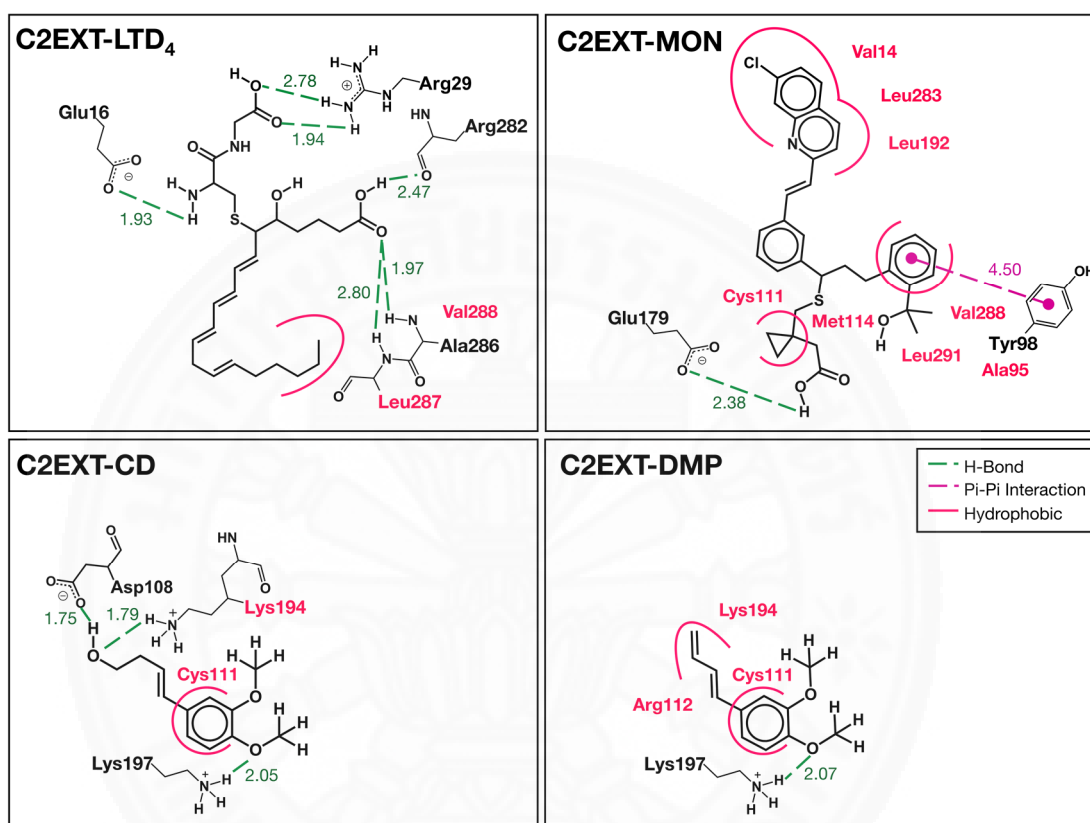


Figure 4.34: 2-D chemical interaction of C2EXT docking. The presented chemical interactions were within 5 Å distance around ligands. Hydrogen bonds shown as green dash lines. Hydrophobic interactions (Van der Waals) shown as pink curve lines and pink amino acid labels represented the amino acid residues that formed hydrophobic interactions with ligands. Pi-Pi interaction shown as purple dash line. All distance labels presented in Å unit.

Binding pocket of CysLTR₂ (C2EXT) is located in extracellular region of receptor forms by boundary of TM2, TM3, TM7 and extracellular loops. All ligand bound within the same area but they interact with different residues similar to the binding on intracellular pocket of CysLTR₁. LTD₄ forms five hydrogen bonds between its two carboxyl groups with guanidium group of Arg29, carbonyl group of Arg282,

and amino group of Leu287 and Ala286. Its amino group also forms hydrogen bond with carboxylate group of Glu16. In addition, the aliphatic hydrocarbon atoms of LTD₄ occur van der Waals interaction with nearby residues. However, the strength of those chemical interactions are weaker than binding on intracellular site of CysLTR₁. Carboxyl group of MON forms a hydrogen bond with carboxylate group of Glu179. Moreover, aromatic hydrocarbon atoms of MON occur the interaction with nearby residues leading by Pi-Pi interaction with aromatic ring of Tyr98 which result in lower B.E. when compare to binding on CysLTR₁. CD forms two hydrogen bonds between its hydroxyl group with protonated amine group of Lys194 and carboxylate group of Asp108. Its oxygen ether atom also forms another hydrogen bond with protonated amine group of Lys197. The aromatic hydrocarbon atoms of CD also occur interaction with nearby residue but strength of those interactions are weaker than binding on extracellular site of CysLTR₁. As expected, DMP and CD have quite similar interaction. The oxygen ether atom of DMP forms hydrogen bond with protonated amine group of Lys197 and its aliphatic and aromatic hydrocarbon atoms also occur interaction with residues which very similar to CD as well.

Since molecular docking calculations have been performed by fixing receptors structure, the simulated environment did not imitate reality. Therefore, the calculated binding possibility might not accurate enough. In addition, the high binding possibility of ligands toward CysLTRs did not mean that it can be used to activate or inhibit activity of receptors because those processes of G-protein couple receptor are very complicated. Structural change of these receptors after binding with ligand is the result upon activation or inhibition process which will allow or prevent consecutive activation of G-protein later on. Consequently, molecular dynamic simulation (MD) can be used to monitor movement of protein over time and predict more accurate binding affinity by including phospholipid bilayer membrane and water environment into complex system.

4.2.3. Molecular Dynamic Simulation Results

According to calculation results from molecular docking, DMP and CD have similar binding characteristic with each other on both CysLTRs. Therefore, in order to reduce simulation time, MD simulation of CysLTRs-DMP complexes will not be

performed because there is recent evidence that DMP can be toxic by accumulation in liver. The selected conformations of the other three ligands (LTD₄, MON, and CD) have been prepared with CysLTRs structures that embedded in phospholipids bilayer membrane with water environment in rectangular box (15 ns snapshot from MD simulation of pure CysLTRs). All complex systems will be minimized and then equilibrated for 30 ns with isothermal-isobaric ensemble (NPAT-anisotropic pressure control) without heating because they have been heated to reach 300 K from the previous MD simulation already. The system energies of all CysLTRs complexes have been calculated in order to observe system's behavior. Moreover, total energy have been averaged every 30 ps for emphasis of system's equilibrium as presented in Figure 4.35, Figure 4.36, and Figure 4.37. As the result, energies of all CysLTRs complexes systems are steady throughout whole simulation and the average total energy can be used to confirm the equilibrium state of all systems shortly after beginning of simulation. Thus, entire 30 ns interval can be used to represent systems equilibrium.

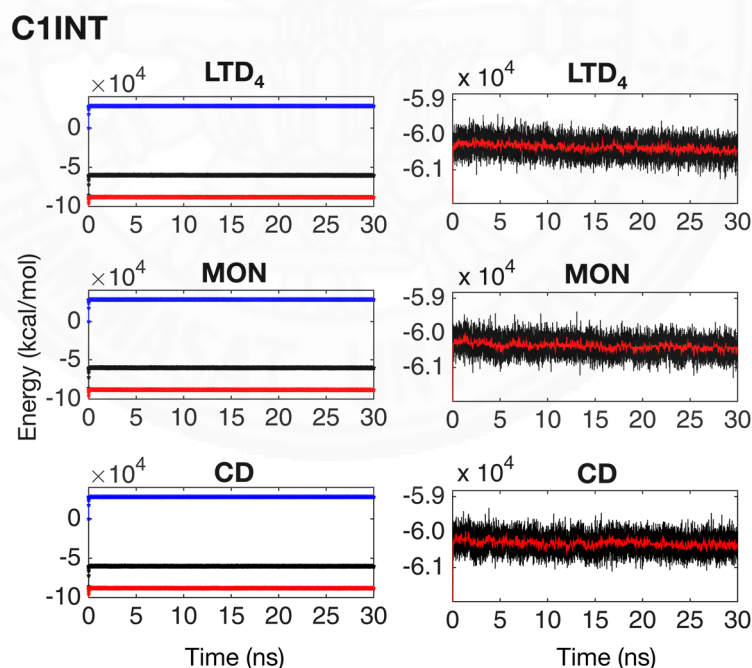


Figure 4.35: C1INT complex system energy. Sub-plots on the left presented system energies with blue, red, and black line which denote kinetic, potential, and total energy, respectively. Sub-plots on the right presented total and average energy as black and red line, respectively. These sub-plots have been magnified in vertical axis for 50 percent.

C1EXT

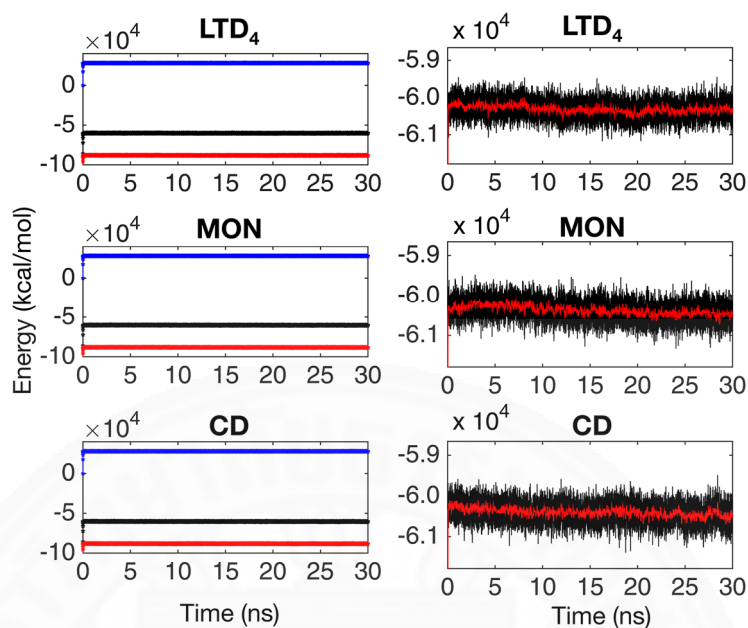


Figure 4.36: C1EXT complex system energy. Sub-plots on the left presented system energies with blue, red, and black line which denote kinetic, potential, and total energy, respectively. Sub-plots on the right presented total and average energy as black and red line, respectively. These sub-plots have been magnified in vertical axis for 50 percent.

C2EXT

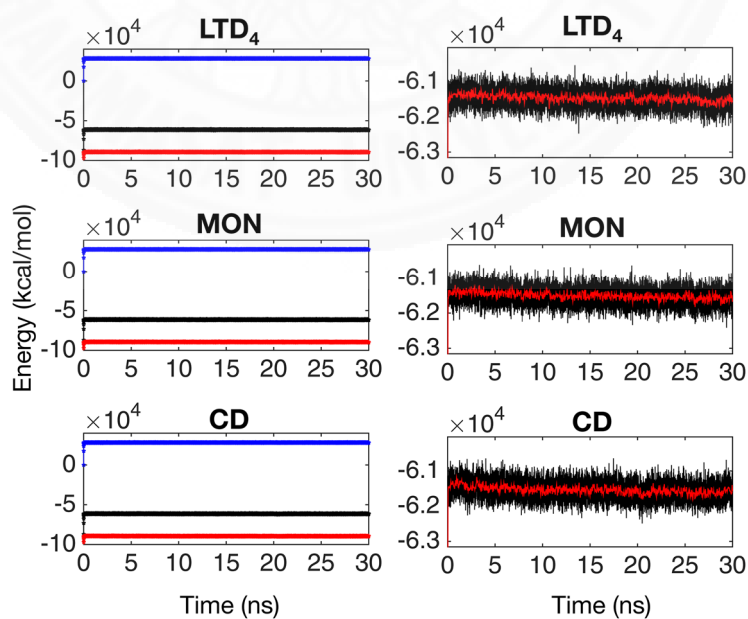


Figure 4.37: C2EXT complex system energy. Sub-plots on the left presented system energies with blue, red, and black line which denote kinetic, potential, and total energy,

respectively. Sub-plots on the right presented total and average energy as black and red line, respectively. These sub-plots have been magnified in vertical axis for 50 percent.

Structural stability of CysLTRs have been investigated based on C_{α} -RMSD with reference frame (last frame of minimization step) as shown in Figure 4.38, Figure 4.39, and Figure 4.40. For C1INT complex systems, all receptor-ligand complexes start to form stable behavior after 6 ns. However, there are noticeable changes in all complexes afterwards. Receptor structure in C1INT-LTD₄ complex has slightly more deviation after 23 ns and then start to form stable pattern again after 25 ns. Reduction of MON structural deviation can be observe after 22 ns and then it start to form stable pattern after 25 ns as well. Receptor structure in C1INT-CD complex has rapid increase in deviation after 23 ns and then start to form stable pattern after 25 ns. For C1EXT complex systems, C1EXT-CD complex presented stable receptor-ligand binding after 15 ns. Unfortunately, there is no evidence of stable receptor-ligand binding in the other two complexes due to high fluctuation of ligands.

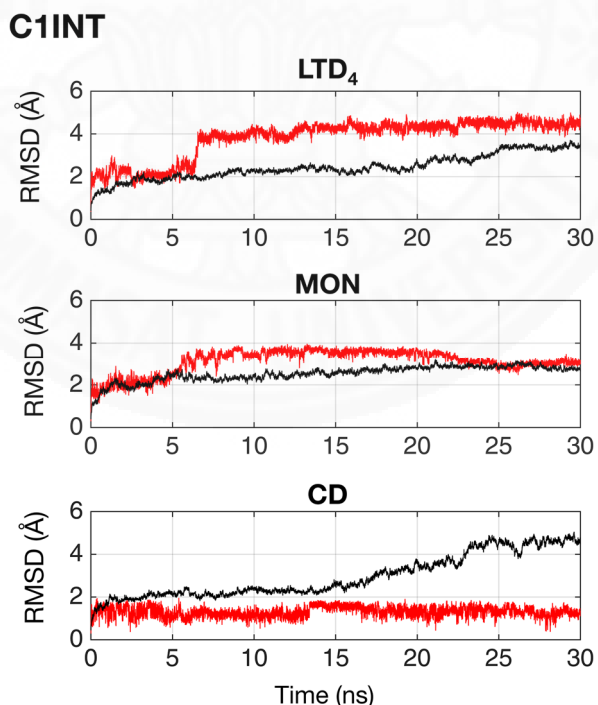


Figure 4.38: RMSD plot of C1INT system. Alpha-carbon RMSD of CysLTR₁ shown as black line. All atoms RMSD of ligands shown as red line.

C1EXT

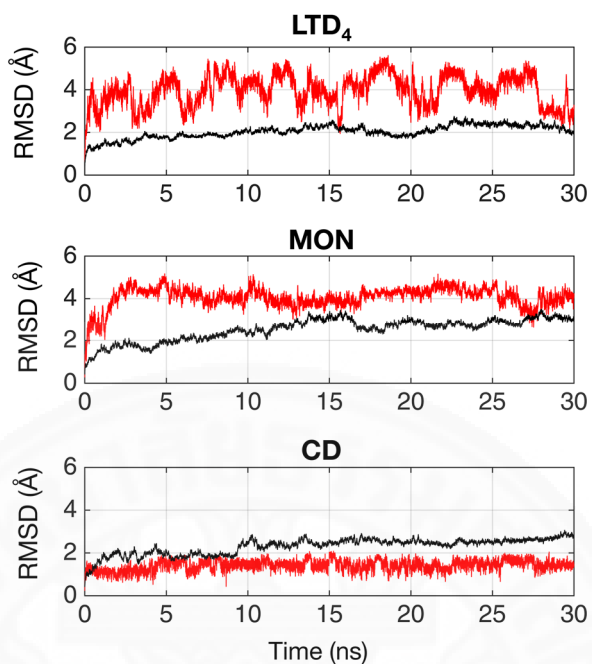


Figure 4.39: RMSD plot of C1EXT system. Alpha-carbon RMSD of CysLTR₁ shown as black line. All atoms RMSD of ligands shown as red line.

C2EXT

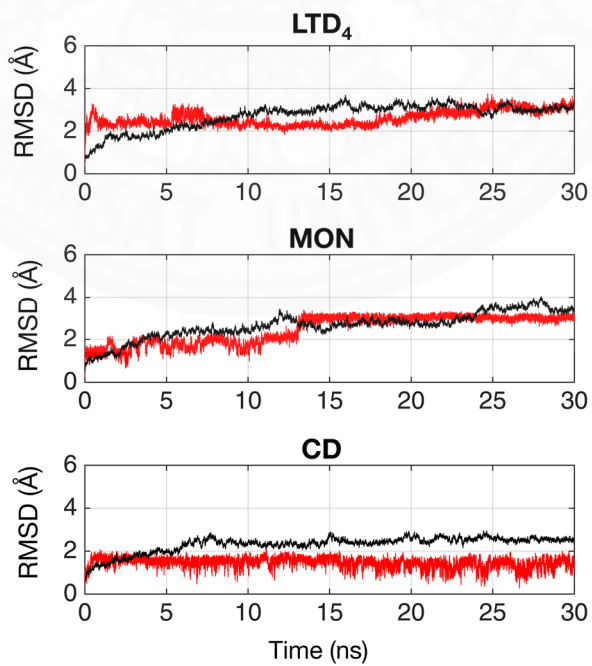
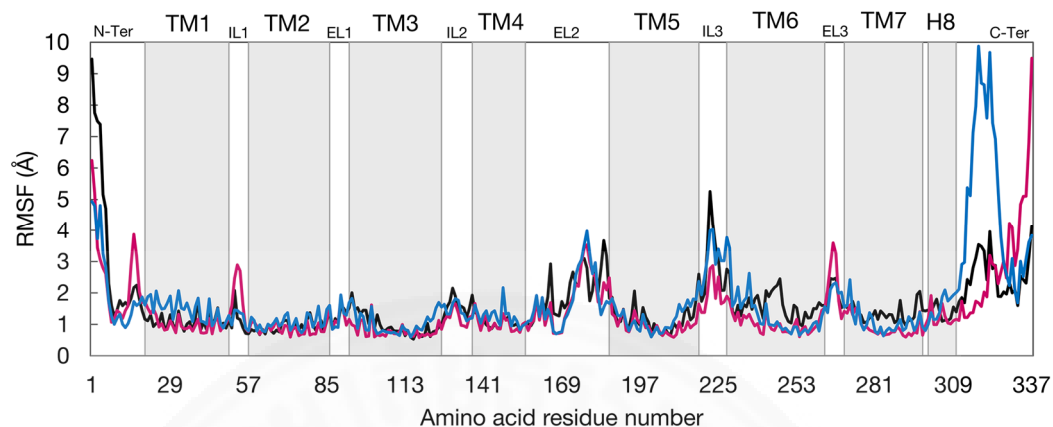


Figure 4.40: RMSD plot of C2EXT system. Alpha-carbon RMSD of CysLTR₁ shown as black line. All atoms RMSD of ligands shown as red line.

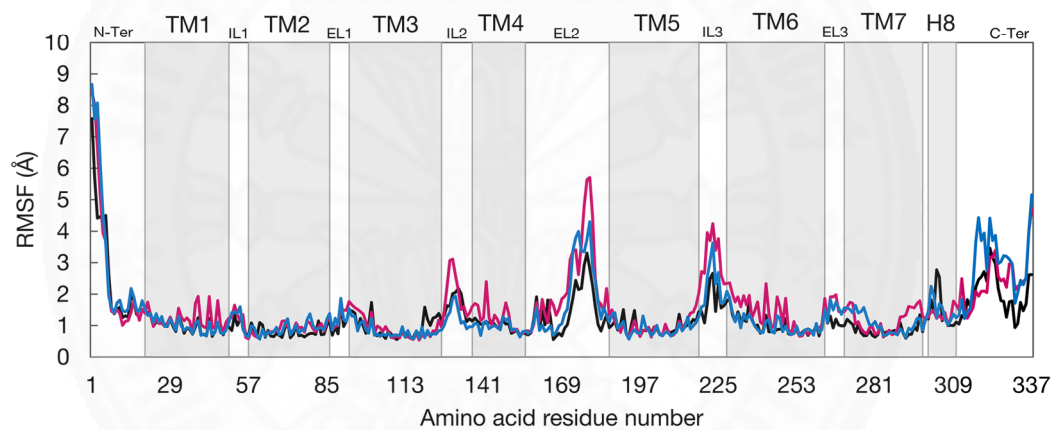
For C2EXT complex systems, C2EXT-MON and C2EXT-CD complexes start to form stable receptor-ligand binding behavior after 15 ns. However, receptor structure in C2EXT-MON complex has higher fluctuation after 23 ns and then it start to form stable pattern again after 25 ns. C2EXT-LTD₄ complex start to form stable receptor-ligand binding behavior after 25 ns. Therefore, behavior of all CysLTRs complex systems within 25 to 30 ns interval have been considered as stable to perform further analysis which involve receptor-ligand interaction.

However, before calculating binding free energy between each ligand and amino acid residues around them, average atomic fluctuation of receptors structure throughout the entire simulation have been calculated first in order to observe movement of receptor in each complex system as shown in Figure 4.41. CysLTR₁ structure in C1INT complex systems have high fluctuation in loops region including N-terminal and C-terminal area especially for C1INT-CD complex, the area near C-terminal is very fluctuate. All transmembrane helixes have quite low fluctuation when compared to loops region. However, higher fluctuation can be found in TM6. CysLTR₁ structure in C1EXT complex systems also have high fluctuation in loops region including N-terminal and C-terminal area. All transmembrane helixes have low fluctuation but higher fluctuation can be observed in TM6 and Helix8. In addition, the fluctuation in C1EXT-MON complex is slightly higher than others for most of CysLTR₁ components. CysLTR₂ structure in C2EXT complex systems have high fluctuation in loops region including N-terminal and C-terminal area but the fluctuation is less than the one in both CysLTR₁ complex systems. All transmembrane helixes have very low fluctuation. Thus, observation on atomic fluctuation of whole receptor in both CysLTRs complex systems revealed less movement in transmembrane helixes when compared to extracellular and intracellular loops region especially in both terminals (N-terminal and C-terminal). These are reasonable because alpha-helix regions were partly immobilized by embedding in phospholipid bilayer membrane. Nevertheless, the high-level in structural change of protein could not be found within short period MD simulation like this. Consequently, observation on activation or inhibition activity of CysLTRs concerning structural change cannot fully perform. But, the binding affinity between each ligand and receptors can still be predicted as discussed in the next part.

C1INT



C1EXT



C2EXT

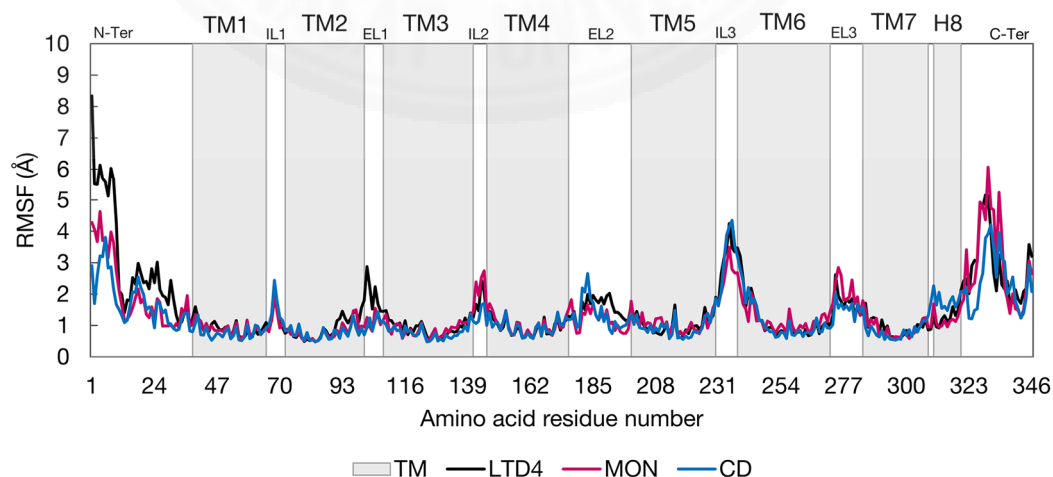


Figure 4.41: Atomic fluctuation of CysLTRs systems.

4.2.3.1. Free Binding Energy Calculation (MM/GBSA)

For CysLTRs systems, 5000 frames (1 frame equals to 1 ps) in specified interval (25-30 ns) have been averaged and calculated binding energy between enzyme and each ligand as shown in Table 4.11.

Table 4.11: Free binding energy calculated from MM/GBSA for CysLTRs systems.

Host	Ligand	MM/GBSA Results (kcal/mol)		
		G_{Total}^a	Entropy (T S)	$G_{Binding}^b$
C1INT	LTD ₄	-43.89 ± 3.91	-64.51	20.61
	MON	-34.93 ± 3.45	-51.74	16.81
	CD	-23.42 ± 3.88	-32.77	9.36
C1EXT	LTD ₄	-32.95 ± 6.17	-75.29	42.35
	MON	-14.19 ± 8.32	-56.04	41.85
	CD	-27.34 ± 3.06	-33.59	6.25
C2EXT	LTD ₄	-41.80 ± 3.33	-60.00	18.20
	MON	-49.55 ± 3.26	-45.95	-3.61
	CD	-24.71 ± 2.47	-33.35	8.64

^a $G_{Total} = G_{complex} - G_{protein} - G_{ligand}$

^b $G_{Binding} = G_{Total} - T S$

By considering only total energy difference between bound and unbound state of CysLTRs (G_{Total}) which neglect the effect of entropy contribution (T S). C1INT complex systems shown high affinity binding with LTD₄ followed by MON and CD. C1EXT complex systems also shown high affinity binding with LTD₄ followed by CD and MON. However, G_{Total} of C1EXT-LTD₄ and C1EXT-MON complexes are higher than the one in C1INT complexes which mean that LTD₄ and MON preferred to bind on CysLTR₁ in intracellular binding pocket. In other hand, G_{Total} of C1EXT-CD complex is lower than the one in C1INT complex which result in higher binding affinity of CD in extracellular binding pocket of CysLTR₁. C2EXT complex systems shown very high affinity binding with MON followed by LTD₄ and CD. Nevertheless, G_{Total}

of C2EXT-LTD₄ and C2EXT-CD complexes are still higher than the one in C1INT complexes. The detail of energy approximation are explained in Appendix C (C-6). However, similar to 5-LO systems, binding energies (G_{Binding}) which include entropy contribution of all CysLTRs complex systems turned out to be positive value except for the C1EXT-MON complex. Therefore, the comparison of binding affinity between CysLTRs and each ligand have been considered from total energy difference (G_{Total}) with the same supported reasons as mentioned in analysis of 5-LO systems result. Next, pairwise energy decomposition between amino acid residues 5 Å around ligand have been calculated in order to investigate major amino acid residues that interact with each ligand. The significant amino acid residues have been considered following criteria that residues with energy lower than -1.0 kcal/mol for one system out of four systems will be selected as shown in Figure 4.42, Figure 4.44, and Figure 4.46. Moreover, the total energy decomposition has been further analyze in context of backbone and sidechain effect as shown in Figure 4.43, Figure 4.45, and Figure 4.47. Energy decomposition of C1INT complex systems revealed different interacting amino acid residues among ligands. LTD₄ mainly interact with Val337, Lys336, Ile334, Phe309 and Lys54. MON interact with Cys335, Gly331, Lys330, Pro328, Leu314, Asn301, and Ile232. CD mainly interact with Arg305 and Lys50. Even though, each ligand interact with different amino acid residues but those residues are closed to each other and can be considered as part of binding pocket. Energy decomposition of C1EXT complex systems revealed different interacting amino acid residues among ligands as well. LTD₄ interact with Cys267, Cys173, Lys172, Asp2, and Met1. However, there are some other residues that show high interaction with LTD₄ but chemical interaction cannot be detect. This could occur due to the position of ligand and amino acid residue is close but not suitable to form any interaction. MON shows very weak binding interaction when compare to other ligands in the same system because it weakly interact with Val270 and Leu7 only. CD interact with Asp268, Pro266, Lys183, and Phe174. Energy decomposition of C2EXT complex systems revealed some similar interacting amino acid residues among ligands. LTD₄ mainly interact with Leu291, Leu287, Ala286, Leu283, Tyr198, Glu16, and Val14. MON interact with Leu287, His284, Lys197, Ala196, Ile195, Lys194, Tyr193, Met114, Cys111, Ty98 and Val14. CD interact with Lys197, Tyr193, and Leu91.

C1INT

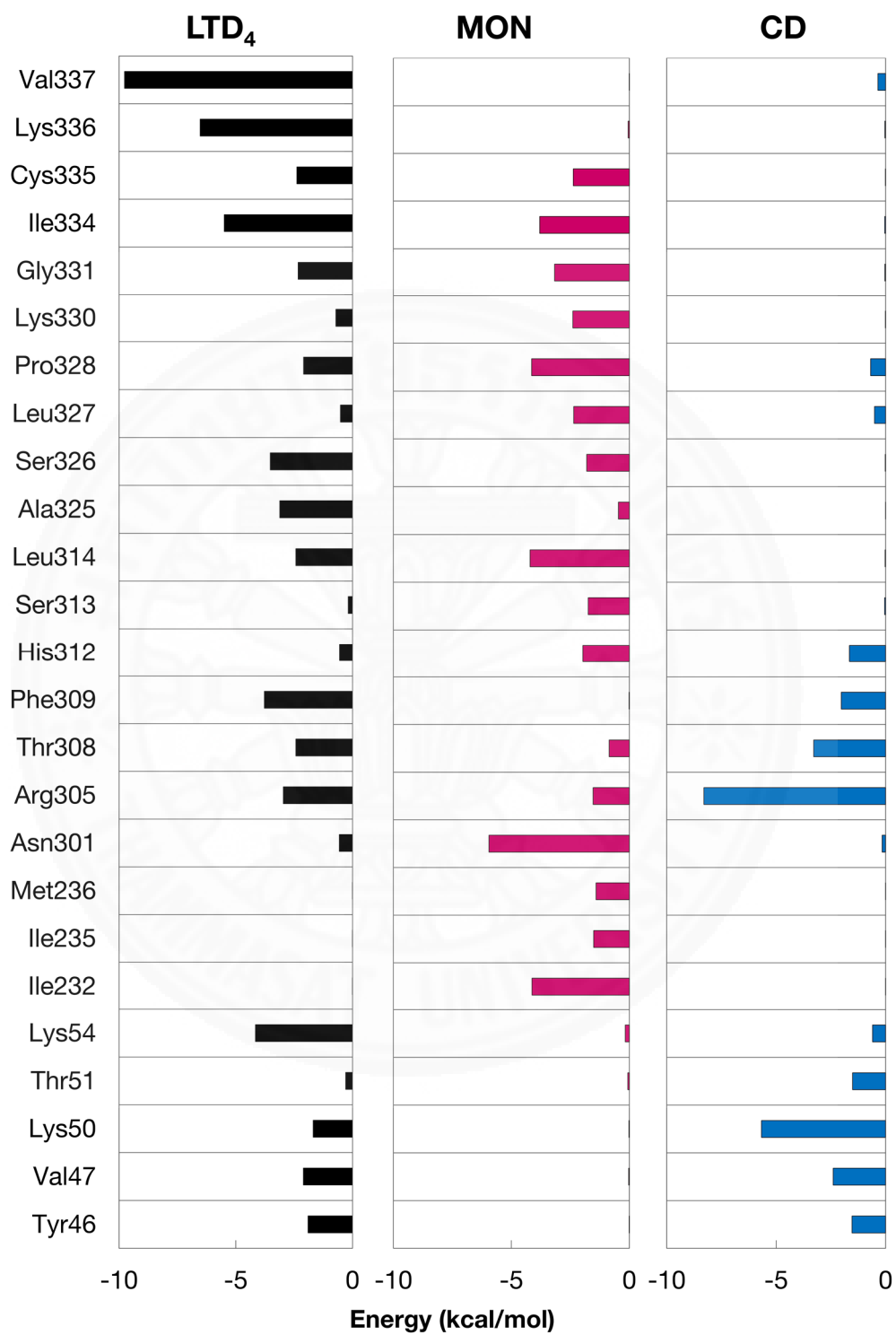


Figure 4.42: Total energy decomposition from selected interval of C1INT systems.

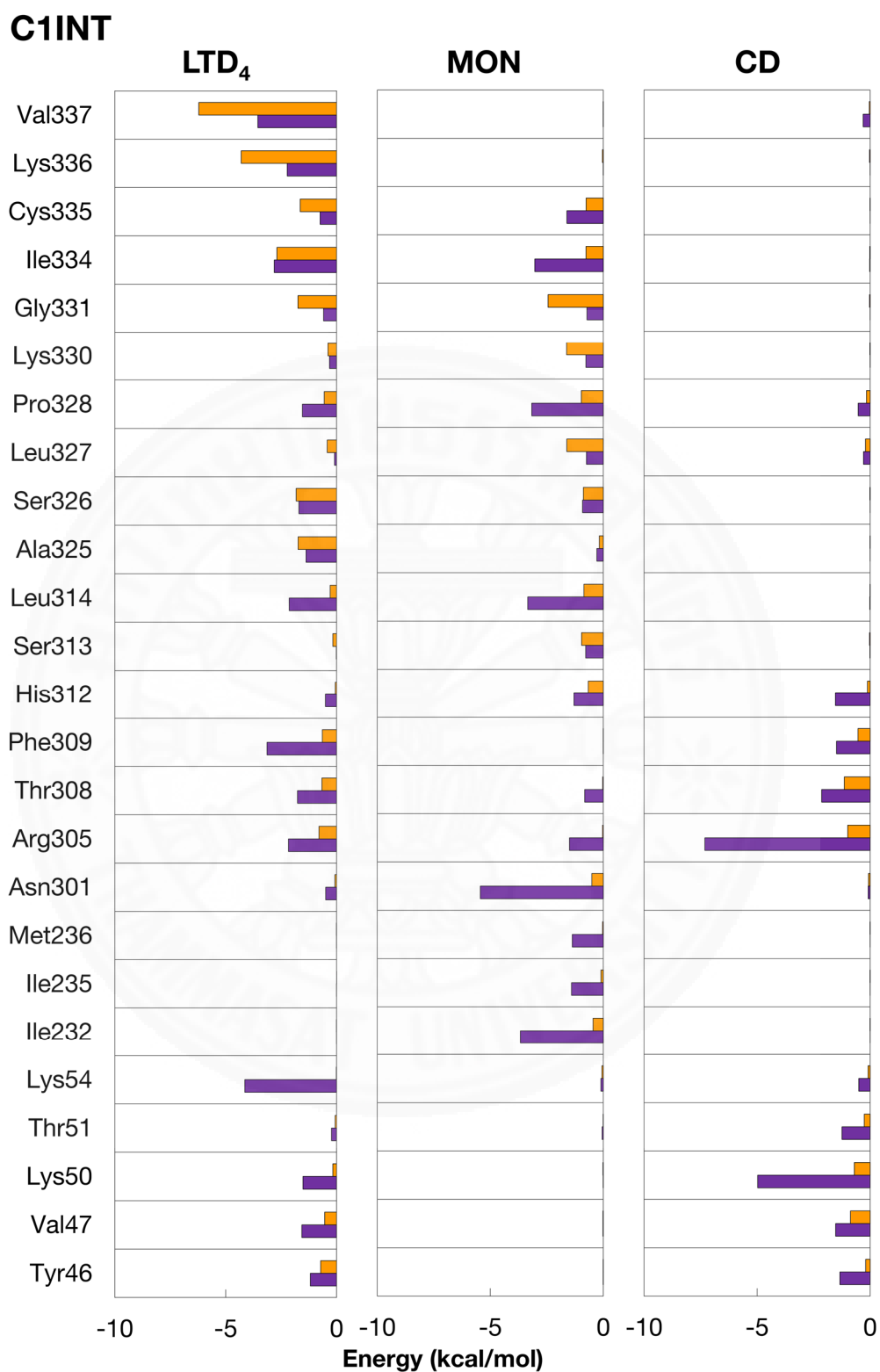


Figure 4.43: Sidechain and backbone energy of C1INT systems. Backbone and sidechain energy shown as orange and purple bar plot, respectively.

C1EXT

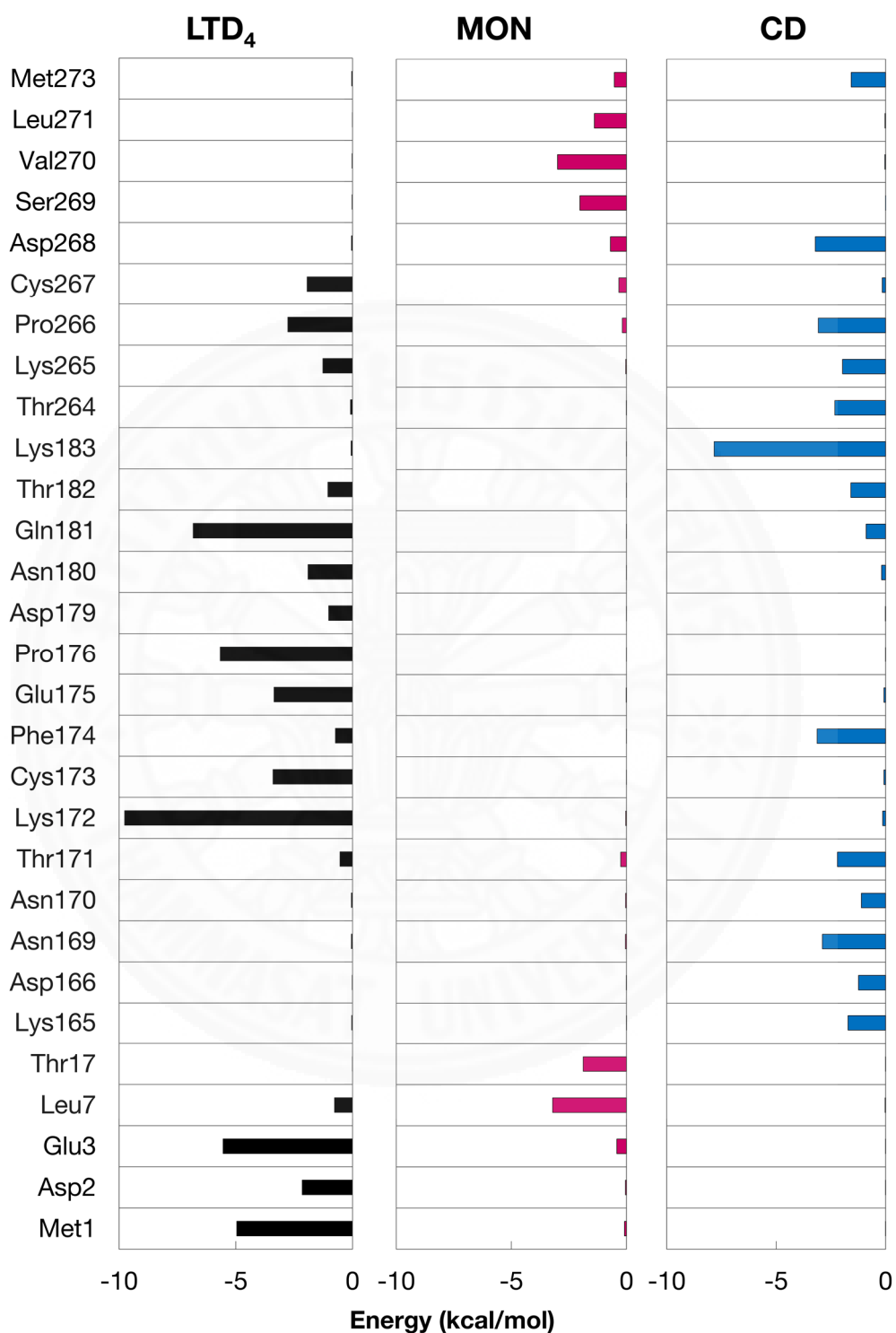


Figure 4.44: Total energy decomposition from selected interval of C1EXT systems.

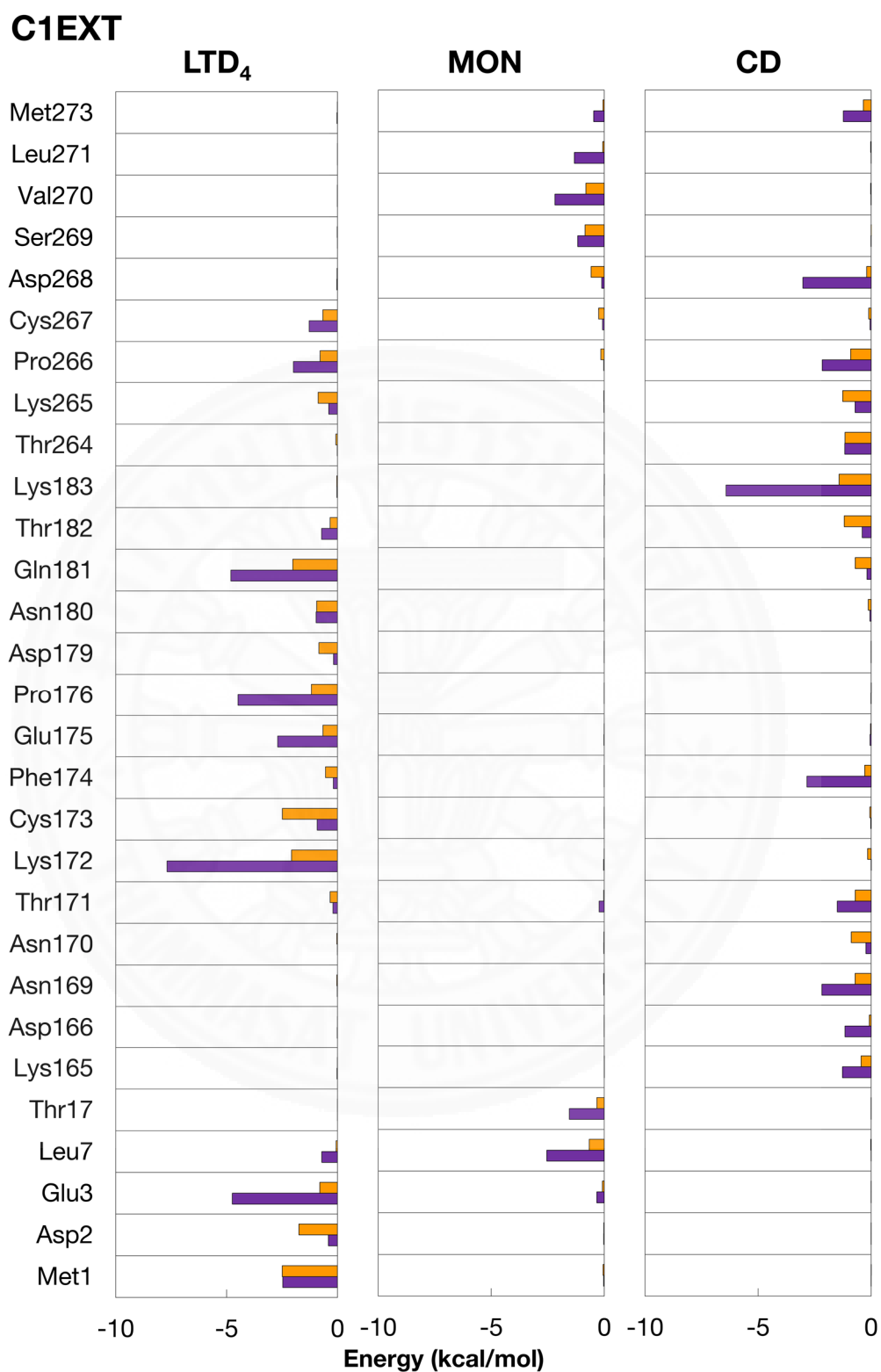


Figure 4.45: Sidechain and backbone energy of C1EXT systems. Backbone and sidechain energy shown as orange and purple bar plot, respectively.

C2EXT

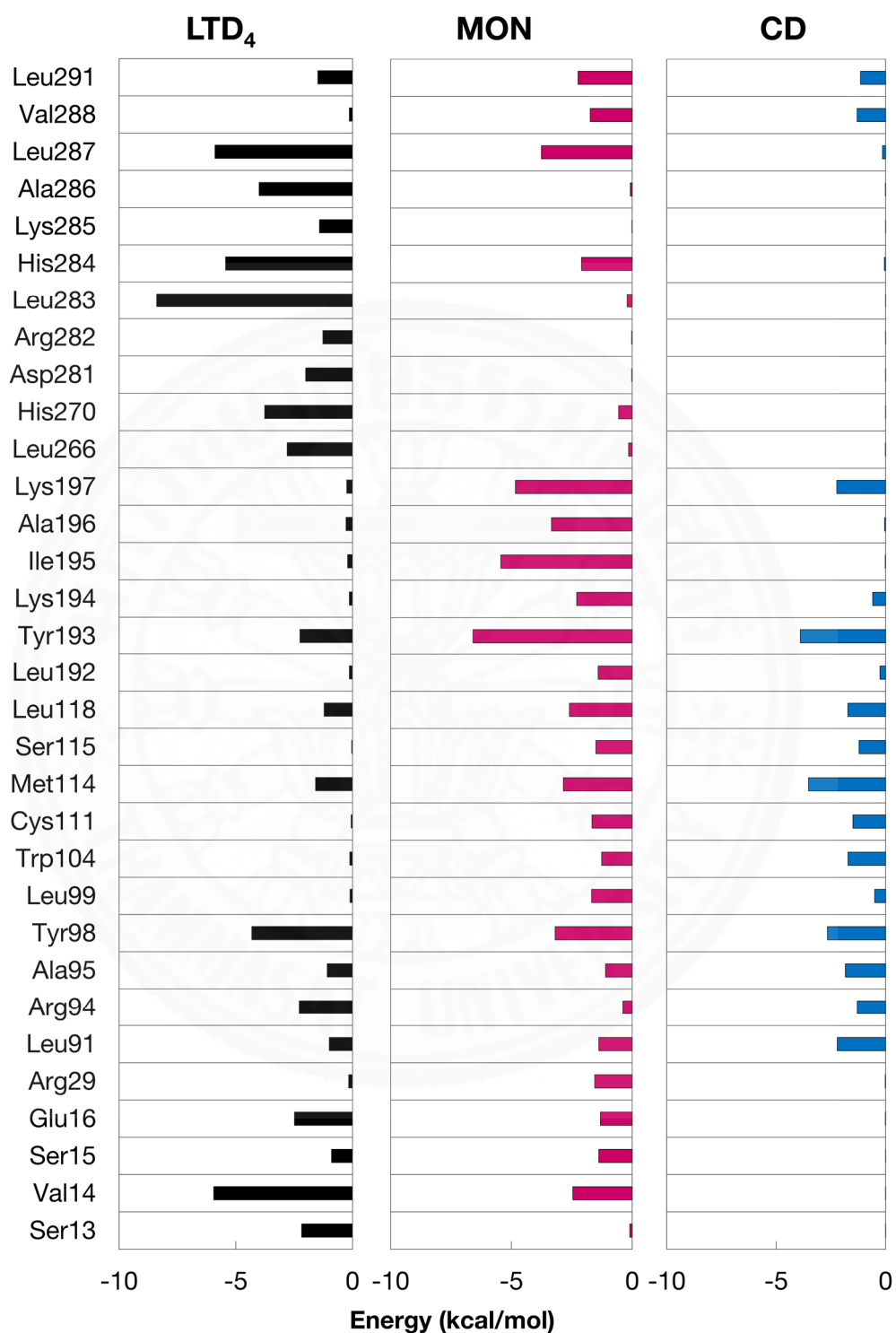


Figure 4.46: Total energy decomposition from selected interval of C2EXT systems.

C2EXT

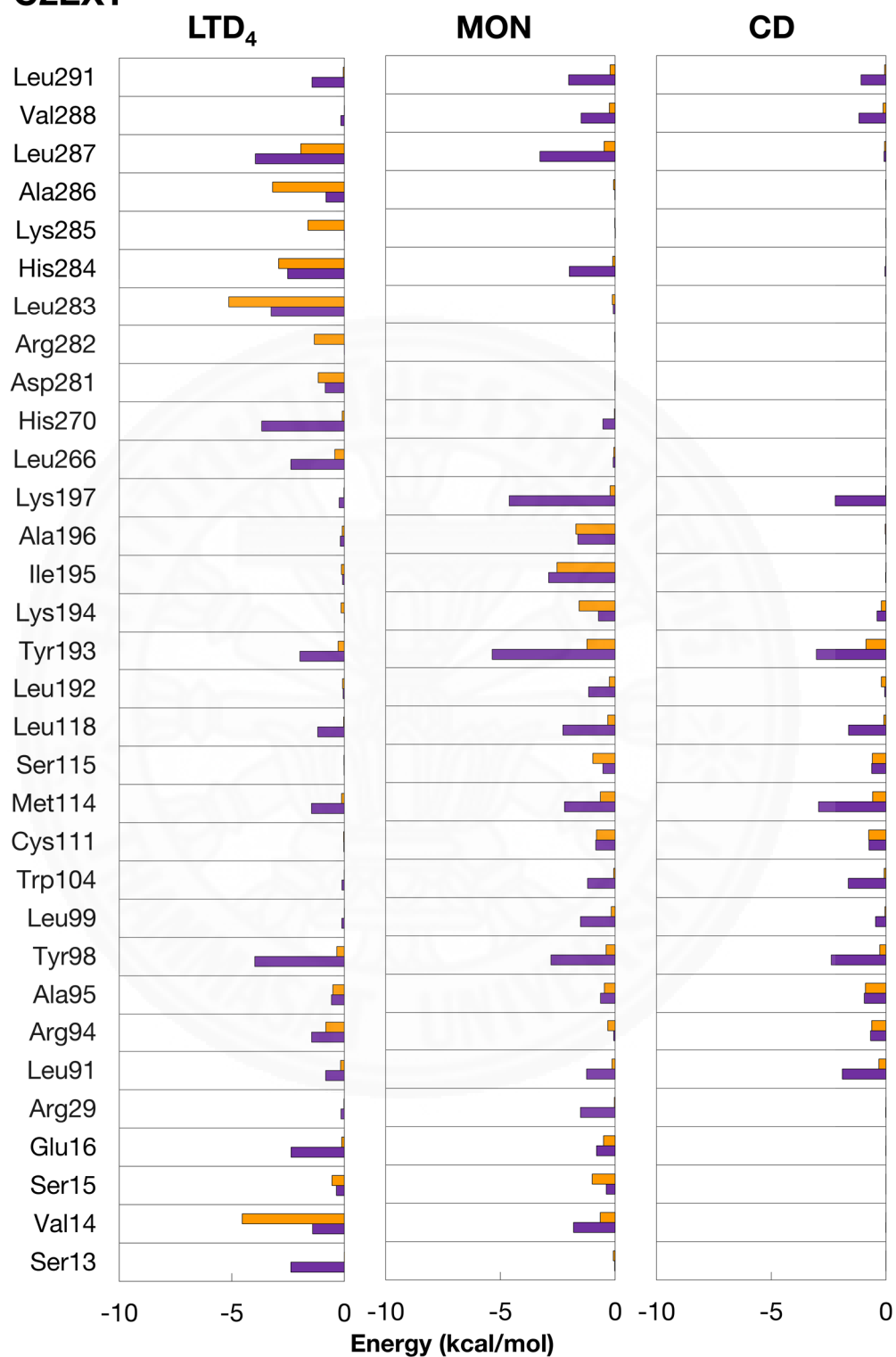


Figure 4.47: Sidechain and backbone energy of C2EXT systems. Backbone and sidechain energy shown as orange and purple bar plot, respectively.

Consequently, specific frame of all 5-LO complex systems within 25 to 30 ns interval can be selected to investigate interaction between both CysLTRs and ligands. However, superimposition between receptor structures in each system have been performed first in order to observe difference between each system as shown in Figure 4.48, Figure 4.49, and Figure 4.50. Incorporated with measurement of C_{α} -RMSD of receptor in each complex system as listed in Table 4.12, Table 4.13, and Table 4.14.

C1INT

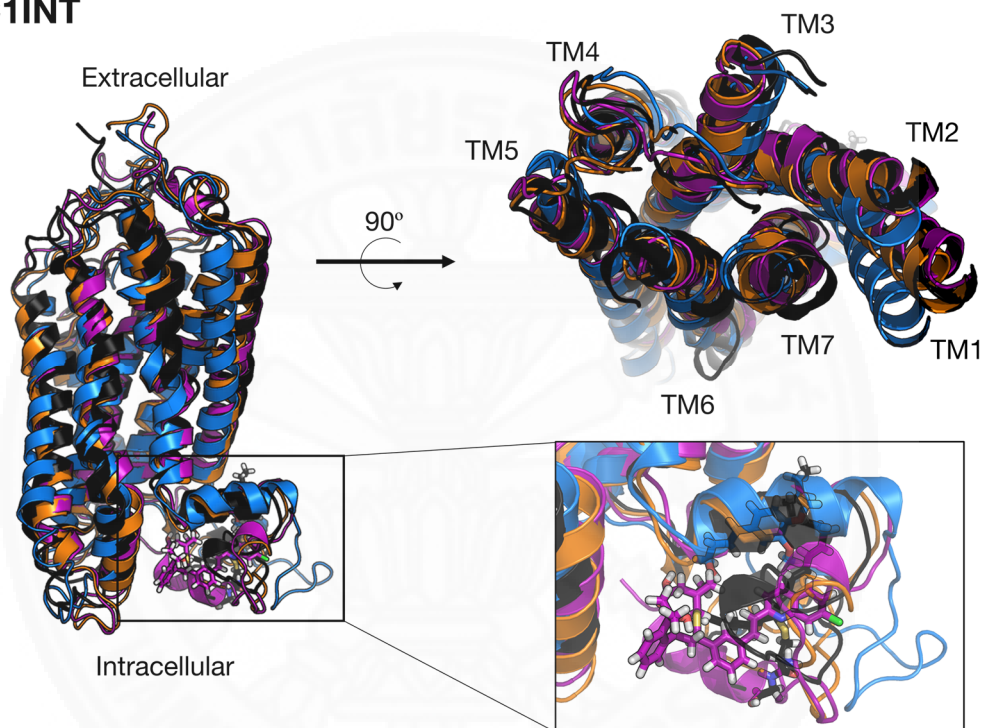


Figure 4.48: Superimposition of C1INT complex systems. CysLTR₁ complex with LTD₄, MON, and CD presented as black, purple, and blue ribbon, respectively. Pure CysLTR₁ presented as orange ribbon. All ligands shown as stick model with the same color as bound CysLTR₁.

Table 4.12: RMSD of selected frame from C1INT complexes and initial structure.

RMSD (Å)	C1_initial	LTD ₄	MON	CD
C1_initial	0.00	3.38	2.82	4.68
LTD₄	3.38	0.00	3.97	4.98
MON	2.82	3.97	0.00	5.67
CD	4.68	4.98	5.67	0.00

C1EXT

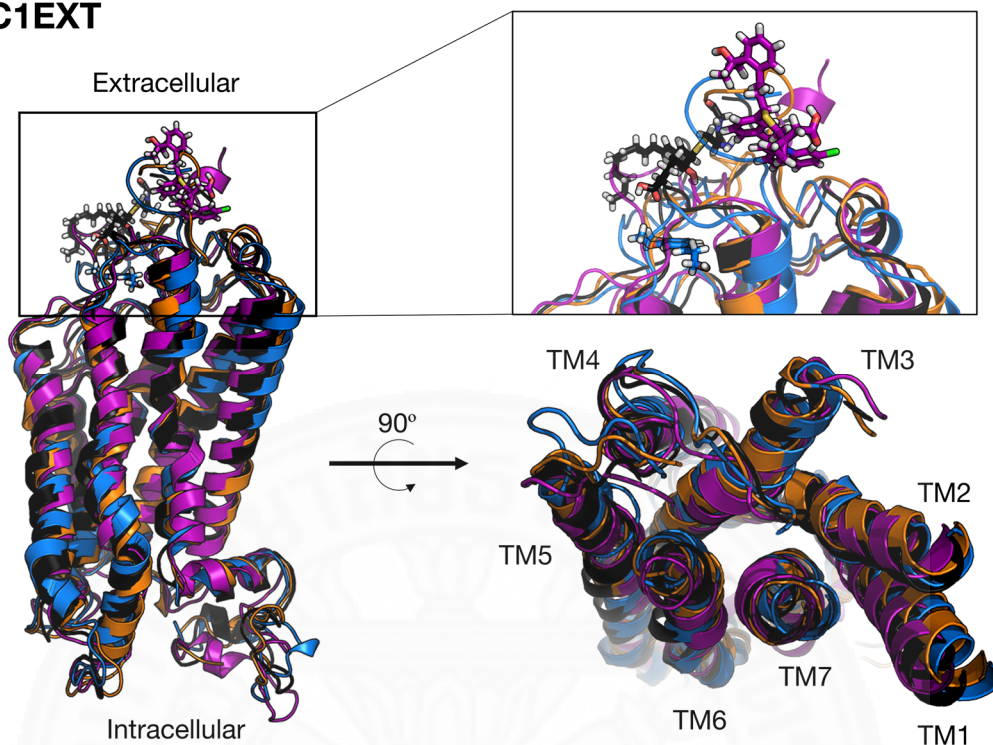


Figure 4.49: Superimposition of C1EXT complex systems. CysLTR₁ complex with LTD₄, MON, and CD presented as black, purple, and blue ribbon, respectively. Pure CysLTR₁ presented as orange ribbon. All ligands shown as stick model with the same color as bound CysLTR₁.

Table 4.13: RMSD of selected frame from C1EXT complexes and initial structure.

RMSD (Å)	C1_initial	LTD ₄	MON	CD
C1_initial	0.00	2.52	3.47	2.70
LTD₄	2.52	0.00	3.03	3.08
MON	3.47	3.03	0.00	3.71
CD	2.70	3.08	3.71	0.00

For C1INT complex systems, the selected snapshots were 28, 29, and 28 ns for C1INT-LTD₄, C1INT-MON, and C1INT-CD complex, respectively. CysLTR₁ shows high deviation from initial structure when it bind with CD especially in TM1, TM2, TM3, and TM5. It has lower deviation when bind with LTD₄. However, there is noticeable deviation in TM3, TM5, TM6, and TM7. The lowest deviation came from binding with MON which result in slight movement of TM1. Thus, this could be an

evidence of inhibition mechanism of MON that restrict movement of transmembrane helices to prevent binding between G-protein and CysLTR₁. Nevertheless, this property could not be applied with binding of CD in the intracellular binding site. For C1EXT complex systems, the selected snapshots were 28, 28, and 29 ns for C2EXT-LTD₄, C1EXT-MON, and C1EXT-CD complex, respectively. CysLTR₁ shows high deviation from initial structure when it bind with MON mainly in TM1 and TM2. It has lower deviation when bind with CD. However, there is some deviation in TM3 and TM7. The lowest deviation came from binding with LTD₄ which result in small movement of TM1. Hence, high deviation of receptor structure after binding with MON on extracellular site is an evidence of unstable receptor-ligand complex which could not prevent structural change of receptor. In other hand, receptor shows less structural movement after binding with CD in the extracellular binding site and this could be evidence of inhibition by CD toward CysLTR₁.

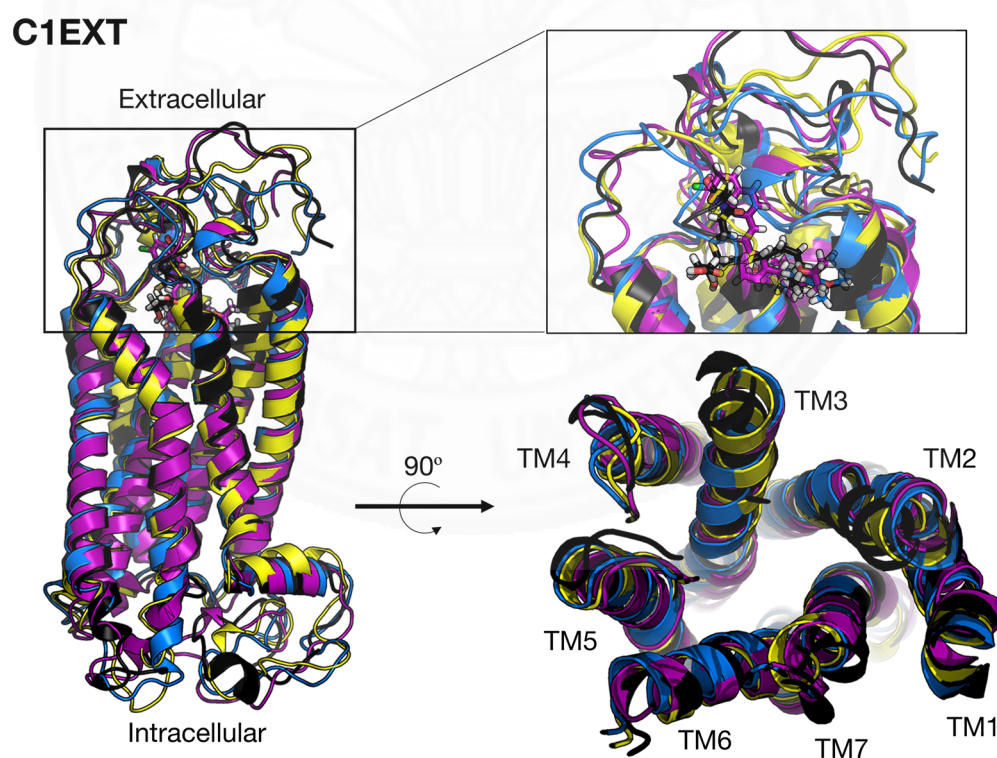


Figure 4.50: Superimposition of C2EXT complex systems. CysLTR₂ complex with LTD₄, MON, and CD presented as black, purple, and blue ribbon, respectively. Pure CysLTR₂ presented as yellow ribbon. All ligands shown as stick model with the same color as bound CysLTR₂.

Table 4.14: RMSD of selected frame from C2EXT complexes and initial structure.

RMSD (Å)	C2_initial	LTD₄	MON	CD
C2_initial	0.00	2.95	3.27	2.39
LTD₄	2.95	0.00	3.17	3.08
MON	3.27	3.17	0.00	3.33
CD	2.39	3.08	3.33	0.00

For C2EXT complex systems, the selected snapshots were 28, 29, and 27 ns for C2EXT-LTD₄, C2EXT-MON, and C2EXT-CD complex, respectively. CysLTR₂ shows high deviation from initial structure when it bind with MON particularly in TM3, TM6, TM7, and Helix8. It has lower deviation when bind with LTD₄. However, there is prominent deviation in TM2 and Helix8. The lowest deviation came from binding with CD which result in small movement of TM3 and Helix8. Therefore, high deviation of receptor after binding with MON is the result of inefficient prevention on structural change of receptor. Even though, binding affinity of MON towards CysLTR₂ is higher than CysLTR₁. In addition, similar to result from C2EXT-CD complex, receptor shows less movement after binding with CD and this could be an evidence of possible inhibition on CysLTR₂.

Selected snapshot from MD (as mentioned in the previous part) have been used to represent ligand's alignment and receptor-ligand interaction as shown in Figure 4.51, Figure 4.52, Figure 4.53, Figure 4.54, Figure 4.55, and Figure 4.56. For C1INT complex systems, all ligands are bound within the same area close to Helix 8 but they have quite different interaction. LTD₄ forms two hydrogen bonds between its two carboxyl and amino group with protonated amine group of Lys54, carbonyl group of Lys336, and carboxylate group of Val337. Its hydroxyl group also forms another hydrogen bonds with carbonyl group of Ile334. Aliphatic hydrocarbon atoms of LTD₄ also occur interaction with nearby residue to stabilize the complex. MON forms one hydrogen bond between its hydroxyl group and amino group of Asn301. Moreover, aromatic hydrocarbon atoms of MON occur the interaction with many nearby residues. CD forms one hydrogen bond between its hydroxyl group and guanidinium group of Arg305. Aromatic hydrocarbon atoms of CD occur interaction with nearby residue leading by

Pi-Cation interaction with protonated amine group of Lys50. For C1EXT complex systems, LTD₄ and MON bound on receptor close to N-terminal area. But, CD bound on extracellular loop region. Thus, binding mode of these ligands are quite different as well. LTD₄ forms two hydrogen bonds between its carboxyl and hydroxyl group with protonated amine group of Lys172 and amino group of Cys267. It also forms another two hydrogen bonds between its two amino groups with carbonyl group of Met1 and Asp2. No evidence of other non-covalent interaction between LTD₄ and nearby residue. Aromatic hydrocarbon atoms of MON occur interaction with only two nearby residues which result in weak receptor-ligand interaction. CD forms one hydrogen bond between its hydroxyl group and carboxylate group of Asp268. Moreover, aromatic hydrocarbon atoms of CD also occur interaction with nearby residue leading by Pi-Pi interaction with aromatic ring of Phe174 and Pi-Cation interaction with protonated amine group of Lys183. For C2EXT complex systems, all ligands bound on extracellular binding pocket near TM2, TM3, and TM7. LTD₄ forms two hydrogen bonds between its two carboxyl groups with carbonyl group of Val14 and amino group of Ala286 and Leu287. Its amino group also forms hydrogen bond with carboxylate group of Glu16. The aliphatic hydrocarbon atoms of LTD₄ occur interaction with nearby residues. MON forms hydrogen bond between its carboxyl group and protonated amine group of Lys197. Aromatic hydrocarbon atoms of MON occur the interaction with nearby residues leading by two Pi-Pi interactions with aromatic ring of Tyr98 and Tyr193. CD forms hydrogen bond between its hydroxyl group and protonated amine group of Lys197. Moreover, aromatic hydrocarbon atoms of CD occur interaction with nearby residue leading by Pi-Pi interaction with aromatic ring of Tyr193 which very similar to MON.

Consequently, all receptor-ligand relationships were in line with result from molecular docking and can be used to confirm prediction from pairwise energy decomposition as well. For this reason, CD has possibility to bind with both CysLTRs but the exact inhibition mechanism cannot be drawn from this short simulation study. However, it has possibility to inhibit both receptors by limit receptor's structural movement in order to prevent binding with G-protein.

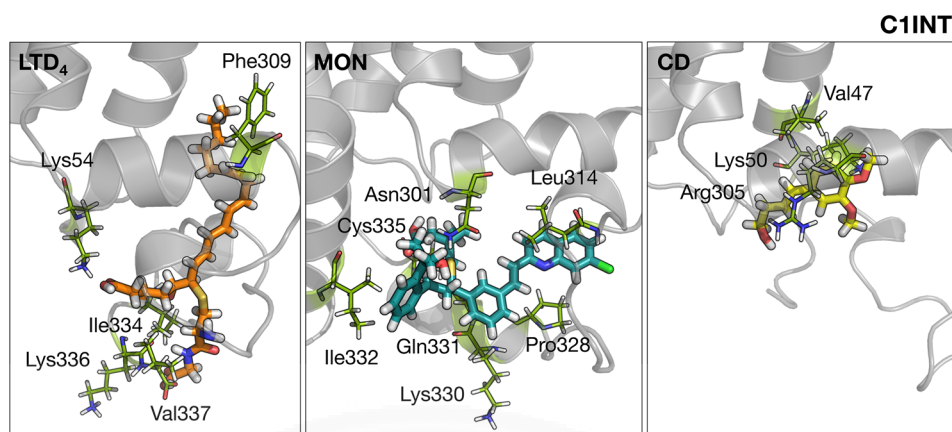


Figure 4.51: Binding site and ligand conformation from selected snapshot of C1INT. Receptor structure shown as grey ribbon. The interacting amino acid residue shown as green stick model. LTD4, MON, and CD shown as orange, teal, and yellow stick model, respectively.

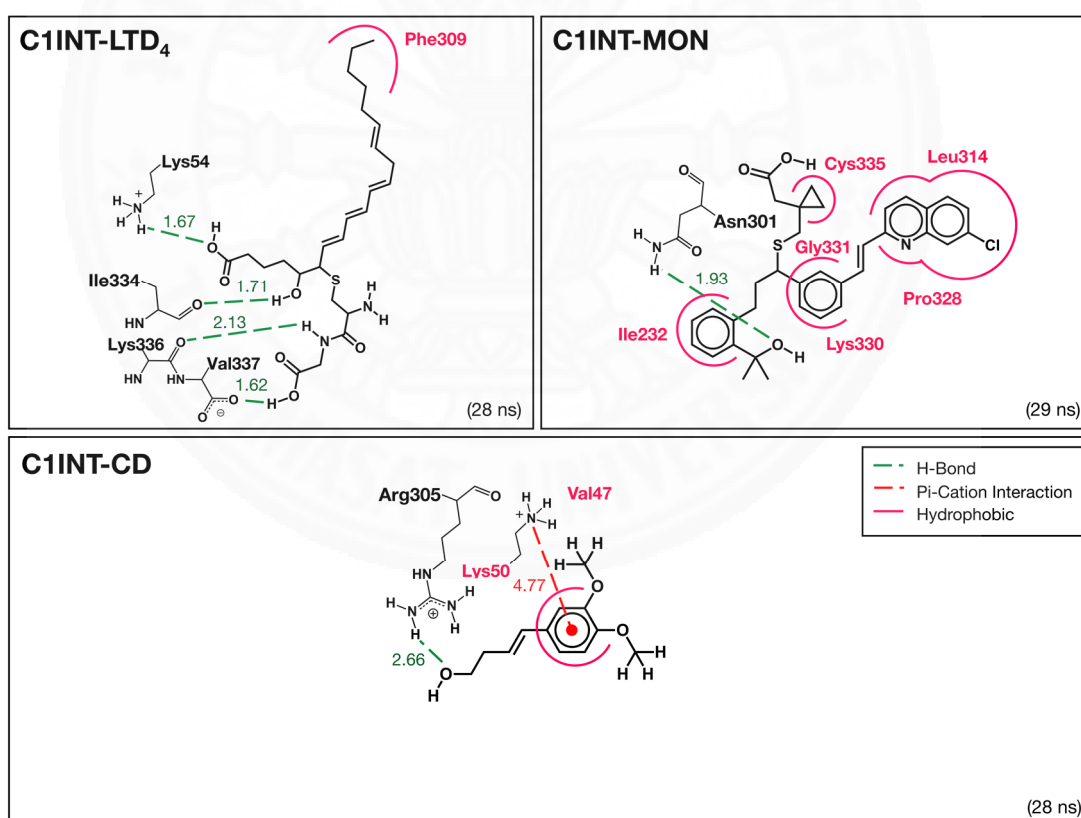


Figure 4.52: 2-D chemical interaction of selected frames from C1INT systems. Hydrogen bonds shown as green dash lines. Hydrophobic interactions (Van der Waals) shown as pink curve lines. Pi-Cation interaction shown as red dash line. All distance labels presented in Å unit

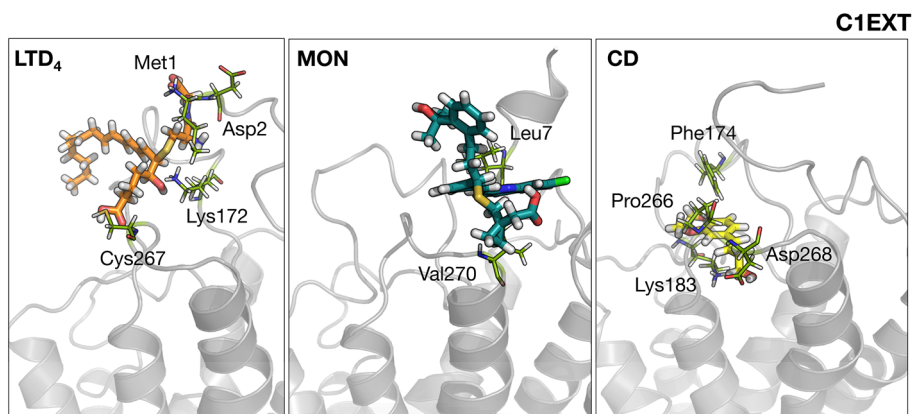


Figure 4.53: Binding site and ligand conformation from selected snapshot of C1EXT. Receptor structure shown as grey ribbon. The interacting amino acid residue shown as green stick model. LTD4, MON, and CD shown as orange, teal, and yellow stick model, respectively.

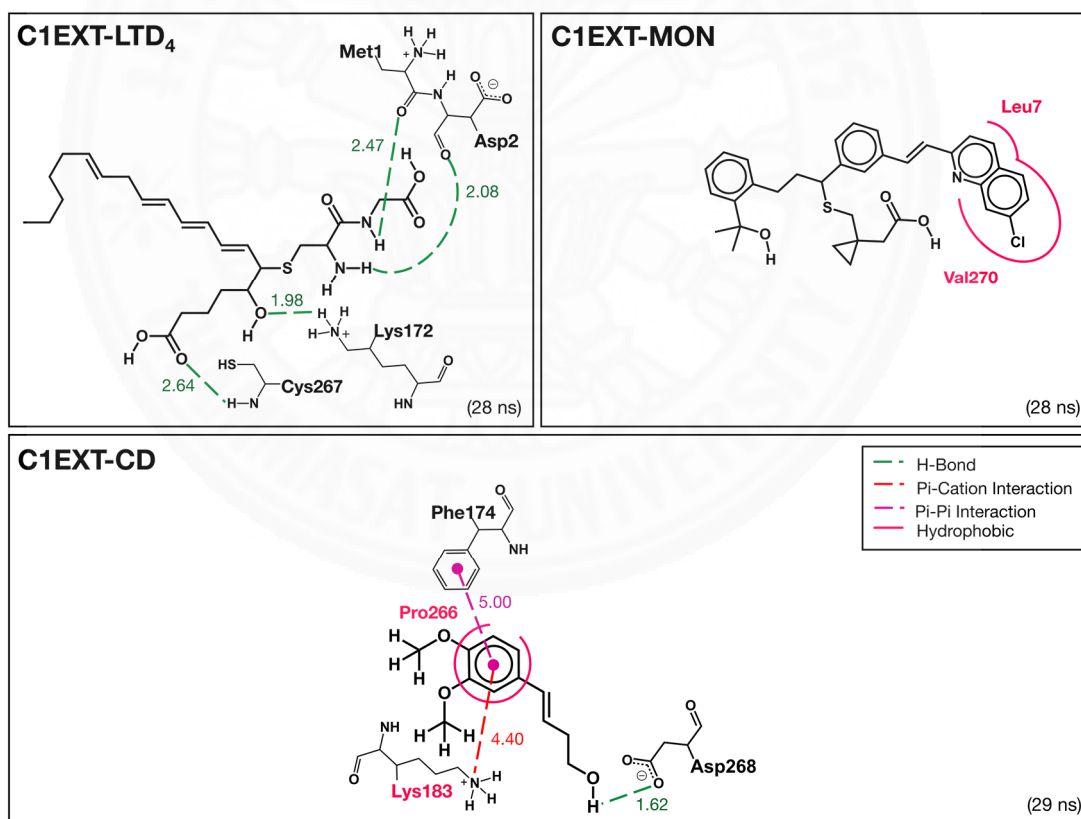


Figure 4.54: 2-D chemical interaction of selected frames from C1EXT systems. Hydrogen bonds shown as green dash lines. Hydrophobic interactions (Van der Waals) shown as pink curve lines. Pi-Pi and Pi-Cation interaction shown as purple and red dash line, respectively. All distance labels presented in Å unit.

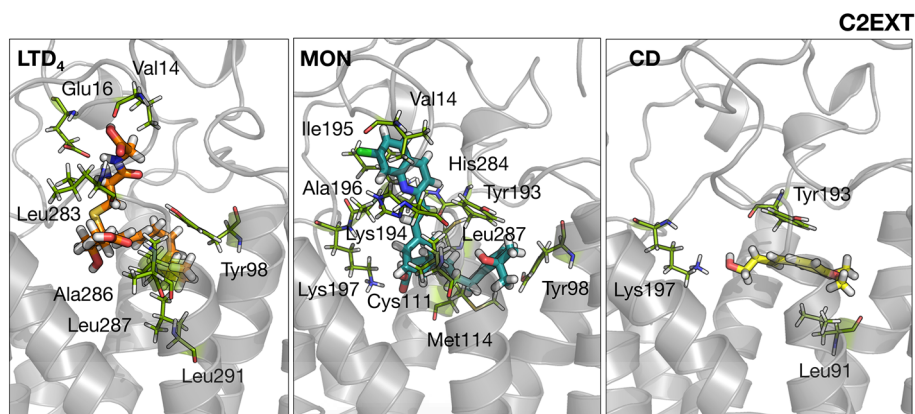


Figure 4.55: Binding site and ligand conformation from selected snapshot of C2EXT. Receptor structure shown as grey ribbon. The interacting amino acid residue shown as green stick model. LTD4, MON, and CD shown as orange, teal, and yellow stick model, respectively.

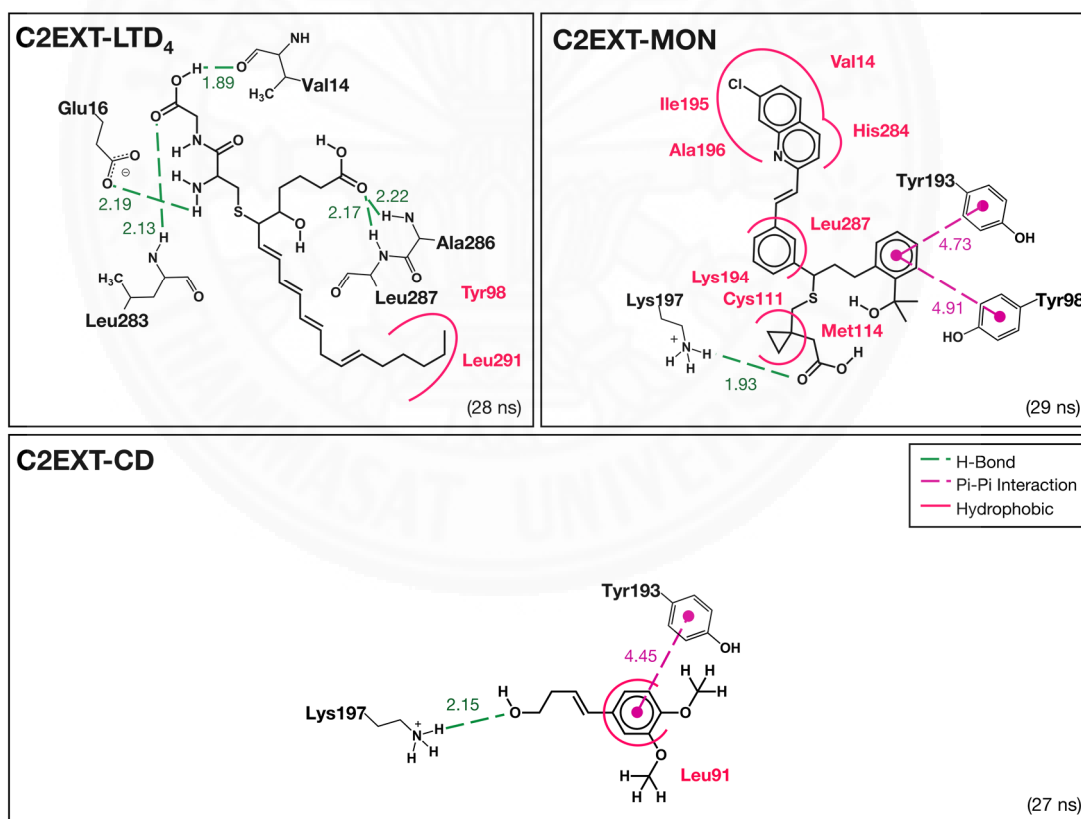


Figure 4.56: 2-D chemical interaction of selected frames from C2EXT systems. Hydrogen bonds shown as green dash lines. Hydrophobic interactions (Van der Waals) shown as pink curve lines. Pi-Pi interaction shown as purple dash line. All distance labels presented in Å unit.

Chapter 5

Conclusions and Recommendations

For 5-LO systems, the calculated mean binding energy from molecular docking of CD and DMP can be considered as similar to AA which is 5-LO natural substrate. Therefore, this lead to possibility that isolated compounds from Plai could bind with 5-LO enzyme. However, analysis of result based on binding energy only are not reliable enough. Thus, binding modes of each ligand revealed that all ligands are possible to bind on 5-LO in the specific region close to Fe^{2+} ion which is an evidence of competitive inhibition behavior. AA and ZIL have similar binding mode. Even though, CD and DMP have the similar chemical structure, but their binding mode on 5-LO are different. DMP has similar binding characteristic as AA and ZIL. Unlike CD that have no similar interaction with other ligands. Nevertheless, it still bound within the same binding pocket. From MD simulations, the calculated binding energy and pairwise energy decomposition can be used to predict binding affinity and major interacting amino acid residues of all 5-LO complex systems. Thus, CD and DMP have possibility to inhibit 5-LO because their calculated binding energy are quite similar to ZIL. However, due to CD bound with 5-LO on different binding site from other ligands, the interacting amino acid residues are quite different. Therefore, binding modes of ligands have been further investigated to reveal the key interacting amino acid residues. As expected, it give the information of key interacting residues following prediction from pairwise energy decomposition. AA and ZIL have Leu420 and Ala424 as key interacting amino acid residue by forming strong hydrogen bonds. But, DMP has Phe421 and Asn425 as key interacting amino acid residues by forming strong hydrogen bond and hydrophobic interaction. Unlike others, CD has Phe177, Asn554, and Ile673 as key interacting amino acid residues by forming strong hydrogen bonds and hydrophobic interactions. This analysis also show similar relationship that we have got from molecular docking. Moreover, solvent accessibility surface area (SASA) calculation revealed the similarity of 5-LO binding pocket cavity between 5-LO complex with AA and CD. In other hand, binding with ZIL and DMP can lead to reduction of 5-LO binding pocket cavity. Both properties give possibility to prevent the binding between 5-LO and AA. Consequently,

all analysis of simulation results have shown that isolated compounds from Plai (CD and DMP) have possibility to be potent inhibitor of 5-LO enzyme.

For CysLTRs systems, the calculated mean binding energy from molecular docking shows possibility of binding between CD and DMP on extracellular site of CysLTR₁ and CysLTR₂. However, LTD₄ and MON are preferred to bind on intracellular site of CysLTR₁ instead. In addition, binding modes of each ligand revealed different chemical interaction between isolated compounds from Plai and the other two ligands with nearby amino acid residues. These could be result from structural difference among ligands. Due to similar properties of CD and DMP incorporated with recent toxicology data of DMP, only CD has been chosen to perform further calculations. From MD simulations, calculated binding energy and pairwise energy decomposition can be used to predict binding affinity and major interacting amino acid residues of all CysLTRs complex systems. As the result, CD have possibility to bind on both CysLTRs with the same binding site as predicted in molecular docking. The investigation on binding mode of each ligand revealed key interacting amino acid residues for each CysLTRs complex. As expected, these major chemical interactions can be used to support calculated binding energy result; the higher strength of interaction, the lower binding energy. Moreover, superimposition between CysLTRs structure in complex systems revealed possible inhibition mechanism of CD on both receptors by limit receptor's structural movement in order to prevent binding with G-protein. These observation came from behavior of CysLTR₁ after binding with MON on intracellular binding site. Consequently, all analysis of simulation results have shown that CD has possibility to bind with both CysLTRs but its inhibition mechanism cannot be clearly explained.

Finally, both isolated compounds have possibility to bind with 5-LO enzyme and CysLTRs receptor. The possibility of their inhibition towards 5-LO is quite high. In other hand, there is possibility that they will also inhibit CysLTRs. But, with short-period MD simulation, movement of receptor cannot be fully investigated and the exact inhibition mechanism cannot be made. Thus, with the current available information, isolated compounds from Plai can be considered as possible antiasthmatic substances from natural source for further study and development in the future.

References

- [1] Asher, I., & Pearce, N. (2014). Global burden of asthma among children. *Int J Tuberc Lung Dis*, 18(11), 1269-1278.
- [2] Pandya, D., Puttanna, A., & Balagopal, V. (2014). Systemic Effects of Inhaled Corticosteroids: An Overview. *Open Respir Med J*, 8, 59-65.
- [3] Luhadia, S. K. (2014). Steroid resistant asthma. *J Assoc Physicians India*, 62(3 Suppl), 38-40.
- [4] Hedi, H., & Norbert, G. (2004). 5-Lipoxygenase Pathway, Dendritic Cells, and Adaptive Immunity. *J Biomed Biotechnol*, 2004(2), 99-105.
- [5] Mastalerz, L., & Kumik, J. (2010). Antileukotriene drugs in the treatment of asthma. *Pol Arch Med Wewn*, 120(3), 103-108.
- [6] Werz, O., & Steinhilber, D. (2006). Therapeutic options for 5-lipoxygenase inhibitors. *Pharmacol Ther*, 112(3), 701-718.
- [7] Panichyupakaranunt, P., & Latae, L. (2013). Plai: Chemical Compositions, Pharmacological Properties, Toxicology, and Quality Control. *J Thai Tradit Altern Med*, 11(2), 123-137.
- [8] *Thai Herbal Pharmacopoeia*. (2009). Department of Medical Sciences, Ministry of Public Health.
- [9] Jeenapongsa, R., Yoovathaworn, K., Sriwatanakul, K. M., Pongprayoon, U., & Sriwatanakul, K. (2003). Anti-inflammatory activity of (E)-1-(3,4-dimethoxyphenyl) butadiene from *Zingiber cassumunar* Roxb. *J Ethnopharmacol*, 87(2-3), 143-148.
- [10] O'Byrne, P. M. (1998). Asthma treatment: antileukotriene drugs. *Can Respir J*, 5 Suppl A, 64a-70a.
- [11] Busse, W. W., & Lemanske, R. F. J. (2001). Asthma. *N Engl J Med*, 344(5), 350-362.
- [12] Drazen, J. M., Israel, E., & O'Byrne, P. M. (1999). Treatment of Asthma with Drugs Modifying the Leukotriene Pathway. *N Engl J Med*, 340(3), 197-206.
- [13] Dahlen, S. E. (2006). Treatment of asthma with antileukotrienes: first line or last resort therapy? *Eur J Pharmacol*, 533(1-3), 40-56.

- [14] Mullane, K. (2011). The increasing challenge of discovering asthma drugs. *Biochem Pharmacol*, 82(6), 586-599.
- [15] O'Byrne, P. M. (1997). Leukotrienes in the pathogenesis of asthma. *Chest*, 111(2 Suppl), 27s-34s.
- [16] Rådmark, O., & Samuelsson, B. (2010). Regulation of the activity of 5-lipoxygenase, a key enzyme in leukotriene biosynthesis. *Biochem Biophys Res Commun*, 396(1), 105-110.
- [17] Rådmark, O., Werz, O., Steinhilber, D., & Samuelsson, B. (2007). 5-Lipoxygenase: regulation of expression and enzyme activity. *Trends Biochem Sci*, 32(7), 332-341.
- [18] Rådmark, O. (2002). Arachidonate 5-lipoxygenase. *Prostaglandins Other Lipid Mediat*, 68-69, 211-234.
- [19] Venugopala, K. N., Govender, R., Khedr, M. A., Venugopala, R., Aldhubiab, B. E., Harsha, S., & Odhav, B. (2015). Design, synthesis, and computational studies on dihydropyrimidine scaffolds as potential lipoxygenase inhibitors and cancer chemopreventive agents. *Drug Des Devel Ther*, 9, 911-921.
- [20] Hui, Y., & Funk, C. D. (2002). Cysteinyl leukotriene receptors. *Biochem Pharmacol*, 64(11), 1549-1557.
- [21] Capra, V. (2004). Molecular and functional aspects of human cysteinyl leukotriene receptors. *Pharmacol Res*, 50(1), 1-11.
- [22] Zhang, M.-Q., & Zwaagstra, M. E. (1997). Structural requirements for leukotriene CysLT1 receptor ligands. *Curr Med Chem*, 4, 229-246.
- [23] Zhang, M.-Q., Zwaagstra, M. E., Nederkoorn, P. H. J., & Timmerman, H. (1997). The Role Of Arginine in The Binding of LTD4 Antagonists to cysLT1 Receptors of Guinea Pig Lung. *Bioorg Med Chem Lett*, 7(10), 1331-1336.
- [24] Zwaagstra, M. E., Schoenmakers, S. H. H. F., Nederkoorn, P. H. J., Gelens, E., Timmerman, H., & Zhang, M.-Q. (1998). Development of a Three-Dimensional CysLT1 (LTD4) Antagonist Model with an Incorporated Amino Acid Residue from the Receptor. *J Med Chem*, 41(9), 1439-1445.
- [25] Dong, X., Zhao, Y., Huang, X., Lin, K., Chen, J., Wei, E., Liu, T., & Hu, Y. (2013). Structure-based drug design using GPCR homology modeling: Toward

- the discovery of novel selective CysLT2 antagonists. *Eur J Med Chem*, 62, 754-763.
- [26] Altschul, S. F., Gish, W., Miller, W., Myers, E. W., & Lipman, D. J. (1990). Basic local alignment search tool. *J Mol Biol*, 215(3), 403-410.
- [27] Chothia, C., & Lesk, A. M. (1986). The relation between the divergence of sequence and structure in proteins. *The EMBO Journal*, 5(4), 823-826.
- [28] Chung, S. Y., & Subbiah, S. (1996). A structural explanation for the twilight zone of protein sequence homology. *Structure*, 4(10), 1123-1127.
- [29] Kelley, L. A., Mezulis, S., Yates, C. M., Wass, M. N., & Sternberg, M. J. E. (2015). The Phyre2 web portal for protein modeling, prediction and analysis. [Protocol]. *Nat Protoc*, 10(6), 845-858.
- [30] Kelley, L. A., & Sternberg, M. J. (2009). Protein structure prediction on the Web: a case study using the Phyre server. *Nat Protoc*, 4(3), 363-371.
- [31] Gopal, S., Schroeder, M., Pieper, U., Sczyrba, A., Aytekin-Kurban, G., Bekiranov, S., Fajardo, J. E., Eswar, N., Sanchez, R., Sali, A., & Gaasterland, T. (2001). Homology-based annotation yields 1,042 new candidate genes in the *Drosophila melanogaster* genome. *Nat Genet*, 27(3), 337-340.
- [32] Baker, D., & Sali, A. (2001). Protein structure prediction and structural genomics. *Science*, 294(5540), 93-96.
- [33] Evans, J. F. (2003). The cysteinyl leukotriene receptors. *Prostaglandins Leukot Essent Fatty Acids*, 69(2-3), 117-122.
- [34] Grossfield, A., Pitman, M. C., Feller, S. E., Soubias, O., & Gawrisch, K. (2008). Internal hydration increases during activation of the G protein-coupled receptor rhodopsin. *J Mol Biol*, 381(2), 478-486.
- [35] Li, F., Chordia, M. D., Woodling, K. A., & Macdonald, T. L. (2007). Irreversible Alkylation of Human Serum Albumin by Zileuton Metabolite 2-Acetylbenzothiophene-S-oxide: A Potential Model for Hepatotoxicity. *Chem Res Toxicol*, 20(12), 1854-1861.
- [36] Panthong, A., Kanjanapothi, D., Niwatananant, W., Tuntiwachwuttikul, P., & Reutrakul, V. (1997). Anti-inflammatory activity of compound D {(E)-4-(3',4'-dimethoxyphenyl)but-3-en-2-ol} isolated from *Zingiber cassumunar* Roxb. *Phytomedicine*, 4(3), 207-212.

- [37] Pongprayoon, U., Tuchinda, P., Claeson, P., Sematong, T., Reutrakul, V., & Soontornsaratune, P. (1997). Topical antiinflammatory activity of the major lipophilic constituents of the rhizome of *Zingiber cassumunar*. Part II: Hexane extractives. *Phytomedicine*, 3(4), 323-326.
- [38] Ozaki, Y., Kawahara, N., & Harada, M. (1991). Anti-inflammatory effect of *Zingiber cassumunar* Roxb. and its active principles. *Chem Pharm Bull (Tokyo)*, 39(9), 2353-2356.
- [39] Poachanukoon, O., Koontongkaew, S., Monthanapisut, P., & Pattanacharoenchai, N. (2017). Mometasone Furoate Suppresses PMA-Induced MUC-5AC and MUC-2 Production in Human Airway Epithelial Cells. *Tuberc Respir Dis (Seoul)*, 80(1), 60-68.
- [40] Thomas, L. H. (1927). The calculation of atomic fields. *Proc Cambridge Philos Soc*, 23(05), 542-548.
- [41] Fermi, E. (1962). *Collected papers : (Note e memorie)*. Chicago: University of Chicago Press.
- [42] Hohenberg, P., & Kohn, W. (1964). Inhomogeneous Electron Gas. *Phys Rev*, 136(3B), B864-B871.
- [43] Kohn, W., & Sham, L. J. (1965). Self-Consistent Equations Including Exchange and Correlation Effects. *Phys Rev*, 140(4A), A1133-A1138.
- [44] Kim, K., & Jordan, K. D. (1994). Comparison of Density Functional and MP2 Calculations on the Water Monomer and Dimer. *J Phys Chem*, 98(40), 10089-10094.
- [45] Stephens, P. J., Devlin, F. J., Chabalowski, C. F., & Frisch, M. J. (1994). Ab Initio Calculation of Vibrational Absorption and Circular Dichroism Spectra Using Density Functional Force Fields. *J Phys Chem*, 98(45), 11623-11627.
- [46] Boys, S. F. (1950). Electronic Wave Functions. I. A General Method of Calculation for the Stationary States of Any Molecular System. *Proc R Soc London, Ser A*, 200(1063), 542.
- [47] Ditchfield, R., Hehre, W. J., & Pople, J. A. (1971). Self-Consistent Molecular-Orbital Methods. IX. An Extended Gaussian-Type Basis for Molecular-Orbital Studies of Organic Molecules. *J Chem Phys*, 54(2), 724-728.

- [48] Ravindranath, P. A., Forli, S., Goodsell, D. S., Olson, A. J., & Sanner, M. F. (2015). AutoDockFR: Advances in Protein-Ligand Docking with Explicitly Specified Binding Site Flexibility. *PLoS Comput Biol*, 11(12), e1004586.
- [49] Goldman, B. B., & Wipke, W. T. (2000). QSD quadratic shape descriptors. 2. Molecular docking using quadratic shape descriptors (QSDock). *Proteins: Struct Funct Bioinform*, 38(1), 79-94.
- [50] Meng, E. C., Shoichet, B. K., & Kuntz, I. D. (1992). Automated docking with grid-based energy evaluation. *J Comput Chem*, 13(4), 505-524.
- [51] Morris, G. M., Goodsell, D. S., Halliday, R. S., Huey, R., Hart, W. E., Belew, R. K., & Olson, A. J. (1998). Automated docking using a Lamarckian genetic algorithm and an empirical binding free energy function. *J Comput Chem*, 19(14), 1639-1662.
- [52] Feig, M., Onufriev, A., Lee, M. S., Im, W., Case, D. A., & Brooks, C. L. (2004). Performance comparison of generalized born and Poisson methods in the calculation of electrostatic solvation energies for protein structures. *J Comput Chem*, 25(2), 265-284.
- [53] Ajay, & Murcko, M. A. (1995). Computational methods to predict binding free energy in ligand-receptor complexes. *J Med Chem*, 38(26), 4953-4967.
- [54] Herron, D. K., Bollinger, N. G., Chaney, M. O., Varshavsky, A. D., Yost, J. B., Sherman, W. R., & Thingvold, J. A. (1995). Visualization and comparison of molecular dynamics simulations of leukotriene C4, leukotriene D4, and leukotriene E4. *J Mol Graph*, 13(6), 337-341.
- [55] Liu, J., Yang, L., & Hopfinger, A. J. (2009). Affinity of drugs and small biologically active molecules to carbon nanotubes: a pharmacodynamics and nanotoxicity factor? *Mol Pharm*, 6(3), 873-882.
- [56] Parravicini, C., Abbracchio, M. P., Fantucci, P., & Raghino, G. (2010). Forced unbinding of GPR17 ligands from wild type and R255I mutant receptor models through a computational approach. *BMC Struct Biol*, 10(1), 1-18.
- [57] Thangapandian, S., John, S., Arooj, M., & Lee, K. W. (2012). Molecular dynamics simulation study and hybrid pharmacophore model development in human LTA4H inhibitor design. *PLoS One*, 7(4), e34593.

- [58] Eren, G., Macchiarulo, A., & Banoglu, E. (2012). From Molecular Docking to 3D-Quantitative Structure-Activity Relationships (3D-QSAR): Insights into the Binding Mode of 5-Lipoxygenase Inhibitors. *Mol Inform*, 31(2), 123-134.
- [59] De Lucia, D., Lucio, O. M., Musio, B., Bender, A., Listing, M., Dennhardt, S., Koeberle, A., Garscha, U., Rizzo, R., Manfredini, S., Werz, O., & Ley, S. V. (2015). Design, synthesis and evaluation of semi-synthetic triazole-containing caffeic acid analogues as 5-lipoxygenase inhibitors. *Eur J Med Chem*, 101, 573-583.
- [60] Loza-Mejía, M. A., & Salazar, J. R. (2015). Sterols and triterpenoids as potential anti-inflammatories: Molecular docking studies for binding to some enzymes involved in inflammatory pathways. *J Mol Graphics Modell*, 62, 18-25.
- [61] Dennington, R., Keith, T., & Millam, J. (2009). GaussView (Version 5). Shawnee Mission, KS: Semichem Inc.
- [62] Frisch, M. J., Trucks, G. W., Schlegel, H. B., Scuseria, G. E., Robb, M. A., Cheeseman, J. R., Scalmani, G., Barone, V., Mennucci, B., Petersson, G. A., Nakatsuji, H., Caricato, M., Li, X., Hratchian, H. P., Izmaylov, A. F., Bloino, J., Zheng, G., Sonnenberg, J. L., Hada, M., Ehara, M., Toyota, K., Fukuda, R., Hasegawa, J., Ishida, M., Nakajima, T., Honda, Y., Kitao, O., Nakai, H., Vreven, T., Montgomery Jr., J. A., Peralta, J. E., Ogliaro, F., Bearpark, M. J., Heyd, J., Brothers, E. N., Kudin, K. N., Staroverov, V. N., Kobayashi, R., Normand, J., Raghavachari, K., Rendell, A. P., Burant, J. C., Iyengar, S. S., Tomasi, J., Cossi, M., Rega, N., Millam, N. J., Klene, M., Knox, J. E., Cross, J. B., Bakken, V., Adamo, C., Jaramillo, J., Gomperts, R., Stratmann, R. E., Yazyev, O., Austin, A. J., Cammi, R., Pomelli, C., Ochterski, J. W., Martin, R. L., Morokuma, K., Zakrzewski, V. G., Voth, G. A., Salvador, P., Dannenberg, J. J., Dapprich, S., Daniels, A. D., Farkas, Ö., Foresman, J. B., Ortiz, J. V., Cioslowski, J., & Fox, D. J. (2009). Gaussian 09. Wallingford, CT, USA: Gaussian, Inc.
- [63] Morris, G. M., Huey, R., Lindstrom, W., Sanner, M. F., Belew, R. K., Goodsell, D. S., & Olson, A. J. (2009). AutoDock4 and AutoDockTools4: Automated docking with selective receptor flexibility. *J Comput Chem*, 30(16), 2785-2791.

- [64] Jo, S., Kim, T., Iyer, V. G., & Im, W. (2008). CHARMM-GUI: a web-based graphical user interface for CHARMM. *J Comput Chem*, 29(11), 1859-1865.
- [65] Jo, S., Kim, T., & Im, W. (2007). Automated Builder and Database of Protein/Membrane Complexes for Molecular Dynamics Simulations. *PLoS ONE*, 2(9), e880.
- [66] Jo, S., Lim, J. B., Klauda, J. B., & Im, W. (2009). CHARMM-GUI Membrane Builder for Mixed Bilayers and Its Application to Yeast Membranes. *Biophys J*, 97(1), 50-58.
- [67] Wu, E. L., Cheng, X., Jo, S., Rui, H., Song, K. C., Davila-Contreras, E. M., Qi, Y., Lee, J., Monje-Galvan, V., Venable, R. M., Klauda, J. B., & Im, W. (2014). CHARMM-GUI Membrane Builder toward realistic biological membrane simulations. *J Comput Chem*, 35(27), 1997-2004.
- [68] Lee, J., Cheng, X., Swails, J. M., Yeom, M. S., Eastman, P. K., Lemkul, J. A., Wei, S., Buckner, J., Jeong, J. C., Qi, Y., Jo, S., Pande, V. S., Case, D. A., Brooks, C. L., 3rd, MacKerell, A. D., Jr., Klauda, J. B., & Im, W. (2016). CHARMM-GUI Input Generator for NAMD, GROMACS, AMBER, OpenMM, and CHARMM/OpenMM Simulations Using the CHARMM36 Additive Force Field. *J Chem Theory Comput*, 12(1), 405-413.
- [69] Brooks, B. R., Brooks, C. L., 3rd, Mackerell, A. D., Jr., Nilsson, L., Petrella, R. J., Roux, B., Won, Y., Archontis, G., Bartels, C., Boresch, S., Caflisch, A., Caves, L., Cui, Q., Dinner, A. R., Feig, M., Fischer, S., Gao, J., Hodoscek, M., Im, W., Kuczera, K., Lazaridis, T., Ma, J., Ovchinnikov, V., Paci, E., Pastor, R. W., Post, C. B., Pu, J. Z., Schaefer, M., Tidor, B., Venable, R. M., Woodcock, H. L., Wu, X., Yang, W., York, D. M., & Karplus, M. (2009). CHARMM: the biomolecular simulation program. *J Comput Chem*, 30(10), 1545-1614.
- [70] Klauda, J. B., Venable, R. M., Freites, J. A., O'Connor, J. W., Tobias, D. J., Mondragon-Ramirez, C., Vorobyov, I., MacKerell, A. D., Jr., & Pastor, R. W. (2010). Update of the CHARMM all-atom additive force field for lipids: validation on six lipid types. *J Phys Chem B*, 114(23), 7830-7843.
- [71] Venable, R. M., Sodt, A. J., Rogaski, B., Rui, H., Hatcher, E., MacKerell, A. D., Jr., Pastor, R. W., & Klauda, J. B. (2014). CHARMM all-atom additive force

- field for sphingomyelin: elucidation of hydrogen bonding and of positive curvature. *Biophys J*, 107(1), 134-145.
- [72] Discovery Studio Modeling Environment. (2016). San Diego: Dassault Systèmes BIOVIA.
- [73] Schrodinger, LLC. (2015). The PyMOL Molecular Graphics System, Version 1.3.
- [74] Grant, B. J., Rodrigues, A. P., ElSawy, K. M., McCammon, J. A., & Caves, L. S. (2006). Bio3d: an R package for the comparative analysis of protein structures. *Bioinformatics*, 22(21), 2695-2696.
- [75] Skjaerven, L., Yao, X. Q., Scarabelli, G., & Grant, B. J. (2014). Integrating protein structural dynamics and evolutionary analysis with Bio3D. *BMC Bioinformatics*, 15, 399.
- [76] Skjaerven, L., Jariwala, S., Yao, X. Q., & Grant, B. J. (2016). Online interactive analysis of protein structure ensembles with Bio3D-web. *Bioinformatics*, 32(22), 3510-3512.
- [77] Allen, W. J., Lemkul, J. A., & Bevan, D. R. (2009). GridMAT-MD: a grid-based membrane analysis tool for use with molecular dynamics. *J Comput Chem*, 30(12), 1952-1958.
- [78] Case, D. A., Darden, T. A., Cheatham, T. E., Simerling, C. L., Wang, J., Duke, R. E., Luo, R., Walker, R. C., Zhang, W., Merz, K. M., Roberts, B., Hayik, S., Roitberg, A., Seabra, G., Swails, J., Götz, A. W., Kolossváry, I., Wong, K. F., Paesani, F., Vanicek, J., Wolf, R. M., Liu, J., Wu, X., Brozell, S. R., Steinbrecher, T., Gohlke, H., Cai, Q., Ye, X., Wang, J., Hsieh, M.-J., Cui, G., Roe, D. R., Mathews, D. H., Seetin, M. G., Salomon-Ferrer, R., Sagui, C., Babin, V., Luchko, T., Gusarov, S., Kovalenko, A., & Kollman, P. A. (2012). AMBER 12. University of California, San Francisco.
- [79] Case, D. A., Betz, R. M., Botello-Smith, W., Cerutti, D. S., Cheatham, T. E., Darden, T. A., Duke, R. E., Giese, T. J., Gohlke, H., Goetz, A. W., Homeyer, N., Izadi, S., Janowski, P., Kaus, J., Kovalenko, A., Lee, T. S., LeGrand, S., Li, P., Lin, C., Luchko, T., Luo, R., Madej, B., Mermelstein, D., Merz, K. M., Monard, G., Nguyen, H., Nguyen, H. T., Omelyan, I., Onufriev, A., Roe, D. R., Roitberg, A., Sagui, C., Simmerling, C. L., Swails, J., Walker, R. C., Wang, J.,

- Wolf, R. M., Wu, X., Xiao, L., York, D. M., & Kollman, P. A. (2016). AMBER 16. University of California, San Francisco.
- [80] Cornell, W. D., Cieplak, P., Bayly, C. I., Gould, I. R., Merz, K. M., Ferguson, D. M., Spellmeyer, D. C., Fox, T., Caldwell, J. W., & Kollman, P. A. (1995). A Second Generation Force Field for the Simulation of Proteins, Nucleic Acids, and Organic Molecules. *J Am Chem Soc*, 117(19), 5179-5197.
- [81] Wang, J., Wolf, R. M., Caldwell, J. W., Kollman, P. A., & Case, D. A. (2004). Development and testing of a general amber force field. *J Comput Chem*, 25(9), 1157-1174.
- [82] Wang, J., Wang, W., Kollman, P. A., & Case, D. A. (2006). Automatic atom type and bond type perception in molecular mechanical calculations. *J Mol Graph Model*, 25(2), 247-260.
- [83] Genheden, S., & Ryde, U. (2015). The MM/PBSA and MM/GBSA methods to estimate ligand-binding affinities. *Exp Op Drug Disc*, 10(5), 449-461.
- [84] Gilbert, N. C., Bartlett, S. G., Waight, M. T., Neau, D. B., Boeglin, W. E., Brash, A. R., & Newcomer, M. E. (2011). The Structure of Human 5-Lipoxygenase. *Science*, 331(6014), 217-219.
- [85] Gilbert, N. C., Rui, Z., Neau, D. B., Waight, M. T., Bartlett, S. G., Boeglin, W. E., Brash, A. R., & Newcomer, M. E. (2012). Conversion of human 5-lipoxygenase to a 15-lipoxygenase by a point mutation to mimic phosphorylation at Serine-663. *FASEB J*, 26(8), 3222-3229.
- [86] Mashaghi, A., Partovi-Azar, P., Jadidi, T., Nafari, N., Maass, P., Tabar, M. R. R., Bonn, M., & Bakker, H. J. (2012). Hydration strongly affects the molecular and electronic structure of membrane phospholipids. *J Chem Phys*, 136(11), 114709.
- [87] Jones, T. R., Labelle, M., Belley, M., Champion, E., Charette, L., Evans, J., Ford-Hutchinson, A. W., Gauthier, J. Y., Lord, A., Masson, P., & et al. (1995). Pharmacology of montelukast sodium (Singulair), a potent and selective leukotriene D4 receptor antagonist. *Can J Physiol Pharmacol*, 73(2), 191-201.
- [88] Nakagawa, N., Fujita, M., Yonetomi, Y., Tanaka, M., & Obata, T. (2002). CysLT1 Antagonism of Pranlukast, Montelukast and Zafirlukast in the Presence of Serum Albumin. *Jpn Pharmacol Ther*, 30, 191-195.

- [89] Nomenclature and Symbolism for Amino Acids and Peptides. (1984). *Eur J Biochem*, 138(1), 9-37.
- [90] Becke, A. D. (1993). Density-functional thermochemistry. III. The role of exact exchange. *J Chem Phys*, 98(7), 5648-5652.



The seal of Thammasat University is a circular emblem. It features a central five-tiered umbrella (parasol) with a flame-like finial. Radiating from the base of the umbrella are eight lotus petals. The entire emblem is encircled by a ring containing the university's name in Thai script (มหาวิทยาลัยธรรมศาสตร์) at the top and 'THAMMASAT UNIVERSITY' at the bottom, separated by small floral motifs.

Appendices

Appendix A

Amino Acids Sequences Information

A-1 CysLTR₁ Receptor Amino Acids Sequence

(UniProt Database: <http://www.uniprot.org/uniprot/Q9Y271#sequences>)

M	D	E	T	G	N	L	T	V	S	S	A	T	C	H	D	T	I	D	D	F	R	N	Q	V	Y	S	T	L	Y
1									10									20											30
S	M	I	S	V	V	G	F	F	G	N	G	F	V	L	Y	V	L	I	K	T	Y	H	K	K	S	A	F	Q	V
									40									50											60
Y	M	I	N	L	A	V	A	D	L	L	C	V	C	T	L	P	L	R	V	V	Y	Y	V	H	K	G	I	W	L
									70									80											90
F	G	D	F	L	C	R	L	S	T	Y	A	L	Y	V	N	L	Y	C	S	I	F	F	M	T	A	M	S	F	F
									100									110											120
R	C	I	A	I	V	F	P	V	Q	N	I	N	L	V	T	Q	K	K	A	R	F	V	C	V	G	I	W	I	F
									130									140											150
V	I	L	T	S	S	P	F	L	M	A	K	P	Q	K	D	E	K	N	N	T	K	C	F	E	P	P	Q	D	N
									160									170											180
Q	T	K	N	H	V	L	V	L	H	Y	V	S	L	F	V	G	F	I	I	P	F	V	I	I	I	V	C	Y	T
									190									200											210
M	I	I	L	T	L	L	K	K	S	M	K	K	N	L	S	S	H	K	K	A	I	G	M	I	M	V	V	T	A
									220									230											240
A	F	L	V	S	F	M	P	Y	H	I	Q	R	T	I	H	L	H	F	L	H	N	E	T	K	P	C	D	S	V
									250									260											270
L	R	M	Q	K	S	V	V	I	T	L	S	L	A	A	S	N	C	C	F	D	P	L	L	Y	F	F	S	G	G
									280									290											300
N	F	R	K	R	L	S	T	F	R	K	H	S	L	S	S	V	T	Y	V	P	R	K	K	A	S	L	P	E	K
									310									320											330
G	E	E	I	C	K	V																							
									337																				

A-2 CysLTR₂ Receptor Amino Acids Sequence

(UniProt Database: <http://www.uniprot.org/uniprot/Q9NS75#sequences>)

M 1	E	R	K	F	M	S	L	Q	P 10	S	I	S	V	S	E	M	E	P	N 20	G	T	F	S	N	N	N	S	R	N 30	
C	T	I	E	N	F	K	R	E	F 40	F	P	I	V	Y	L	I	I	F	F 50	W	G	V	L	G	N	G	L	S	I 60	
Y	V	F	L	Q	P	Y	K	K	S 70	T	S	V	N	V	F	M	L	N	L 80	A	I	S	D	L	L	F	I	S	T 90	
L	P	F	R	A	D	Y	Y	L	R 100	G	S	N	W	I	F	G	D	L	A 110	C	R	I	M	S	Y	S	L	Y	V 120	
N	M	Y	S	S	I	Y	F	L	T 130	V	L	S	V	V	R	F	L	A	M 140	V	H	P	F	R	L	L	H	V	T 150	
S	I	R	S	A	W	I	L	C	G 160	I	I	W	I	L	I	M	A	S	S 170	I	M	L	L	D	S	G	S	E	Q 180	
N	G	S	V	T	S	C	L	E	L 190	N	L	Y	K	I	A	K	L	Q	T 200	M	N	Y	I	A	L	V	V	G	C 210	
L	L	P	F	F	T	L	S	I	C 220	Y	L	L	I	I	R	V	L	L	K 230	V	E	V	P	E	S	G	L	R	V 240	
S	H	R	K	A	L	T	T	I	I 250	I	T	L	I	I	F	F	L	C	F 260	L	P	Y	H	T	L	R	T	V	H 270	
L	T	T	W	K	V	G	L	C	K 280	D	R	L	H	K	A	L	V	I	T 290	L	A	L	A	A	A	N	A	C	F 300	
N	P	L	L	Y	Y	F	A	G	E 310	N	F	K	D	R	L	K	S	A	L 320	R	K	G	H	P	Q	K	A	K	T 330	
K	C	V	F	P	V	S	V	W	L 340	R	K	E	T	R	V	346														

Remark: The definition of 1 letter amino acid abbreviation is shown in Appendix A: A-5.

114

CysLTR ₁	M	D	E	T	G	N	L	T	V	S	S	A	T	C	H	D	T	I	D	D	F	R	N	Q	V	Y	S	T	L	Y
CysLTR ₂	M	E	R	K	F	M	S	L	Q	P	S	I	S	V	S	E	M	E	P	N	G	T	F	S	N	N	N	S	R	N
	1									10									20										30	
CysLTR ₁	S	M	I	S	V	V	G	F	F	G	N	G	F	V	L	Y	V	L	I	K	T	Y	H	K	K	S	A	F	Q	V
CysLTR ₂	C	T	I	E	N	F	K	R	E	F	F	P	I	V	Y	L	I	I	F	F	W	G	V	L	G	N	G	L	S	I
										40										50									60	
CysLTR ₁	Y	M	I	N	L	A	V	A	D	L	L	C	V	C	T	L	P	L	R	V	V	Y	Y	V	H	K	G	I	W	L
CysLTR ₂	Y	V	F	L	Q	P	Y	K	K	S	T	S	V	N	V	F	M	L	N	L	A	I	S	D	L	L	F	I	S	T
										70										80									90	
CysLTR ₁	F	G	D	F	L	C	R	L	S	T	Y	A	L	Y	V	N	L	Y	C	S	I	F	F	M	T	A	M	S	F	F
CysLTR ₂	L	P	F	R	A	D	Y	Y	L	R	G	S	N	W	I	F	G	D	L	A	C	R	I	M	S	Y	S	L	Y	V
										100										110									120	
CysLTR ₁	R	C	I	A	I	V	F	P	V	Q	N	I	N	L	V	T	Q	K	K	A	R	F	V	C	V	G	I	W	I	F
CysLTR ₂	N	M	Y	S	S	I	Y	F	L	T	V	L	S	V	V	R	F	L	A	M	V	H	P	F	R	L	L	H	V	T
										130										140									150	
CysLTR ₁	V	I	L	T	S	S	P	F	L	M	A	K	P	Q	K	D	E	K	N	N	T	K	C	F	E	P	P	Q	D	N
CysLTR ₂	S	I	R	S	A	W	I	L	C	G	I	I	W	I	L	I	M	A	S	S	I	M	L	L	D	S	G	S	E	Q
										160										170									180	
CysLTR ₁	Q	T	K	N	H	V	L	V	L	H	Y	V	S	L	F	V	G	F	I	I	P	F	V	I	I	I	V	C	Y	T
CysLTR ₂	N	G	S	V	T	S	C	L	E	L	N	L	Y	K	I	A	K	L	Q	T	M	N	Y	I	A	L	V	V	G	C
										190										200									210	
CysLTR ₁	M	I	I	L	T	L	L	K	K	S	M	K	K	N	L	S	S	H	K	K	A	I	G	M	I	M	V	V	T	A
CysLTR ₂	L	L	P	F	F	T	L	S	I	C	Y	L	L	I	I	R	V	L	L	K	V	E	V	P	E	S	G	L	R	V
										220										230									240	
CysLTR ₁	A	F	L	V	S	F	M	P	Y	H	I	Q	R	T	I	H	L	H	F	L	H	N	E	T	K	P	C	D	S	V
CysLTR ₂	S	H	R	K	A	L	T	T	I	I	I	T	L	I	I	F	F	L	C	F	L	P	Y	H	T	L	R	T	V	H
										250										260									270	

CysLTR ₁	L	R	M	Q	K	S	V	V	I	T	L	S	L	A	A	S	N	C	C	F	D	P	L	L	Y	F	F	S	G	G							
CysLTR ₂	L	T	T	W	K	V	G	L	C	280			K	D	R	L	H	K	A	L	V	290			I	T	L	A	L	A	A	A	N	A	C	F	300
CysLTR ₁	N	F	R	K	R	L	S	T	F	R	K	H	S	L	S	S	V	T	Y	V	P	R	K	K	A	S	L	P	E	K							
CysLTR ₂	N	P	L	L	Y	Y	F	A	G	310			E	N	F	K	D	R	L	K	S	320			A	L	R	K	G	H	P	Q	K	A	K	T	330
CysLTR ₁	G	E	E	I	C	K	V																														
CysLTR ₂	K	C	V	F	P	V	S	V	W	L	R	K	E	T	R	V																					
	337						340				346																										

Sequences Comparison Summary

Receptor	Total Residues	Matched Residues	Similarity (%)
CysLTR ₁	337	22	6.53
CysLTR ₂	346	22	6.35

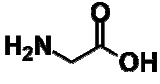
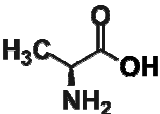
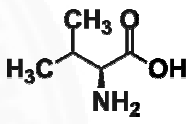
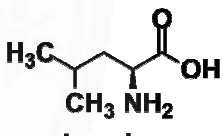
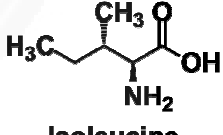
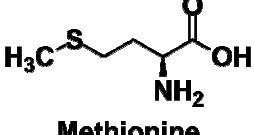
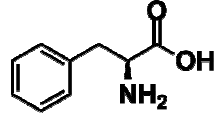
116

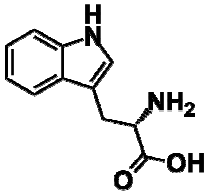
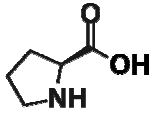
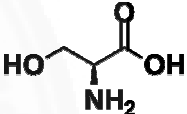
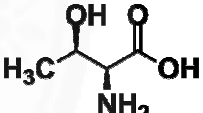
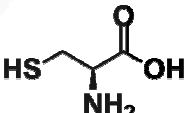
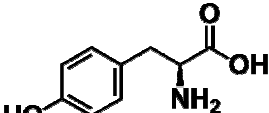
308Y	-	-	-	P	S	Y	T	V	T	V	A	T	G	S	Q	E	H	A	G	T	D	D	Y	I	Y	L	S	L	V	G
3V99	-	-	-	-	S	Y	T	V	T	V	A	T	G	S	Q	E	H	A	G	T	D	D	Y	I	Y	L	S	L	V	G
	1									10						20						30								
308Y	S	A	G	C	S	E	K	H	L	L	D	K	G	S	F	E	R	G	A	V	D	S	Y	D	V	T	V	D	E	E
3V99	S	A	G	C	S	E	K	H	L	L	D	K	G	S	F	E	R	G	A	V	D	S	Y	D	V	T	V	D	E	E
							40						50						60											
308Y	L	G	E	I	Q	L	V	R	I	E	K	R	K	Y	G	S	N	D	D	W	Y	L	K	Y	I	T	L	K	T	P
3V99	L	G	E	I	Q	L	V	R	I	E	K	R	K	Y	G	S	N	D	D	W	Y	L	K	Y	I	T	L	K	T	P
							70						80						90											
308Y	H	G	D	Y	I	E	F	P	C	Y	R	W	I	T	G	D	V	E	V	V	L	R	D	G	R	A	K	L	A	R
3V99	H	G	D	Y	I	E	F	P	C	Y	R	W	I	T	G	D	V	E	V	V	L	R	D	G	R	A	K	L	A	R
							100						110						120											
308Y	D	D	Q	I	H	I	L	K	Q	H	R	R	K	E	L	E	T	R	Q	K	Q	Y	R	W	M	E	W	N	P	G
3V99	D	D	Q	I	H	I	L	K	Q	H	R	R	K	E	L	E	T	R	Q	K	Q	Y	R	W	M	E	W	N	P	G
							130						140						150											
308Y	F	P	L	S	I	D	A	K	C	H	K	D	L	P	R	D	I	Q	F	D	S	E	K	G	V	D	F	V	L	N
3V99	F	P	L	S	I	D	A	K	C	H	K	D	L	P	R	D	I	Q	F	D	S	-	-	-	-	-	F	V	L	N
							160						170						180											
308Y	Y	S	K	A	M	E	N	L	F	I	N	R	F	M	H	M	F	Q	S	S	W	N	D	F	A	D	F	E	K	I
3V99	Y	S	K	A	M	E	N	L	F	-	-	-	-	-	-	-	-	Q	S	S	W	N	D	F	A	D	F	E	K	I
							190						200						210											
308Y	F	V	K	I	S	N	T	I	S	E	R	V	M	N	H	W	Q	E	D	L	M	F	G	Y	Q	F	L	N	G	A
3V99	F	V	K	I	S	N	T	I	S	E	R	V	M	N	H	W	Q	E	D	L	M	F	G	Y	Q	F	L	N	G	A
							220						230						240											
308Y	N	P	V	L	I	R	R	C	T	E	L	P	E	K	L	P	V	T	T	E	M	V	E	C	S	L	E	R	Q	L
3V99	N	P	V	L	I	R	R	C	T	E	L	P	E	K	L	P	V	T	T	E	M	V	E	C	S	L	E	R	Q	L
							250						260						270											

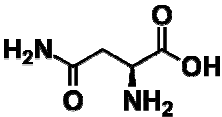
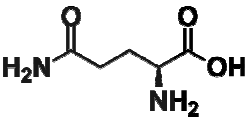
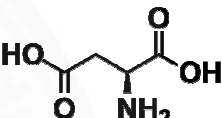
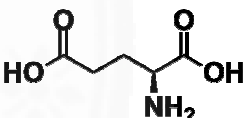
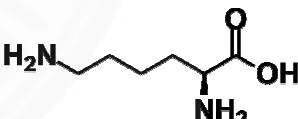
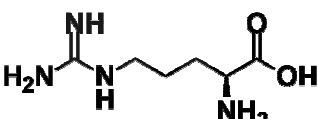
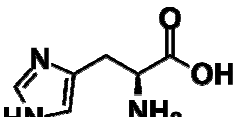
308Y	S	L	E	Q	E	V	Q	Q	G	N	I	F	I	V	D	F	E	L	L	D	G	I	D	A	N	K	T	D	P	C
3V99	S	L	E	Q	E	V	Q	Q	G	N	I	F	I	V	D	F	E	L	L	D	G	I	D	-	-	-	-	-	-	C
										280										290									300	
308Y	T	L	Q	F	L	A	A	P	I	C	L	L	Y	K	N	L	A	N	K	I	V	P	I	A	I	Q	L	N	Q	I
3V99	T	L	Q	F	L	A	A	P	I	C	L	L	Y	K	N	L	A	N	K	I	V	P	I	A	I	Q	L	N	Q	I
										310										320									330	
308Y	P	G	D	E	N	P	I	F	L	P	S	D	A	K	Y	D	W	L	L	A	K	I	W	V	R	S	S	D	F	H
3V99	P	G	D	E	N	P	I	F	L	P	S	D	A	K	Y	D	W	L	L	A	K	I	W	V	R	S	S	D	F	H
										340										350									360	
308Y	V	H	Q	T	I	T	H	L	L	R	T	H	L	V	S	E	V	F	G	I	A	M	Y	R	Q	L	P	A	V	H
3V99	V	H	Q	T	I	T	H	L	L	R	T	H	L	V	S	E	V	F	G	I	A	M	Y	R	Q	L	P	A	V	H
										370										380									390	
308Y	P	I	F	K	L	L	V	A	H	V	R	F	T	I	A	I	N	T	K	A	R	E	Q	L	I	C	E	C	G	L
3V99	P	I	F	K	L	L	V	A	H	V	R	F	T	I	A	I	N	T	K	A	R	E	Q	-	-	-	-	-	-	-
										400										410									420	
308Y	F	D	K	A	N	A	T	G	G	G	G	H	V	Q	M	V	Q	R	A	M	K	D	L	T	Y	A	S	L	C	F
3V99	-	-	-	-	-	-	-	-	-	G	G	H	V	Q	M	V	Q	R	A	M	K	D	L	T	Y	A	S	L	C	F
										430										440									450	
308Y	P	E	A	I	K	A	R	G	M	E	S	K	E	D	I	P	Y	Y	F	Y	R	D	D	G	L	L	V	W	E	A
3V99	P	E	A	I	K	A	R	G	M	E	S	K	E	D	I	P	Y	Y	F	Y	R	D	D	G	L	L	V	W	E	A
										460										470									480	
308Y	I	R	T	F	T	A	E	V	V	D	I	Y	Y	E	G	D	Q	V	V	E	E	D	P	E	L	Q	D	F	V	N
3V99	I	R	T	F	T	A	E	V	V	D	I	Y	Y	E	G	D	Q	V	V	E	E	D	P	E	L	Q	D	F	V	N
										490										500									510	
308Y	D	V	Y	V	Y	G	M	R	G	R	K	S	S	G	F	P	K	S	V	K	S	R	E	Q	L	S	E	Y	L	T
3V99	D	V	Y	V	Y	G	M	R	G	R	K	S	S	G	F	P	K	S	V	K	S	R	E	Q	L	S	E	Y	L	T
										520										530									540	
308Y	V	V	I	F	T	A	S	A	Q	H	A	A	V	N	F	G	Q	Y	D	W	A	S	W	I	P	N	A	P	P	T
3V99	V	V	I	F	T	A	S	A	Q	H	A	A	V	N	F	G	Q	Y	D	W	A	S	W	I	P	N	A	P	P	T
										550										560									570	

3O8Y	M	R	A	P	P	P	T	A	K	G	V	V	T	I	E	Q	I	V	D	T	L	P	D	R	G	R	S	C	W	H
3V99	M	R	A	P	P	P	T	A	K	G	V	V	T	I	E	Q	I	V	D	T	L	P	D	R	G	R	S	C	W	H
										580										590										600
3O8Y	L	G	A	V	W	A	L	S	Q	F	Q	E	N	E	L	F	L	G	M	Y	P	E	E	H	F	I	E	K	P	V
3V99	L	G	A	V	W	A	L	S	Q	F	-	-	-	E	L	F	L	G	M	Y	P	E	E	H	F	I	E	K	P	V
										610										620										630
3O8Y	K	E	A	M	A	R	F	R	K	N	L	E	A	I	V	S	V	I	A	E	R	N	E	N	L	Q	L	P	Y	Y
3V99	K	E	A	M	A	R	F	R	K	N	L	E	A	I	V	S	V	I	A	E	R	N	E	N	L	Q	L	P	Y	Y
										640										650										660
3O8Y	Y	L	S	P	D	R	I	P	N	S	V	A	I																	
3V99	Y	L	D	P	D	R	I	P	N	S	V	A	-																	
										670			673																	

A-5 Essential Amino Acid Abbreviation and Property

Amino acid	Three letter code	Single letter code	Property	Chemical Structure
Glycine	Gly	G	Nonpolar	 Glycine
Alanine	Ala	A	Nonpolar	 Alanine
Valine	Val	V	Nonpolar	 Valine
Leucine	Leu	L	Nonpolar	 Leucine
Isoleucine	Ile	I	Nonpolar	 Isoleucine
Methionine	Met	M	Nonpolar, contain sulfur	 Methionine
Phenylalanine	Phe	F	Nonpolar	 Phenylalanine

Amino acid	Three letter code	Single letter code	Property	Chemical Structure
Tryptophan	Trp	W	Nonpolar	 Tryptophan
Proline	Pro	P	Nonpolar	 Proline
Serine	Ser	S	Polar, can be phosphorylated	 Serine
Threonine	Thr	T	Polar, can be phosphorylated	 Threonine
Cysteine	Cys	C	Polar, contain sulfur	 Cysteine
Tyrosine	Tyr	Y	Polar, can be phosphorylated	 Tyrosine

Amino acid	Three letter code	Single letter code	Property	Chemical Structure
Asparagine	Asn	N	Polar	 <p>Asparagine</p>
Glutamine	Gln	Q	Polar	 <p>Glutamine</p>
Aspartic acid	Asp	D	Negative charge	 <p>Aspartic acid</p>
Glutamic acid	Glu	E	Negative charge	 <p>Glutamic acid</p>
Lysine	Lys	K	Positive charge	 <p>Lysine</p>
Arginine	Arg	R	Positive charge	 <p>Arginine</p>
Histidine	His	H	Positive charge	 <p>Histidine</p>

Reference [89] and Website: <http://www.bio.davidson.edu/biology/aatable.html>

Appendix B

Calculation Theory

B-1 Kohn-Sham Theorem

Kohn-Sham equation is described by external potential of non-interacting particles motions, typically denoted as $V_s(r)$ called as Kohn-Sham potential term. Since, particles in this imaginary system that they have set do not have interaction, thus, the wave function has been determined from lowest energy orbitals set in eq. (B1-1)

$$\left(\frac{\hbar^2}{2m} \nabla^2 + V_s(r) \right) \phi_i(r) = \varepsilon_i \phi_i(r) \quad (\text{B1-1})$$

Where ε_i denotes orbital energy and ϕ_i denotes Kohn-Sham orbitals.

This equation have been developed based on Schrödinger equation (eq.(B1-2)), as described below.

$$\hat{H}\Psi = [\hat{T} + \hat{V} + \hat{U}]\Psi = \left[\sum_i^N \left(\frac{\hbar^2}{2m} \nabla^2 \right) + \sum_i^N V(r_i) + \sum_{i<j}^N U(r_i, r_j) \right] = E\Psi \quad (\text{B1-2})$$

For system with N-electrons, \hat{H} is Hamiltonian

E is total energy

\hat{T} is kinetic energy

\hat{V} is potential energy due to positive charge

\hat{U} is electron-electron interaction energy

The kinetic energy and electron-electron interaction operator are the same with any N-electron system, but, the potential energy operator is system dependent. However, the complicated system with interacting particles cannot be divided into

single-particle equation due to present of electron interaction operator. By development of Schrödinger equation to DFT, it provided much easier method to solve many-body system with electron interactions by consider it as single-body system without electron interaction, hence, the main variable for DFT is electron density denoted as $n(r)$ instead in order to normalize the Hamiltonian (eq. (B1-3)).

$$n(r) = N \int d^3r_2 \dots \int d^3r_N \Psi(r, r_2, \dots, r_N) \Psi(r, r_2, \dots, r_N) \quad (B1-3)$$

In the other hand, this electron density relationship can be considered in reverse, from ground-state electron density $n_0(r)$ you can calculate the corresponded ground-state wave function $\Psi_0(r, r_2, \dots, r_N)$. In this regard, Ψ_0 can be considered as function of n_0 as shown in eq.(B1-4).

$$\Psi_0 = \Psi_0[n_0] \quad (B1-4)$$

Consequently, the ground-state energy can also be considered as function of n_0 as shown in eq. (B1-5).

$$E_0 = E[n_0] = \langle \Psi[n_0] | \hat{T} + \hat{V} + \hat{U} | \Psi[n_0] \rangle \quad (B1-5)$$

Then, the external potential energy operator can be rewritten in term of ground-state density (n_0) as described in eq. (B1-6).

$$V[n_0] = \int V(r) n_0(r) d^3r \quad (B1-6)$$

Therefore, in general the external potential of system can also be consider in term of density (n) as shown in eq.(B1-7).

$$V[n] = \int V(r) n(r) d^3r \quad (B1-7)$$

Because of dependency on system of potential energy operator (\hat{V}) and independency of kinetic energy operator (\hat{T}) and electron-electron interaction operator (\hat{U}), the total energy can be written as eq.(B1-8), and when consider with respect to $n(r)$ with reliable $T[n]$ and $U[n]$; the energy minimization will give the ground-state density (n_0) and all other ground-state observables also.

$$E[n] = T[n] + U[n] + \int V(r)n(r)d^3r \quad (B1-8)$$

By applying the Lagrangian method of determined multiplier [43], the minimization of energy $E[n]$ can be solved with exclusion of electron-electron interaction energy term (\hat{U}), thus, the energy function can be rewritten as eq.(B1-9).

$$E[n] = \langle \Psi_s[n] | \hat{T} + \hat{V}_s | \Psi_s[n] \rangle \quad (B1-9)$$

Where, \hat{T} denotes kinetic energy

\hat{V}_s denotes potential energy of non-interacting moving particle

Thus, $n_s(r) \equiv n(r)$

As the result, Kohn and Sham have solved this problem and proposed eq. (B1-1), which produced the Kohn-Sham orbitals (ϕ_i) and can be used to rewritten in term of electron density $n(r)$ of many interacting atoms system as described in eq. (B1-10).

$$n_s(r) \equiv n(r) = \sum_i^N |\phi_i(r)|^2 \quad (B1-10)$$

The Kohn-Sham potential term can also be described in further detail as shown in eq. (B1-11).

$$V_s(r) = V(r) + \int \frac{e^2 n_s(r')}{|r - r'|} d^3 r' + V_{xc}[n(r)] \quad (B1-11)$$

Where, $\int \frac{e^2 n_s(r')}{|r - r'|} d^3 r'$ denotes Hatree term, which described repulsion between electrons

V_{xc} denotes exchange-correlation potential, which included all interaction between particles.

Therefore, both Hatree term and exchange-correlation potential term are depend on electron density which also made them depend on Kohn-Sham orbitals and Kohn-Sham potential. Hence, to solve Kohn-Sham equation, you have to do it iteratively by initially guessing value of electron density, then calculate the Kohn-Sham potential and finally solved for Kohn-Sham orbitals and calculated for new density again with the repeated steps until converge. However, there are alternative method to solve this equation without iteratively calculated it, called Harris functional.

B-2 Becke, three-parameter, Lee-Yang-Parr (B3LYP)

The exchange-correlation function is shown in eq. (B2-1).

$$E_{xc}^{B3LYP} = E_X^{LDA} + a_0(E_X^{HF} - E_X^{LDA}) + a_x(E_X^{GGA} - E_X^{LDA}) + E_C^{LDA} + a_c(E_C^{GGA} - E_C^{LDA}) \quad (B2-1)$$

Where, $a_0 = 0.20$

$$a_x = 0.72$$

$$a_c = 0.81$$

E_X^{HF} is Hatree-Fock exchange functional

E_X^{LDA} is local-density approximation

E_X^{GGA} , E_C^{GGA} are generalized gradient approximations

E_C^{LDA} is local density approximation to the correlation functional

Three defined parameter have been taken from Reference [90].

The Hatree-Fock exchange functional can be described in detail in eq. (B2-2).

$$E_X^{HF} = \frac{1}{2} \sum_{i,j} \int \int \Psi_i(r_1) \Psi_j(r_1) \frac{1}{r_{12}} \Psi_i(r_2) \Psi_j(r_2) dr_1 dr_2 \quad (B2-2)$$

B-3 Integration of Equations of Motion

From Newton's second law, the equation of motion is described in eq. (B3-1).

$$F_i = m_i a_i \quad (B3-1)$$

Where, F_i denotes force exerted on particle i

m_i denotes mass of particle i

a_i denotes acceleration of particle i

In addition the force (F_i) can be written in tern of potential energy gradient as shown in eq. (B3-2).

$$F_i = -\nabla_i V \quad (B3-2)$$

Thus, combination of eq. (B3-1) and (B3-2) will produce the relationship between change in potential energy and position of particles in the system as described in eq. (B3-3).

$$\frac{dV}{dx_i} = m_i \frac{d^2x_i}{dt^2} \quad (B3-3)$$

Where, V denoted potential energy of system
 x_i denotes position of particle i
 dt denotes time change of the system

Hence, if consider the system to have constant acceleration, the acceleration term can be written as shown in eq. (B3-4).

$$a_i = \frac{dv_i}{dt} \quad (B3-4)$$

Where, v_i denotes velocity of particle

After integration of eq. (B3-4), the velocity expression can be obtained as shown in eq. (B3-5).

$$v_i = \frac{1}{2}a_i t + v_0 \quad (B3-5)$$

Where, v_0 denotes the initial velocity

Since, originally, the general velocity expression can be written as shown in eq.(B3-6)

$$v_i = \frac{dx_i}{dt} \quad (B3-6)$$

With the integrated definition as shown in eq. (B3-7)

$$x_i = v_i t + x_0 \quad (B3-7)$$

Where, x_0 denotes the initial position of particle

After combining eq.(B3-5) and (B3-7), the position definition can be rewritten as described in eq.(B3-8) .

$$x_i = \frac{1}{2}a_it^2 + v_0t + x_0 \quad (B3-8)$$

B-4 Leap-frog Algorithm and Kinetic Energy Calculation

Firstly, the definition of average kinetic energy (K_{avg}) and potential energy (V_{avg}) that derived from configurations of particles in the system have to be investigated as described in eq. (B4-1) and (B4-2).

$$K_{avg} = \frac{1}{M} \sum_{i=1}^M \left\{ \left(\sum_{i=1}^N \frac{m_i}{2} v_i \right) \times v_i \right\} \quad (B4-1)$$

$$V_{avg} = \frac{1}{M} \sum_{i=1}^M V_i \quad (B4-2)$$

Where, M denotes number of configurations
 N denotes number of particles

The average potential energy was depended on potential energy of each particle in the system, which can refer to its previous definition in eq. (B3-3). It have shown obvious relationship between potential energy and position of each particle in the system unlike the kinetic energy that can easily be calculated. Consequently, the leap-frog algorithm can be used to solve for the potential energy of the system based on Taylor series expansion as explained below.

From in eq. (B3-3), potential energy difference depend on particle's position difference with respect to time, therefore, in order to obtained the position of all particles in the system this algorithm have started by calculation of the velocity at time $(t + \frac{1}{2}dt)$ as shown in eq. (B4-3)

$$v\left(t + \frac{1}{2}dt\right) = v\left(t - \frac{1}{2}dt\right) + a(t)dt \quad (B4-3)$$

Then, the velocity at time $(t + \frac{1}{2}dt)$ will be used to calculate position of particle at time $(t + dt)$ as described in eq.(B4-4)

$$x(t + dt) = x(t) + v\left(t + \frac{1}{2}dt\right) dt \quad (B4-4)$$

Thus, from these two definition, the calculated velocities have leap over positions and in the other way positions also leap over velocities. Even though the velocities can be calculated explicitly but they were not calculated at the same time as position. However, the velocities at time (t) can be estimated by eq. (B4-5).

$$v(t) = \frac{1}{2}\left[v\left(t - \frac{1}{2}dt\right) + v\left(t + \frac{1}{2}dt\right)\right] \quad (B4-5)$$

B-5 Total Energy of System Calculation

After obtaining the kinetic energy and total energy of system (E_{tot}), the total energy can also be calculated followed the definition of mechanical energy as shown in eq. (B5-1)

$$E_{tot} = V + K \quad (B5-1)$$

Appendix C

Calculation Results

C-1 Molecular Docking Results of 5-LO Systems

5-LO and AA

Cluster rank	Lowest B.E. (kcal/mol)	Mean B.E. (kcal/mol)	Number in cluster (Frequency)	K _i (μM)	K _{i,avg} (μM)
1	-7.49	-6.68 ± 0.40	26	3.21	12.63 ± 11.18
2	-7.35	-6.85 ± 0.36	5	4.06	9.36 ± 5.94
3	-6.97	-6.37 ± 0.33	32	7.72	21.17 ± 14.72
4	-6.85	-6.34 ± 0.72	2	9.45	22.37 ± 30.75
5	-6.61	-6.61 ± 0.00	1	14.18	14.18 ± 0.00
6	-6.61	-6.61 ± 0.00	1	14.18	14.18 ± 0.00
7	-6.57	-6.57 ± 0.00	1	15.17	15.17 ± 0.00
8	-6.53	-6.40 ± 0.20	3	16.23	20.33 ± 7.53
9	-6.35	-6.10 ± 0.22	7	21.99	33.63 ± 14.87
10	-6.34	-5.83 ± 0.47	3	22.37	52.64 ± 41.74
11	-6.22	-6.22 ± 0.00	1	27.39	27.39 ± 0.00
12	-6.11	-5.67 ± 0.39	3	32.99	68.58 ± 44.11
13	-6.07	-5.56 ± 0.73	2	35.29	84.22 ± 117.17
14	-5.90	-5.90 ± 0.00	1	47.03	47.03 ± 0.00
15	-5.89	-5.86 ± 0.04	2	47.83	49.89 ± 2.98
16	-5.78	-5.61 ± 0.25	2	57.60	77.40 ± 32.83
17	-5.71	-5.28 ± 0.52	3	64.83	113.26 ± 115.12
18	-5.61	-5.61 ± 0.00	1	76.75	76.75 ± 0.00
19	-5.59	-5.53 ± 0.09	2	79.39	88.60 ± 13.78
20	-5.40	-5.40 ± 0.00	1	109.43	109.43 ± 0.00
21	-5.35	-5.35 ± 0.00	1	119.07	119.07 ± 0.00

5-LO and ZIL

Cluster rank	Lowest B.E. (kcal/mol)	Mean B.E. (kcal/mol)	Number in cluster (Frequency)	K _i (μM)	K _{i,avg} (μM)
1	-7.80	-7.60 ± 0.36	8	1.90	2.65 ± 3.41
2	-7.28	-7.22 ± 0.05	51	4.57	5.09 ± 0.43
3	-6.88	-6.88 ± 0.00	1	8.99	8.99 ± 0.00
4	-6.84	-6.83 ± 0.02	37	9.61	9.81 ± 0.25
5	-6.75	-6.75 ± 0.01	2	11.19	11.29 ± 0.14
6	-6.61	-6.61 ± 0.00	1	14.18	14.18 ± 0.00

5-LO and CD

Cluster rank	Lowest B.E. (kcal/mol)	Mean B.E. (kcal/mol)	Number in cluster (Frequency)	K _i (μM)	K _{i,avg} (μM)
1	-5.93	-5.73 ± 0.12	32	44.71	62.54 ± 12.82
2	-5.72	-5.58 ± 0.10	36	63.74	80.10 ± 14.49
3	-5.66	-5.54 ± 0.06	30	70.54	86.78 ± 9.35
4	-5.60	-5.60 ± 0.00	1	78.06	78.06 ± 0.00
5	-5.43	-5.43 ± 0.00	1	104.02	104.02 ± 0.00

5-LO and DMP

Cluster rank	Lowest B.E. (kcal/mol)	Mean B.E. (kcal/mol)	Number in cluster (Frequency)	K _i (μM)	K _{i,avg} (μM)
1	-5.94	-5.94 ± 0.00	1	43.96	43.96 ± 0.00
2	-5.74	-5.70 ± 0.06	50	61.62	65.97 ± 8.26
3	-5.65	-5.49 ± 0.07	23	71.74	94.07 ± 11.13
4	-5.60	-5.56 ± 0.03	26	78.06	84.22 ± 4.08

C-2 MM/GBSA Calculation Results of 5-LO Systems

Entropy Approximation for 5-LO Complex Systems.

Ligand		Entropy approximation at T = 298.15 K (kcal/mol)			
		Translational	Rotational	Vibrational	Total
AA	Complex	17.59	18.60	5372.36	5408.55
	Receptor	17.58	18.60	5351.79	5387.97
	Ligand	12.82	10.70	58.22	81.75
	T S	-12.82	-10.70	-37.65	-61.17
ZIL	Complex	17.74	18.93	5841.43	5878.10
	Receptor	17.74	18.93	5834.46	5871.13
	Ligand	12.60	9.74	15.91	38.25
	T S	-12.60	-9.74	-8.94	-31.28
CD	Complex	17.74	18.95	8687.81	8724.50
	Receptor	17.74	18.95	8664.66	8701.34
	Ligand	12.48	9.78	28.46	50.73
	T S	-12.48	-9.78	-5.31	-27.57
DMP	Complex	17.74	18.94	5844.55	5881.23
	Receptor	17.74	18.94	5835.59	5872.27
	Ligand	12.40	9.62	23.01	45.03
	T S	-12.40	-9.62	-14.05	-36.07

Generalized Born Binding Energy Approximation.

Ligand	Generalized Born (Complex - Receptor-Ligand)			
	Energy Component	Average (kcal/mol)	S.D.	Total (kcal/mol)
AA	VDWAALS	-51.99	2.58	
	EEL	-15.92	2.84	
	EGB	27.20	1.87	
	ESURF	-7.51	0.18	
	G _{gas}	-67.90	3.17	
	G _{solv}	19.69	1.88	
	G_{Total}	-48.21	2.78	
	G_{binding}			12.96
ZIL	VDWAALS	-35.28	2.50	
	EEL	-23.69	4.73	
	EGB	34.24	4.15	
	ESURF	-4.67	0.09	
	G _{gas}	-58.97	4.80	
	G _{solv}	29.57	4.11	
	G_{Total}	-29.40	2.78	
	G_{binding}			1.88
CD	VDWAALS	-33.08	2.27	
	EEL	-16.19	3.49	
	EGB	27.17	2.71	
	ESURF	-4.72	0.09	
	G _{gas}	-49.28	3.52	
	G _{solv}	22.45	2.70	
	G_{Total}	-26.83	2.58	
	G_{binding}			0.74
DMP	VDWAALS	-32.92	1.64	
	EEL	-5.19	1.80	
	EGB	13.68	1.71	
	ESURF	-4.71	0.12	
	G _{gas}	-38.12	2.30	
	G _{solv}	8.97	1.74	
	G_{Total}	-29.15	1.87	
	G_{binding}			6.92

VDWAALS denotes van der Waals energy.

EEL denotes electrostatic energy.

EGB denotes as polar solvation free energy.

ESURF denotes as nonpolar solvation free energy.

G_{gas} denotes total gas phase free energy.

G_{solv} denotes total solvation free energy.

C-3 Comparison of MD Simulation Results of Pure CysLTRs

MD simulations of pure CysLTRs can be divided into two systems which are CysLTRs solvated in truncated octahedral water box and CysLTRs embedded in phospholipid bilayer membrane with water environment on both extracellular side and intracellular side (rectangular box). The first systems (water only) were heated from 0 to 300 K within 20 ps and then equilibrated for 5 ns with NPT ensemble (isotropic pressure control). The second systems (with membrane) were heated in two subsequent steps which are 0 to 100 K for 5 ps and 100 to 300 K for 100 ps in order to slowly increase system's temperature because membrane system is more sensitive than water-only system. Afterward, equilibrate systems for 5 ns with NPAT ensemble (use anisotropic pressure control). Hence, the comparison based on C_{α} -RMSD of CysLTRs in both systems have been performed to observe receptor stability as shown in Figure C3-1

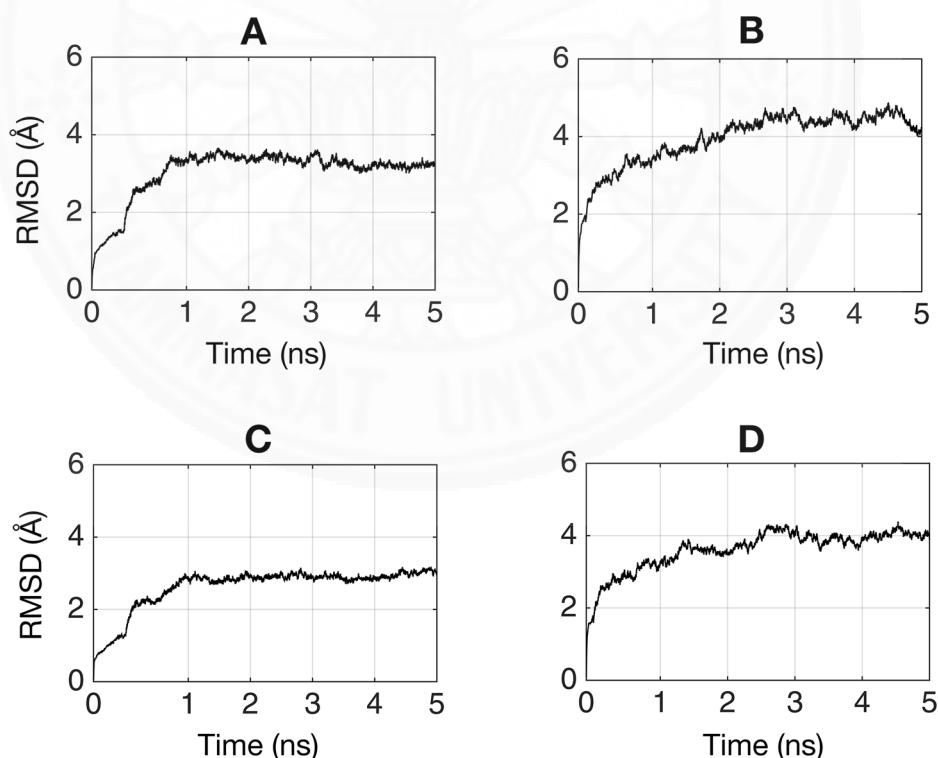


Figure C3-1: Alpha-carbon RMSD comparison of pure CysLTRs systems. A refer to CysLTR₁ embedded in membrane. B refer to CysLTR₁ solvated in water. C refer to CysLTR₂ embedded in membrane. D refer to CysLTR₂ solvated in water.

There are distinctive difference in CysLTRs structure stability between two systems after 1 ns. CysLTRs that were embedded in phospholipid bilayer membrane show higher stability due to immobilization of transmembrane helix. Moreover, superimposition of 5 ns snapshots from both systems have been carried out as shown in Figure C3-2 in order to emphasize the difference between membrane bounded system and water-only system. C_{α} -RMSD are 4.18 Å and 4.74 Å for CysLTR₁ systems and CysLTR₂ systems, respectively. As expected, there are clearly deviation of alpha-helix region of CysLTRs between the two systems including some loops regions that link between those helices. For this reason, the water-only system cannot be used to represent behavior of membrane-bound receptor because there are distinct motion of protein's structure which can lead to incorrect simulation result even though water-only system can be used to reduce simulation time.

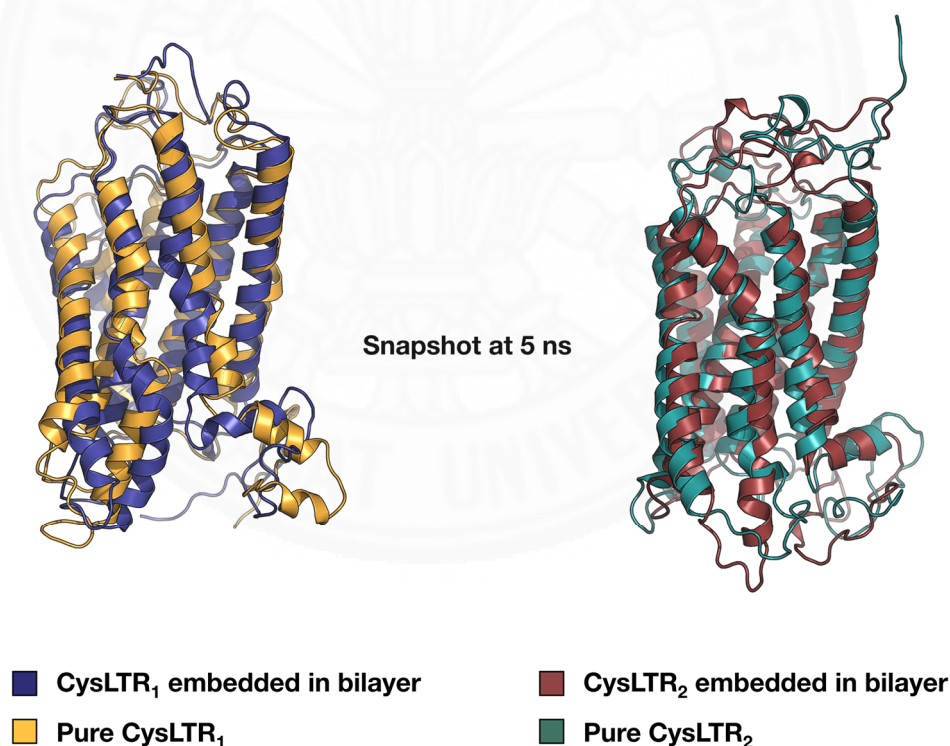


Figure C3-2: Superimposition of pure CysLTRs systems.

C-4 AutoSite Calculation for CysLTRs

CysLTR₁ AutoSite Score

Rank	AS Score	Fills Points	Radius of Gyration	Buriedness
1	46.58	277	4.74	0.89
2	27.2	87	2.97	0.96
3	27.08	74	2.63	0.98
4	25.09	98	2.97	0.87
5	24.18	137	3.86	0.83
6	23.47	50	2.13	1.00
7	22.83	63	2.67	0.98
8	21.92	83	2.33	0.78
9	21.72	87	2.67	0.82
10	21.50	77	2.57	0.85
11	18.14	78	2.68	0.79
12	17.92	106	3.53	0.78
13	16.64	98	3.41	0.76
14	16.44	84	2.95	0.76
15	16.31	81	2.99	0.78
16	16.22	88	2.76	0.71
17	14.37	53	2.17	0.77
18	14.31	63	2.39	0.74

CysLTR₂ Autosite Score

Rank	AS Score	Fills Points	Radius of Gyration	Buriedness
1	61.50	558	7.31	0.90
2	44.85	323	5.79	0.90
3	35.85	176	3.52	0.85
4	29.19	111	3.01	0.89
5	26.72	137	3.71	0.85
6	24.60	200	4.16	0.71
7	20.22	73	2.40	0.82
8	20.20	66	2.63	0.90
9	19.80	143	3.71	0.72
10	19.73	56	2.59	0.96
11	18.24	95	3.16	0.78
12	16.64	103	3.20	0.72
13	14.29	54	2.12	0.75
14	13.71	116	4.26	0.71
15	12.98	58	2.31	0.72
16	9.21	85	3.43	0.61

C-5 Molecular Docking Results of CysLTRs Systems

CIINT-LTD₄

Cluster rank	Lowest B.E. (kcal/mol)	Mean B.E. (kcal/mol)	Frequency	K _i (μM)	K _{i,avg} (μM)
1	-7.68	-7.68 ± 0.00	1	2.33	2.33 ± 0.00
2	-7.28	-5.73 ± 1.35	3	4.57	62.67 ± 141.33
3	-7.27	-6.57 ± 0.10	2	4.65	15.30 ± 32.29
4	-7.01	-7.01 ± 0.00	1	7.21	7.21 ± 0.00
5	-6.91	-5.50 ± 0.84	7	8.54	92.42 ± 119.20
6	-6.91	-6.91 ± 0.00	1	8.54	8.54 ± 0.00
7	-6.54	-5.12 ± 1.28	4	15.96	177.08 ± 1,371.46
8	-6.42	-4.89 ± 1.84	4	19.54	257.86 ± 10,768.42
9	-6.40	-6.40 ± 0.00	1	20.21	20.21 ± 0.00
10	-6.28	-5.04 ± 0.86	4	24.75	202.70 ± 256.19
11	-6.26	-6.26 ± 0.00	1	25.60	25.60 ± 0.00
12	-5.64	-5.13 ± 0.73	2	72.96	174.12 ± 242.22
13	-5.56	-5.56 ± 0.00	1	83.52	83.52 ± 0.00
14	-5.43	-5.43 ± 0.00	1	104.02	104.02 ± 0.00
15	-5.39	-5.39 ± 0.00	1	111.29	111.29 ± 0.00
16	-5.34	-4.00 ± 1.37	3	121.10	1,170.75 ± 6,823.47
17	-5.32	-5.32 ± 0.00	1	125.26	125.26 ± 0.00
18	-5.29	-5.29 ± 0.00	1	131.77	131.77 ± 0.00
19	-5.10	-5.10 ± 0.00	1	181.63	181.63 ± 0.00
20	-5.02	-5.02 ± 0.00	1	207.90	207.90 ± 0.00
21	-4.68	-4.68 ± 0.00	1	369.19	369.19 ± 0.00
22	-4.68	-4.29 ± 0.56	2	369.19	719.41 ± 730.21
23	-4.65	-4.65 ± 0.00	1	388.37	388.37 ± 0.00
24	-4.61	-4.61 ± 0.00	1	415.52	415.52 ± 0.00
25	-4.61	-4.61 ± 0.00	1	415.52	415.52 ± 0.00
26	-4.56	-3.95 ± 0.87	2	452.13	1,277.51 ± 2,232.69
27	-4.46	-4.46 ± 0.00	1	535.32	535.32 ± 0.00
28	-4.33	-3.86 ± 0.67	3	666.76	1,474.72 ± 2,678.98
29	-4.28	-4.28 ± 0.00	1	725.51	725.51 ± 0.00
30	-4.25	-4.25 ± 0.00	1	763.22	763.22 ± 0.00
31	-4.22	-4.22 ± 0.00	1	802.88	802.88 ± 0.00
32	-4.20	-4.20 ± 0.00	1	830.47	830.47 ± 0.00
33	-4.06	-3.96 ± 0.14	2	1,051.99	1,245.55 ± 298.92
34	-3.98	-3.58 ± 0.57	2	1,204.18	2,386.47 ± 2,492.83
35	-3.97	-3.97 ± 0.00	1	1,224.69	1,224.69 ± 0.00
36	-3.91	-3.91 ± 0.00	1	1,355.30	1,355.30 ± 0.00

Cluster rank	Lowest B.E. (kcal/mol)	Mean B.E. (kcal/mol)	Frequency	K _i (μM)	K _{i,avg} (μM)
37	-3.91	-3.91 ± 0.00	1	1,355.30	1,355.30 ± 0.00
38	-3.82	-3.82 ± 0.00	1	1,577.79	1,577.79 ± 0.00
39	-3.76	-3.76 ± 0.00	1	1,746.06	1,746.06 ± 0.00
40	-3.63	-3.63 ± 0.00	1	2,174.77	2,174.77 ± 0.00
41	-3.62	-3.62 ± 0.00	1	2,211.82	2,211.82 ± 0.00
42	-3.57	-3.57 ± 0.00	1	2,406.71	2,406.71 ± 0.00
43	-3.49	-3.49 ± 0.00	1	2,754.88	2,754.88 ± 0.00
44	-3.44	-2.46 ± 0.75	5	2,997.63	15,583.64 ± 32,417.85
45	-3.43	-3.43 ± 0.00	1	3,048.69	3,048.69 ± 0.00
46	-3.42	-3.42 ± 0.00	1	3,100.61	3,100.61 ± 0.00
47	-3.41	-3.41 ± 0.00	1	3,153.43	3,153.43 ± 0.00
48	-3.35	-3.35 ± 0.00	1	3,489.73	3,489.73 ± 0.00
49	-3.05	-3.05 ± 0.00	1	5,792.16	5,792.16 ± 0.00
50	-3.04	-2.82 ± 0.32	2	5,890.82	8,614.14 ± 4,741.60
51	-3.00	-3.00 ± 0.00	1	6,302.54	6,302.54 ± 0.00
52	-2.99	-2.99 ± 0.00	1	6,409.89	6,409.89 ± 0.00
53	-2.94	-2.94 ± 0.00	1	6,974.70	6,974.70 ± 0.00
54	-2.84	-2.84 ± 0.00	1	8,258.00	8,258.00 ± 0.00
55	-2.77	-2.77 ± 0.00	1	9,294.36	9,294.36 ± 0.00
56	-2.75	-2.75 ± 0.00	1	9,613.67	9,613.67 ± 0.00
57	-2.47	-2.47 ± 0.00	1	15,426.52	15,426.52 ± 0.00
58	-2.35	-2.25 ± 0.09	3	18,892.40	22,494.78 ± 3,327.23
59	-2.33	-2.33 ± 0.00	1	19,541.46	19,541.46 ± 0.00
60	-2.31	-2.31 ± 0.00	1	20,212.82	20,212.82 ± 0.00
61	-2.13	-2.13 ± 0.00	1	27,394.04	27,394.04 ± 0.00
62	-1.96	-1.96 ± 0.00	1	36,504.82	36,504.82 ± 0.00
63	-1.86	-1.86 ± 0.00	1	43,221.48	43,221.48 ± 0.00
64	-1.82	-1.82 ± 0.00	1	46,242.30	46,242.30 ± 0.00
65	-1.15	-1.15 ± 0.00	1	143,377.49	143,377.49 ± 0.00
66	-0.57	-0.57 ± 0.00	1	381,863.33	381,863.33 ± 0.00

CIINT-MON

Cluster rank	Lowest B.E. (kcal/mol)	Mean B.E. (kcal/mol)	Frequency	K _i (μM)	K _{i,avg} (μM)
1	-11.37	-10.56 ± 0.59	8	0.005	0.02 ± 0.03
2	-10.84	-9.42 ± 1.18	9	0.01	0.12 ± 0.61
3	-10.62	-9.49 ± 1.09	6	0.02	0.11 ± 0.84
4	-10.43	-10.17 ± 0.39	4	0.02	0.03 ± 0.03

Cluster rank	Lowest B.E. (kcal/mol)	Mean B.E. (kcal/mol)	Frequency	K _i (μM)	K _{i,avg} (μM)
5	-10.33	-10.18 ± 0.22	2	0.03	0.03 ± 0.01
6	-10.22	-9.13 ± 1.55	2	0.03	0.20 ± 0.89
7	-9.99	-9.26 ± 0.79	4	0.05	0.16 ± 0.28
8	-9.89	-8.60 ± 1.83	2	0.06	0.50 ± 3.09
9	-9.80	-8.89 ± 0.62	4	0.06	0.30 ± 0.25
10	-9.40	-8.75 ± 0.92	2	0.13	0.38 ± 0.72
11	-9.38	-7.06 ± 2.32	3	0.13	6.59 ± 190.71
12	-9.16	-9.16 ± 0.00	1	0.19	0.19 ± 0.00
13	-9.13	-9.13 ± 0.00	1	0.20	0.20 ± 0.00
14	-9.06	-7.38 ± 1.46	3	0.23	3.84 ± 9.81
15	-9.02	-7.36 ± 1.19	4	0.24	3.99 ± 11.30
16	-8.80	-8.80 ± 0.00	1	0.35	0.35 ± 0.00
17	-8.74	-8.74 ± 0.00	1	0.39	0.39 ± 0.00
18	-8.72	-8.72 ± 0.00	1	0.40	0.40 ± 0.00
19	-8.67	-8.67 ± 0.00	1	0.44	0.44 ± 0.00
20	-8.48	-8.48 ± 0.00	1	0.60	0.60 ± 0.00
21	-8.46	-8.46 ± 0.00	1	0.62	0.62 ± 0.00
22	-8.35	-7.88 ± 0.67	2	0.75	1.66 ± 2.07
23	-8.24	-8.24 ± 0.00	1	0.90	0.90 ± 0.00
24	-8.21	-8.21 ± 0.00	1	0.95	0.95 ± 0.00
25	-8.16	-8.16 ± 0.00	1	1.03	1.03 ± 0.00
26	-8.15	-8.15 ± 0.00	1	1.05	1.05 ± 0.00
27	-8.10	-8.10 ± 0.00	1	1.14	1.14 ± 0.00
28	-7.93	-7.25 ± 0.96	2	1.53	4.81 ± 9.65
29	-7.72	-7.48 ± 0.34	2	2.17	3.26 ± 1.92
30	-7.69	-7.69 ± 0.00	1	2.29	2.29 ± 0.00
31	-7.54	-7.54 ± 0.00	1	2.95	2.95 ± 0.00
32	-7.48	-7.48 ± 0.00	1	3.26	3.26 ± 0.00
33	-7.33	-7.33 ± 0.00	1	4.20	4.20 ± 0.00
34	-7.25	-7.25 ± 0.00	1	4.81	4.81 ± 0.00
35	-7.04	-7.04 ± 0.00	1	6.86	6.86 ± 0.00
36	-7.00	-7.00 ± 0.00	1	7.34	7.34 ± 0.00
37	-6.90	-6.90 ± 0.00	1	8.69	8.69 ± 0.00
38	-6.90	-6.07 ± 1.18	2	8.69	35.59 ± 96.97
39	-6.89	-6.89 ± 0.00	1	8.84	8.84 ± 0.00
40	-6.88	-6.88 ± 0.00	1	8.99	8.99 ± 0.00
41	-6.87	-6.87 ± 0.00	1	9.14	9.14 ± 0.00
42	-6.84	-6.84 ± 0.00	1	9.61	9.61 ± 0.00
43	-6.60	-6.60 ± 0.00	1	14.42	14.42 ± 0.00

Cluster rank	Lowest B.E. (kcal/mol)	Mean B.E. (kcal/mol)	Frequency	K _i (μM)	K _{i,avg} (μM)
44	-6.34	-6.34 ± 0.00	1	22.37	22.37 ± 0.00
45	-6.21	-6.21 ± 0.00	1	27.86	27.86 ± 0.00
46	-6.13	-6.13 ± 0.00	1	31.89	31.89 ± 0.00
47	-5.96	-5.96 ± 0.00	1	42.50	42.50 ± 0.00
48	-5.61	-5.61 ± 0.00	1	76.75	76.75 ± 0.00
49	-5.47	-5.47 ± 0.00	1	97.23	97.23 ± 0.00
50	-5.44	-5.44 ± 0.00	1	102.28	102.28 ± 0.00
51	-5.33	-5.33 ± 0.00	1	123.16	123.16 ± 0.00
52	-4.54	-4.54 ± 0.00	1	467.66	467.66 ± 0.00
53	-4.22	-4.22 ± 0.00	1	802.88	802.88 ± 0.00
54	-3.72	-3.72 ± 0.00	1	1,868.10	1,868.10 ± 0.00
55	-3.28	-3.28 ± 0.00	1	3,927.69	3,927.69 ± 0.00
56	-2.84	-2.84 ± 0.00	1	8,258.00	8,258 ± 0.00

C1INT-CD

Cluster rank	Lowest B.E. (kcal/mol)	Mean B.E. (kcal/mol)	Frequency	K _i (μM)	K _{i,avg} (μM)
1	-6.49	-6.00 ± 0.38	8	17.36	39.81 ± 29.25
2	-5.76	-5.44 ± 0.19	54	59.58	101.48 ± 35.41
3	-5.61	-5.49 ± 0.13	21	76.75	93.85 ± 22.82
4	-5.43	-5.26 ± 0.09	8	104.02	138.32 ± 21.24
5	-5.06	-5.06 ± 0.00	1	194.32	194.32 ± 0.00
6	-5.05	-5.05 ± 0.00	1	197.63	197.63 ± 0.00
7	-5.03	-4.90 ± 0.10	6	204.42	255.33 ± 43.41
8	-4.73	-4.73 ± 0.00	1	339.29	339.29 ± 0.00

C1INT-DMP

Cluster rank	Lowest B.E. (kcal/mol)	Mean B.E. (kcal/mol)	Frequency	K _i (μM)	K _{i,avg} (μM)
1	-6.17	-5.98 ± 0.13	36	29.81	40.82 ± 9.10
2	-5.52	-5.36 ± 0.13	30	89.35	117.01 ± 29.72
3	-5.40	-5.40 ± 0.00	1	109.43	109.43 ± 0.00
4	-5.37	-5.30 ± 0.08	7	115.12	130.19 ± 19.19
5	-5.31	-5.24 ± 0.05	14	127.39	142.52 ± 12.87
6	-5.28	-5.28 ± 0.00	1	134.01	134.01 ± 0.00
7	-5.25	-5.22 ± 0.05	10	140.98	147.81 ± 13.47
8	-5.08	-5.08 ± 0.00	1	187.87	187.87 ± 0.00

C1EXT-LTD₄

Cluster rank	Lowest B.E. (kcal/mol)	Mean B.E. (kcal/mol)	Frequency	K _i (μM)	K _{i,avg} (μM)
1	-6.35	-5.35 ± 1.02	3	21.99	118.40 ± 362.88
2	-5.70	-5.15 ± 0.77	2	65.93	165.51 ± 247.20
3	-5.29	-5.29 ± 0.00	1	131.77	131.77 ± 0.00
4	-5.22	-5.22 ± 0.00	1	148.31	148.31 ± 0.00
5	-5.06	-5.06 ± 0.00	1	194.32	194.32 ± 0.00
6	-4.72	-4.72 ± 0.00	1	345.07	345.07 ± 0.00
7	-4.69	-4.08 ± 0.86	2	363.00	1,017.05 ± 1,758.24
8	-4.34	-4.34 ± 0.00	1	655.59	655.59 ± 0.00
9	-4.27	-4.27 ± 0.00	1	737.87	737.87 ± 0.00
10	-4.18	-4.18 ± 0.00	1	859.00	859.00 ± 0.00
11	-3.95	-3.95 ± 0.00	1	1,266.76	1,266.76 ± 0.00
12	-3.87	-3.76 ± 0.16	2	1,450.02	1,746.06 ± 461.40
13	-3.83	-3.83 ± 0.00	1	1,551.37	1,551.37 ± 0.00
14	-3.79	-3.79 ± 0.00	1	1,659.80	1,659.80 ± 0.00
15	-3.48	-2.39 ± 1.54	2	2,801.81	17,658.24 ± 76,712.85
16	-3.45	-3.45 ± 0.00	1	2,947.43	2,947.43 ± 0.00
17	-3.44	-2.63 ± 1.14	2	2,997.63	11,674.58 ± 30,030.99
18	-3.43	-3.43 ± 0.00	1	3,048.69	3,048.69 ± 0.00
19	-3.18	-3.04 ± 0.19	2	4,650.36	5,841.28 ± 1,899.88
20	-2.96	-2.96 ± 0.00	1	6,743.03	6,743.03 ± 0.00
21	-2.95	-2.95 ± 0.00	1	6,857.89	6,857.89 ± 0.00
22	-2.91	-2.91 ± 0.00	1	7,337.20	7,337.20 ± 0.00
23	-2.75	-2.75 ± 0.00	1	9,613.67	9,613.67 ± 0.00
24	-2.68	-2.68 ± 0.00	1	10,820.17	10,820.17 ± 0.00
25	-2.57	-2.57 ± 0.00	1	13,029.22	13,029.22 ± 0.00
26	-2.39	-2.39 ± 0.00	1	17,658.24	17,658.24 ± 0.00
27	-2.39	-2.39 ± 0.00	1	17,658.24	17,658.24 ± 0.00
28	-2.38	-2.38 ± 0.00	1	17,959.01	17,959.01 ± 0.00
29	-2.27	-2.27 ± 0.00	1	21,625.53	21,625.53 ± 0.00
30	-2.26	-2.26 ± 0.00	1	21,993.87	21,993.87 ± 0.00
31	-2.24	-2.24 ± 0.00	1	22,749.49	22,749.49 ± 0.00
32	-2.23	-2.23 ± 0.00	1	23,136.98	23,136.98 ± 0.00
33	-2.22	-2.22 ± 0.00	1	23,531.06	23,531.06 ± 0.00
34	-2.19	-2.19 ± 0.00	1	24,754.06	24,754.06 ± 0.00
35	-2.13	-2.13 ± 0.00	1	27,394.04	27,394.04 ± 0.00
36	-2.10	-2.10 ± 0.00	1	28,817.81	28,817.81 ± 0.00
37	-2.06	-2.06 ± 0.00	1	30,831.93	30,831.93 ± 0.00
38	-1.99	-1.99 ± 0.00	1	34,701.27	34,701.27 ± 0.00

Cluster rank	Lowest B.E. (kcal/mol)	Mean B.E. (kcal/mol)	Frequency	K _i (μM)	K _{i,avg} (μM)
39	-1.99	-1.99 ± 0.00	1	34,701.27	34,701.27 ± 0.00
40	-1.91	-1.91 ± 0.00	1	39,721.43	39,721.43 ± 0.00
41	-1.83	-1.83 ± 0.00	1	45,467.86	45,467.86 ± 0.00
42	-1.71	-1.17 ± 0.40	4	55,683.16	137,449.64 ± 95,119.72
43	-1.63	-1.63 ± 0.00	1	63,738.74	63,738.74 ± 0.00
44	-1.44	-1.44 ± 0.00	1	87,855.20	87,855.20 ± 0.00
45	-1.38	-1.38 ± 0.00	1	97,224.82	97,224.82 ± 0.00
46	-1.37	-1.37 ± 0.00	1	98,880.83	98,880.83 ± 0.00
47	-1.34	-1.34 ± 0.00	1	104,020.03	104,020.03 ± 0.00
48	-1.30	-1.30 ± 0.00	1	111,290.16	111,290.16 ± 0.00
49	-1.26	-1.26 ± 0.00	1	119,068.41	119,068.41 ± 0.00
50	-1.12	-1.12 ± 0.00	1	150,829.34	150,829.34 ± 0.00
51	-1.10	-1.10 ± 0.00	1	156,011.18	156,011.18 ± 0.00
52	-1.04	-1.04 ± 0.00	1	172,649.53	172,649.53 ± 0.00
53	-1.04	-1.04 ± 0.00	1	172,649.53	172,649.53 ± 0.00
54	-0.86	-0.86 ± 0.00	1	233,988.48	233,988.48 ± 0.00
55	-0.82	-0.82 ± 0.00	1	250,342.31	250,342.31 ± 0.00
56	-0.76	-0.76 ± 0.00	1	277,040.94	277,040.94 ± 0.00
57	-0.72	-0.37 ± 0.50	2	296,403.78	535,311.93 ± 474,031.42
58	-0.66	-0.66 ± 0.00	1	328,014.79	328,014.79 ± 0.00
59	-0.64	-0.64 ± 0.00	1	339,283.96	339,283.96 ± 0.00
60	-0.61	-0.61 ± 0.00	1	356,917.77	356,917.77 ± 0.00
61	-0.57	-0.57 ± 0.00	1	381,863.33	381,863.33 ± 0.00
62	-0.55	-0.03 ± 0.74	2	394,982.50	950,594.19 ± 1,338,403.22
63	-0.44	-0.44 ± 0.00	1	475,622.38	475,622.38 ± 0.00
64	-0.42	-0.42 ± 0.00	1	491,962.71	491,962.71 ± 0.00
65	-0.32	-0.32 ± 0.00	1	582,480.86	582,480.86 ± 0.00
66	-0.29	-0.29 ± 0.00	1	612,754.50	612,754.50 ± 0.00
67	-0.25	-0.25 ± 0.00	1	655,580.91	655,580.91 ± 0.00
68	-0.18	-0.18 ± 0.00	1	737,854.85	737,854.85 ± 0.00
69	-0.08	-0.08 ± 0.00	1	873,615.67	873,615.67 ± 0.00
70	-0.07	-0.07 ± 0.00	1	888,495.77	888,495.77 ± 0.00
71	-0.05	-0.05 ± 0.00	1	919,020.63	919,020.63 ± 0.00
72	0.05	0.05 ± 0.00	1	1,088,114.86	1,088,114.86 ± 0.00
73	0.10	0.10 ± 0.00	1	1,183,993.94	1,183,993.94 ± 0.00
74	0.19	0.19 ± 0.00	1	1,378,364.29	1,378,364.29 ± 0.00
75	0.22	0.22 ± 0.00	1	1,450,002.85	1,450,002.85 ± 0.00
76	0.26	0.26 ± 0.00	1	1,551,345.93	1,551,345.93 ± 0.00
77	0.50	0.50 ± 0.00	1	2,326,737.57	2,326,737.57 ± 0.00
78	0.58	0.58 ± 0.00	1	2,663,342.30	2,663,342.30 ± 0.00

Cluster rank	Lowest B.E. (kcal/mol)	Mean B.E. (kcal/mol)	Frequency	K_i (μ M)	$K_{i,avg}$ (μ M)
79	0.59	0.59 ± 0.00	1	2,708,706.41	$2,708,706.41 \pm 0.00$
80	0.75	0.75 ± 0.00	1	3,549,123.43	$3,549,123.43 \pm 0.00$
81	0.85	0.85 ± 0.00	1	4,202,140.65	$4,202,140.65 \pm 0.00$
82	0.87	0.87 ± 0.00	1	4,346,507.97	$4,346,507.97 \pm 0.00$
83	0.94	0.94 ± 0.00	1	4,891,985.00	$4,891,985.00 \pm 0.00$
84	1.02	1.02 ± 0.00	1	5,599,699.23	$5,599,699.23 \pm 0.00$
85	1.22	1.22 ± 0.00	1	7,849,891.65	$7,849,891.65 \pm 0.00$
86	1.53	1.53 ± 0.00	1	13,250,951.11	$13,250,951.11 \pm 0.00$
87	2.39	2.39 ± 0.00	1	56,630,785.32	$56,630,785.32 \pm 0.00$

C1EXT-MON

Cluster rank	Lowest B.E. (kcal/mol)	Mean B.E. (kcal/mol)	Frequency	K_i (μ M)	$K_{i,avg}$ (μ M)
1	-8.36	-8.36 ± 0.00	1	0.74	0.74 ± 0.00
2	-8.27	-7.44 ± 1.38	3	0.86	3.49 ± 29.02
3	-8.18	-8.18 ± 0.00	1	1.00	1.00 ± 0.00
4	-8.01	-7.51 ± 0.71	2	1.33	3.13 ± 4.25
5	-7.85	-7.85 ± 0.00	1	1.75	1.75 ± 0.00
6	-7.71	-7.18 ± 0.89	4	2.21	5.44 ± 24.29
7	-7.55	-7.55 ± 0.00	1	2.90	2.90 ± 0.00
8	-7.55	-7.55 ± 0.00	1	2.90	2.90 ± 0.00
9	-7.45	-7.45 ± 0.00	1	3.43	3.43 ± 0.00
10	-7.35	-7.35 ± 0.00	1	4.06	4.06 ± 0.00
11	-7.17	-7.17 ± 0.00	1	5.51	5.51 ± 0.00
12	-6.90	-6.90 ± 0.00	1	8.69	8.69 ± 0.00
13	-6.86	-6.56 ± 0.43	2	9.29	15.56 ± 11.84
14	-6.81	-6.81 ± 0.00	1	10.11	10.11 ± 0.00
15	-6.75	-6.75 ± 0.00	1	11.19	11.19 ± 0.00
16	-6.68	-6.68 ± 0.00	1	12.60	12.60 ± 0.00
17	-6.66	-6.66 ± 0.00	1	13.03	13.03 ± 0.00
18	-6.65	-6.65 ± 0.00	1	13.25	13.25 ± 0.00
19	-6.61	-6.61 ± 0.00	1	14.18	14.18 ± 0.00
20	-6.60	-6.60 ± 0.00	1	14.42	14.42 ± 0.00
21	-6.59	-6.59 ± 0.00	1	14.66	14.66 ± 0.00
22	-6.56	-6.48 ± 0.12	2	15.43	17.81 ± 3.63
23	-6.56	-6.56 ± 0.00	1	15.43	15.43 ± 0.00
24	-6.54	-6.54 ± 0.00	1	15.96	15.96 ± 0.00
25	-6.46	-6.46 ± 0.00	1	18.27	18.27 ± 0.00
26	-6.45	-6.45 ± 0.00	1	18.58	18.58 ± 0.00
27	-6.45	-5.97 ± 0.40	4	18.58	42.14 ± 29.03

Cluster rank	Lowest B.E. (kcal/mol)	Mean B.E. (kcal/mol)	Frequency	K _i (μM)	K _{i,avg} (μM)
28	-6.37	-6.04 ± 0.47	2	21.26	37.44 ± 31.58
29	-6.19	-6.19 ± 0.00	1	28.82	28.82 ± 0.00
30	-6.17	-5.91 ± 0.37	2	29.81	46.24 ± 29.65
31	-6.11	-6.11 ± 0.00	1	32.99	32.99 ± 0.00
32	-6.11	-5.81 ± 0.43	2	32.99	55.22 ± 42.03
33	-6.10	-6.10 ± 0.00	1	33.55	33.55 ± 0.00
34	-6.08	-6.08 ± 0.00	1	34.70	34.70 ± 0.00
35	-6.08	-6.08 ± 0.00	1	34.70	34.70 ± 0.00
36	-6.01	-6.01 ± 0.00	1	39.06	39.06 ± 0.00
37	-5.99	-5.99 ± 0.00	1	40.40	40.40 ± 0.00
38	-5.98	-5.98 ± 0.00	1	41.09	41.09 ± 0.00
39	-5.94	-5.94 ± 0.00	1	43.96	43.96 ± 0.00
40	-5.83	-5.83 ± 0.00	1	52.93	52.93 ± 0.00
41	-5.77	-5.77 ± 0.00	1	58.58	58.58 ± 0.00
42	-5.72	-5.72 ± 0.00	1	63.74	63.74 ± 0.00
43	-5.72	-5.52 ± 0.29	2	63.74	90.11 ± 45.01
44	-5.71	-5.71 ± 0.00	1	64.83	64.83 ± 0.00
45	-5.69	-5.69 ± 0.00	1	67.05	67.05 ± 0.00
46	-5.68	-5.68 ± 0.00	1	68.19	68.19 ± 0.00
47	-5.67	-5.67 ± 0.00	1	69.36	69.36 ± 0.00
48	-5.66	-5.66 ± 0.00	1	70.54	70.54 ± 0.00
49	-5.59	-5.59 ± 0.00	1	79.39	79.39 ± 0.00
50	-5.57	-5.57 ± 0.00	1	82.12	82.12 ± 0.00
51	-5.52	-5.52 ± 0.00	1	89.35	89.35 ± 0.00
52	-5.51	-5.51 ± 0.00	1	90.87	90.87 ± 0.00
53	-5.49	-5.49 ± 0.00	1	94.00	94.00 ± 0.00
54	-5.43	-5.43 ± 0.00	2	104.02	104.02 ± 0.00
55	-5.42	-5.42 ± 0.00	1	105.79	105.79 ± 0.00
56	-5.40	-4.40 ± 1.41	2	109.43	592.41 ± 2,190.41
57	-5.36	-5.36 ± 0.00	1	117.08	117.08 ± 0.00
58	-5.29	-5.29 ± 0.00	1	131.77	131.77 ± 0.00
59	-5.24	-5.24 ± 0.00	1	143.38	143.38 ± 0.00
60	-5.22	-5.22 ± 0.00	1	148.31	148.31 ± 0.00
61	-5.21	-5.21 ± 0.00	1	150.83	150.83 ± 0.00
62	-5.19	-5.19 ± 0.00	1	156.01	156.01 ± 0.00
63	-5.19	-5.19 ± 0.00	1	156.01	156.01 ± 0.00
64	-5.18	-5.18 ± 0.00	1	158.67	158.67 ± 0.00
65	-5.13	-5.13 ± 0.00	1	172.65	172.65 ± 0.00
66	-5.11	-5.11 ± 0.00	1	178.58	178.58 ± 0.00
67	-5.02	-5.02 ± 0.00	1	207.90	207.90 ± 0.00

Cluster rank	Lowest B.E. (kcal/mol)	Mean B.E. (kcal/mol)	Frequency	K _i (μM)	K _{i,avg} (μM)
68	-4.92	-4.92 ± 0.00	1	246.15	246.15 ± 0.00
69	-4.87	-4.87 ± 0.00	1	267.84	267.84 ± 0.00
70	-4.72	-4.72 ± 0.00	1	345.07	345.07 ± 0.00
71	-4.60	-4.60 ± 0.00	1	422.59	422.59 ± 0.00
72	-4.52	-4.52 ± 0.00	1	483.73	483.73 ± 0.00
73	-4.51	-4.51 ± 0.00	1	491.97	491.97 ± 0.00
74	-4.50	-4.50 ± 0.00	1	500.35	500.35 ± 0.00
75	-4.37	-4.37 ± 0.00	1	623.20	623.20 ± 0.00
76	-4.22	-4.22 ± 0.00	1	802.88	802.88 ± 0.00
77	-4.19	-4.19 ± 0.00	1	844.61	844.61 ± 0.00
78	-4.10	-4.10 ± 0.00	1	983.27	983.27 ± 0.00
79	-3.97	-3.97 ± 0.00	1	1,224.69	1,224.69 ± 0.00
80	-3.84	-3.84 ± 0.00	1	1,525.39	1,525.39 ± 0.00
81	-3.36	-3.36 ± 0.00	1	3,431.29	3,431.29 ± 0.00
82	-2.46	-2.46 ± 0.00	1	15,689.27	15,689.27 ± 0.00
83	-1.93	-1.93 ± 0.00	1	38,402.10	38,402.10 ± 0.00

C1EXT-CD

Cluster rank	Lowest B.E. (kcal/mol)	Mean B.E. (kcal/mol)	Frequency	K _i (μM)	K _{i,avg} (μM)
1	-6.98	-6.68 ± 0.21	96	7.59	12.65 ± 5.29
2	-5.86	-5.75 ± 0.11	4	50.32	60.85 ± 11.71

C1EXT-DMP

Cluster rank	Lowest B.E. (kcal/mol)	Mean B.E. (kcal/mol)	Frequency	K _i (μM)	K _{i,avg} (μM)
1	-6.56	-6.50 ± 0.06	99	15.43	16.96 ± 2.26
2	-5.92	-5.92 ± 0.00	1	45.47	45.46 ± 0.00

C2EXT-LTD₄

Cluster rank	Lowest B.E. (kcal/mol)	Mean B.E. (kcal/mol)	Frequency	K _i (μM)	K _{i,avg} (μM)
1	-7.18	-6.36 ± 0.89	3	5.41	21.63 ± 54.76
2	-6.94	-5.90 ± 0.92	3	8.12	46.77 ± 76.72
3	-6.86	-6.86 ± 0.00	1	9.29	9.29 ± 0.00
4	-6.81	-6.81 ± 0.00	1	10.11	10.11 ± 0.00
5	-6.65	-6.10 ± 0.78	2	13.25	33.55 ± 50.69
6	-6.12	-5.63 ± 0.70	2	32.43	74.83 ± 99.14
7	-6.06	-5.72 ± 0.37	3	35.89	63.38 ± 45.43

Cluster rank	Lowest B.E. (kcal/mol)	Mean B.E. (kcal/mol)	Frequency	K _i (μM)	K _{i,avg} (μM)
8	-5.97	-5.97 ± 0.00	1	41.79	41.79 ± 0.00
9	-5.97	-5.97 ± 0.00	1	41.79	41.79 ± 0.00
10	-5.96	-5.96 ± 0.00	1	42.50	42.50 ± 0.00
11	-5.96	-5.96 ± 0.00	1	42.50	42.50 ± 0.00
12	-5.89	-5.89 ± 0.00	1	47.83	47.83 ± 0.00
13	-5.84	-5.84 ± 0.00	1	52.05	52.05 ± 0.00
14	-5.82	-5.82 ± 0.00	1	53.83	53.83 ± 0.00
15	-5.82	-5.82 ± 0.00	1	53.83	53.83 ± 0.00
16	-5.74	-5.04 ± 1.00	2	61.62	202.70 ± 427.90
17	-5.69	-4.72 ± 0.80	4	67.05	347.99 ± 556.29
18	-5.68	-5.68 ± 0.00	1	68.19	68.19 ± 0.00
19	-5.67	-4.40 ± 1.80	2	69.36	592.41 ± 3,529.01
20	-5.63	-4.54 ± 0.99	3	74.20	470.30 ± 942.77
21	-5.53	-5.53 ± 0.00	1	87.86	87.86 ± 0.00
22	-5.48	-4.56 ± 1.31	2	95.60	455.96 ± 1,470.20
23	-5.46	-5.46 ± 0.00	1	98.88	98.88 ± 0.00
24	-5.39	-5.39 ± 0.00	1	111.29	111.29 ± 0.00
25	-5.38	-5.38 ± 0.00	1	113.19	113.19 ± 0.00
26	-5.30	-4.74 ± 0.79	2	129.56	333.61 ± 515.79
27	-5.26	-5.26 ± 0.00	1	138.62	138.62 ± 0.00
28	-5.25	-5.25 ± 0.00	1	140.98	140.98 ± 0.00
29	-5.22	-5.22 ± 0.00	1	148.31	148.31 ± 0.00
30	-5.19	-5.19 ± 0.00	1	156.01	156.01 ± 0.00
31	-5.18	-5.18 ± 0.00	1	158.67	158.67 ± 0.00
32	-5.16	-4.27 ± 1.30	4	164.12	737.87 ± 9314.54
33	-5.16	-5.16 ± 0.00	1	164.12	164.12 ± 0.00
34	-5.02	-4.72 ± 0.42	2	207.90	345.07 ± 257.98
35	-5.02	-5.02 ± 0.00	1	207.90	207.90 ± 0.00
36	-4.94	-4.94 ± 0.00	1	237.98	237.98 ± 0.00
37	-4.93	-4.93 ± 0.00	1	242.03	242.03 ± 0.00
38	-4.92	-4.78 ± 0.20	2	246.15	311.81 ± 105.24
39	-4.91	-4.91 ± 0.00	1	250.35	250.35 ± 0.00
40	-4.88	-4.88 ± 0.00	1	263.36	263.36 ± 0.00
41	-4.88	-3.44 ± 1.25	3	263.36	2,980.80 ± 6,001.51
42	-4.83	-4.20 ± 0.90	2	286.56	837.51 ± 1,528.16
43	-4.80	-4.80 ± 0.00	1	301.46	301.46 ± 0.00
44	-4.68	-4.68 ± 0.00	1	369.19	369.19 ± 0.00
45	-4.67	-4.67 ± 0.00	1	375.47	375.47 ± 0.00
46	-4.54	-4.54 ± 0.00	1	467.66	467.66 ± 0.00

Cluster rank	Lowest B.E. (kcal/mol)	Mean B.E. (kcal/mol)	Frequency	K _i (μM)	K _{i,avg} (μM)
47	-4.52	-3.27 ± 1.77	2	483.73	3,994.59 ± 22,983.16
48	-4.52	-4.52 ± 0.00	1	483.73	483.73 ± 0.00
49	-4.32	-4.32 ± 0.00	1	678.11	678.11 ± 0.00
50	-4.28	-4.28 ± 0.00	1	725.51	725.51 ± 0.00
51	-4.28	-4.28 ± 0.00	1	725.51	725.51 ± 0.00
52	-4.28	-4.28 ± 0.00	1	725.51	725.51 ± 0.00
53	-4.27	-3.27 ± 1.42	2	737.87	4,028.46 ± 15,030.27
54	-4.11	-4.11 ± 0.00	1	966.80	966.80 ± 0.00
55	-4.09	-4.09 ± 0.00	1	1,000.01	1,000.01 ± 0.00
56	-4.08	-4.08 ± 0.00	1	1,017.05	1,017.05 ± 0.00
57	-3.96	-3.96 ± 0.00	1	1,245.55	1,245.55 ± 0.00
58	-3.86	-3.86 ± 0.00	1	1,474.72	1,474.72 ± 0.00
59	-3.82	-3.82 ± 0.00	1	1,577.79	1,577.79 ± 0.00
60	-3.78	-3.78 ± 0.00	1	1,688.07	1,688.07 ± 0.00
61	-3.48	-3.48 ± 0.00	1	2,801.81	2,801.81 ± 0.00
62	-3.48	-3.48 ± 0.00	1	2,801.81	2,801.81 ± 0.00
63	-3.38	-3.38 ± 0.00	1	3,317.32	3,317.32 ± 0.00
64	-3.34	-3.34 ± 0.00	1	3,549.17	3,549.17 ± 0.00
65	-3.07	-3.07 ± 0.00	1	5,599.78	5,599.78 ± 0.00
66	-2.99	-2.99 ± 0.00	1	6,409.89	6,409.89 ± 0.00
67	-2.81	-2.81 ± 0.00	1	8,687.20	8,687.20 ± 0.00
68	-2.67	-2.67 ± 0.00	1	11,004.46	11,004.46 ± 0.00
69	-2.65	-2.65 ± 0.00	1	11,382.53	11,382.53 ± 0.00
70	-2.62	-2.62 ± 0.00	1	11,974.12	11,974.12 ± 0.00
71	-2.57	-2.57 ± 0.00	1	13,029.22	13,029.22 ± 0.00
72	-2.50	-2.50 ± 0.00	1	14,664.36	14,664.36 ± 0.00
73	-2.17	-2.17 ± 0.00	1	25,604.50	25,604.50 ± 0.00

C2EXT-MON

Cluster rank	Lowest B.E. (kcal/mol)	Mean B.E. (kcal/mol)	Frequency	K _i (μM)	K _{i,avg} (μM)
1	-12.44	-11.39 ± 0.95	3	0.00075	0.00440 ± 0.01
2	-11.43	-11.06 ± 0.53	2	0.00413	0.00778 ± 0.01
3	-11.33	-11.33 ± 0.00	1	0.00489	0.00489 ± 0.00
4	-11.30	-11.30 ± 0.00	1	0.00515	0.00515 ± 0.00
5	-11.30	-10.57 ± 0.73	4	0.00515	0.01781 ± 0.03
6	-11.28	-10.15 ± 0.68	5	0.00532	0.03589 ± 0.04
7	-11.25	-11.25 ± 0.00	1	0.00560	0.00560 ± 0.00
8	-11.24	-10.38 ± 0.70	4	0.00570	0.02424 ± 0.04
9	-11.19	-11.06 ± 0.18	2	0.00620	0.00772 ± 0.002

Cluster rank	Lowest B.E. (kcal/mol)	Mean B.E. (kcal/mol)	Frequency	K _i (μM)	K _{i,avg} (μM)
10	-11.10	-10.21 ± 0.87	3	0.00721	0.03225 ± 0.07
11	-11.04	-10.82 ± 0.32	2	0.00798	0.01167 ± 0.01
12	-10.96	-10.53 ± 0.48	4	0.00914	0.01881 ± 0.02
13	-10.84	-10.30 ± 0.46	8	0.01119	0.02780 ± 0.03
14	-10.83	-10.83 ± 0.00	1	0.01138	0.01138 ± 0.00
15	-10.82	-10.82 ± 0.00	1	0.01158	0.01158 ± 0.00
16	-10.75	-10.75 ± 0.00	1	0.01303	0.01303 ± 0.00
17	-10.71	-10.71 ± 0.00	1	0.01394	0.01394 ± 0.00
18	-10.70	-10.70 ± 0.00	1	0.01418	0.01418 ± 0.00
19	-10.68	-9.75 ± 1.32	2	0.01466	0.07114 ± 0.23
20	-10.65	-10.53 ± 0.17	2	0.01543	0.01889 ± 0.01
21	-10.63	-10.02 ± 0.87	2	0.01596	0.04509 ± 0.08
22	-10.61	-10.61 ± 0.00	1	0.01651	0.01651 ± 0.00
23	-10.59	-10.59 ± 0.00	1	0.01707	0.01707 ± 0.00
24	-10.57	-10.57 ± 0.00	1	0.01766	0.01766 ± 0.00
25	-10.52	-10.52 ± 0.00	1	0.01921	0.01921 ± 0.00
26	-10.47	-10.47 ± 0.00	1	0.02091	0.02091 ± 0.00
27	-10.45	-10.45 ± 0.00	1	0.02163	0.02163 ± 0.00
28	-10.43	-10.41 ± 0.03	2	0.02237	0.02314 ± 0.001
29	-10.41	-10.41 ± 0.00	1	0.02314	0.02314 ± 0.00
30	-10.40	-10.40 ± 0.00	1	0.02353	0.02353 ± 0.00
31	-10.37	-10.37 ± 0.00	1	0.02475	0.02475 ± 0.00
32	-10.37	-10.37 ± 0.00	1	0.02475	0.02475 ± 0.00
33	-10.31	-10.31 ± 0.00	1	0.02739	0.02739 ± 0.00
34	-10.27	-9.82 ± 0.64	2	0.02931	0.06267 ± 0.07
35	-10.27	-10.27 ± 0.00	1	0.02931	0.02931 ± 0.00
36	-10.09	-10.09 ± 0.00	1	0.03972	0.03972 ± 0.00
37	-10.08	-10.08 ± 0.00	1	0.04040	0.04040 ± 0.00
38	-10.01	-10.01 ± 0.00	1	0.04547	0.04547 ± 0.00
39	-9.97	-9.88 ± 0.13	2	0.04865	0.05711 ± 0.01
40	-9.93	-9.93 ± 0.00	1	0.05205	0.05205 ± 0.00
41	-9.93	-9.93 ± 0.00	1	0.05205	0.05205 ± 0.00
42	-9.86	-9.86 ± 0.00	1	0.05858	0.05858 ± 0.00
43	-9.85	-9.85 ± 0.00	1	0.05958	0.05958 ± 0.00
44	-9.66	-9.66 ± 0.00	1	0.08212	0.08212 ± 0.00
45	-9.66	-9.66 ± 0.00	1	0.08212	0.08212 ± 0.00
46	-9.63	-9.63 ± 0.00	1	0.08639	0.08639 ± 0.00
47	-9.59	-9.59 ± 0.00	1	0.09242	0.09242 ± 0.00
48	-9.58	-8.97 ± 0.86	2	0.09400	0.26336 ± 0.46
49	-9.52	-9.52 ± 0.00	1	0.10402	0.10402 ± 0.00

Cluster rank	Lowest B.E. (kcal/mol)	Mean B.E. (kcal/mol)	Frequency	K_i (μ M)	$K_{i,avg}$ (μ M)
50	-9.50	-9.02 ± 0.68	2	0.10760	0.24203 ± 0.31
51	-9.49	-9.49 ± 0.00	1	0.10943	0.10943 ± 0.00
52	-9.45	-9.45 ± 0.00	1	0.11708	0.11708 ± 0.00
53	-9.43	-9.43 ± 0.00	1	0.12110	0.12110 ± 0.00
54	-9.41	-9.34 ± 0.10	2	0.12526	0.14098 ± 0.02
55	-9.38	-9.38 ± 0.00	1	0.13177	0.13177 ± 0.00
56	-9.26	-9.26 ± 0.00	1	0.16138	0.16138 ± 0.00
57	-9.12	-9.12 ± 0.00	1	0.20442	0.20442 ± 0.00
58	-9.10	-9.10 ± 0.00	1	0.21144	0.21144 ± 0.00
59	-9.05	-9.05 ± 0.00	1	0.23008	0.23008 ± 0.00
60	-8.87	-8.79 ± 0.12	2	0.31182	0.35995 ± 0.07
61	-8.83	-8.83 ± 0.00	1	0.33361	0.33361 ± 0.00
62	-8.73	-8.73 ± 0.00	1	0.39499	0.39499 ± 0.00
63	-8.03	-8.03 ± 0.00	1	1.28836	1.28836 ± 0.00

C2EXT-CD

Cluster rank	Lowest B.E. (kcal/mol)	Mean B.E. (kcal/mol)	Frequency	K_i (μ M)	$K_{i,avg}$ (μ M)
1	-6.25	-5.63 ± 0.34	23	26.04	74.31 ± 43.72
2	-5.76	-5.61 ± 0.10	16	59.58	76.51 ± 12.35
3	-5.71	-5.32 ± 0.11	19	64.83	126.15 ± 18.09
4	-5.47	-5.27 ± 0.34	3	97.23	136.30 ± 95.44
5	-5.43	-5.19 ± 0.35	2	104.02	157.34 ± 94.72
6	-5.33	-5.33 ± 0.00	1	123.16	123.16 ± 0.00
7	-5.31	-5.22 ± 0.08	3	127.39	148.31 ± 20.09
8	-5.22	-5.11 ± 0.16	2	148.31	180.10 ± 49.78
9	-5.17	-5.00 ± 0.14	10	161.37	216.87 ± 57.18
10	-5.14	-5.14 ± 0.00	1	169.76	169.76 ± 0.00
11	-5.10	-5.00 ± 0.10	5	181.63	214.32 ± 37.79
12	-5.08	-5.08 ± 0.00	1	187.87	187.87 ± 0.00
13	-5.04	-5.04 ± 0.00	2	201.00	201.00 ± 0.00
14	-5.02	-4.85 ± 0.19	3	207.90	277.04 ± 92.44
15	-4.99	-4.99 ± 0.00	1	218.71	218.71 ± 0.00
16	-4.95	-4.85 ± 0.15	2	233.99	279.39 ± 70.44
17	-4.89	-4.71 ± 0.26	3	258.95	350.95 ± 179.36
18	-4.78	-4.78 ± 0.00	1	311.81	311.81 ± 0.00
19	-4.63	-4.63 ± 0.00	1	401.72	401.72 ± 0.00
20	-4.56	-4.56 ± 0.00	1	452.13	452.13 ± 0.00

C2EXT-DMP

Cluster rank	Lowest B.E. (kcal/mol)	Mean B.E. (kcal/mol)	Frequency	K _i (μM)	K _{i,avg} (μM)
1	-5.61	-5.50 ± 0.07	68	76.75	91.80 ± 10.25
2	-5.54	-5.34 ± 0.18	13	86.39	120.31 ± 37.80
3	-5.45	-5.41 ± 0.06	3	100.57	106.99 ± 11.85
4	-5.25	-5.25 ± 0.01	2	140.98	142.17 ± 1.70
5	-5.23	-5.12 ± 0.07	10	145.82	175.59 ± 20.88
6	-5.11	-5.07 ± 0.04	3	178.58	189.99 ± 11.23
7	-4.98	-4.98 ± 0.00	1	222.43	222.43 ± 0.00

C-6 MM/GBSA Calculation of CysLTRs Systems

Entropy Approximation for 5-LO Complex Systems.

Host	Ligand	Entropy approximation at T = 298.15 K (kcal/mol)				
			Translational	Rotational	Vibrational	Total
C1INT	LTD ₄	Complex	17.13	18.01	3977.72	4012.86
		Receptor	17.12	17.99	3931.58	3966.69
		Ligand	13.26	11.81	85.61	110.68
		T S	-13.25	-11.79	-39.47	-64.51
	MON	Complex	17.14	18.01	3975.06	4010.21
		Receptor	17.12	18.00	3936.24	3971.36
		Ligand	13.40	11.80	65.39	90.59
		T S	-13.39	-11.78	-26.57	-51.74
	CD	Complex	17.13	18.04	3993.68	4028.84
		Receptor	17.12	18.03	3971.22	4006.37
		Ligand	12.49	9.76	32.99	55.24
		T S	-12.48	-9.76	-10.53	-32.77
C1EXT	LTD ₄	Complex	17.13	18.02	3987.67	4022.82
		Receptor	17.12	17.99	3931.41	3966.53
		Ligand	13.26	11.61	106.72	131.58
		T S	-13.25	-11.59	-50.46	-75.29
	MON	Complex	17.14	18.02	4034.47	4069.63
		Receptor	17.12	17.99	3974.70	4009.82
		Ligand	13.40	11.78	90.67	115.86
		T S	-13.39	-11.75	-30.90	-56.04
	CD	Complex	17.13	18.01	3948.75	3983.89
		Receptor	17.12	18.00	3928.55	3963.68

Host	Ligand	Entropy approximation at T = 298.15 K (kcal/mol)				
		Translational	Rotational	Vibrational	Total	
C2EXT	LTD ₄	Ligand	12.49	9.79	31.52	53.80
		T S	-12.48	-9.79	-11.32	-33.59
		Complex	17.16	18.05	4064.12	4099.33
		Receptor	17.15	18.04	4024.02	4059.21
	MON	Ligand	13.26	11.68	75.18	100.12
		T S	-13.25	-11.67	-35.08	-60.00
		Complex	17.16	18.04	3997.85	4033.06
		Receptor	17.15	18.03	3963.55	3998.73
	CD	Ligand	13.40	11.77	55.09	80.27
		T S	-13.39	-11.76	-20.79	-45.95
		Complex	17.15	18.04	3953.74	3988.94
		Receptor	17.15	18.04	3930.90	3966.09
		Ligand	12.49	9.77	33.94	56.20
		T S	-12.48	-9.77	-11.10	-33.35

Generalized Born Binding Energy Approximation.

Host	Ligand	Generalized Born (Complex - Receptor-Ligand)			
		Energy Component	Average (kcal/mol)	S.D.	Total (kcal/mol)
C1INT	LTD ₄	DIHED	-0.35	0.17	
		VDWAALS	-51.79	3.50	
		EEL	-55.99	13.95	
		EGB	72.59	11.91	
		ESURF	-8.35	0.31	
		G _{gas}	-108.13	13.41	
		G _{solv}	64.23	11.84	
		G_{Total}	-43.89	3.91	
	MON	G_{binding}			20.61
		DIHED	0.00	0.01	
		VDWAALS	-51.26	3.36	
		EEL	-3.26	6.13	
		EGB	26.23	5.30	
		ESURF	-6.65	0.33	
		G _{gas}	-54.51	7.24	
		G _{solv}	19.58	5.19	
	CD	G_{Total}	-34.93	3.45	
		G_{binding}			16.81
		VDWAALS	-28.79	2.34	
		EEL	-20.48	8.68	

Host	Ligand	Generalized Born (Complex - Receptor-Ligand)			
		Energy Component	Average (kcal/mol)	S.D.	Total (kcal/mol)
C1EXT	LTD ₄	EGB	30.28	6.87	
		ESURF	-4.43	0.26	
		G _{gas}	-49.27	8.92	
		G _{solv}	25.85	6.78	
		G_{Total}	-23.42	3.88	
		G_{binding}			9.36
		DIHED	-0.36	0.18	
		VDWAALS	-42.36	4.77	
		EEL	-54.93	19.10	
		EGB	71.41	16.84	
	MON	ESURF	-6.72	0.72	
		G _{gas}	-97.64	20.62	
		G _{solv}	64.70	16.30	
		G_{Total}	-32.95	6.17	
		G_{binding}			42.35
		DIHED	0.01	0.01	
		VDWAALS	-21.46	10.17	
		EEL	-6.64	7.62	
		EGB	16.62	10.31	
		ESURF	-2.71	1.26	
C2EXT	CD	G _{gas}	-28.10	16.43	
		G _{solv}	13.90	9.26	
		G_{Total}	-14.19	8.32	
		G_{binding}			41.85
		VDWAALS	-35.16	2.72	
		EEL	-22.60	4.93	
	LTD ₄	EGB	35.43	3.75	
		ESURF	-5.02	0.13	
		G _{gas}	-57.75	4.64	
		G _{solv}	30.41	3.74	
		G_{Total}	-27.34	3.06	
		G_{binding}			6.25
	LTD ₄	DIHED	-0.35	0.17	
		VDWAALS	-60.36	2.99	
		EEL	-55.86	7.51	
		EGB	83.47	5.97	
		ESURF	-8.69	0.25	
		G _{gas}	-116.57	7.26	

Host	Ligand	Generalized Born (Complex - Receptor-Ligand)			
		Energy Component	Average (kcal/mol)	S.D.	Total (kcal/mol)
MON	CD	G_{solv}	74.77	5.91	
		G_{Total}	-41.80	3.33	
		G_{binding}			18.20
		DIHED	0.01	0.01	
		VDWAALS	-71.75	2.84	
		EEL	-17.10	3.38	
		EGB	48.26	2.69	
		ESURF	-8.96	0.25	
		G_{gas}	-88.85	3.99	
		G_{solv}	39.29	2.67	
		G_{Total}	-49.55	3.26	
		G_{binding}			-3.61
		VDWAALS	-32.45	2.06	
		EEL	-6.65	3.56	
CD	MON	EGB	19.19	2.36	
		ESURF	-4.80	0.16	
		G_{gas}	-39.10	3.57	
		G_{solv}	14.39	2.37	
		G_{Total}	-24.71	2.47	
		G_{binding}			8.64

DIHED	denotes dihedral energy.
VDWAALS	denotes van der Waals energy.
EEL	denotes electrostatic energy.
EGB	denotes as polar solvation free energy.
ESURF	denotes as nonpolar solvation free energy.
G_{gas}	denotes total gas phase free energy.
G_{solv}	denotes total solvation free energy.